FACULTY OF
PHARMACEUTICAL SCIENCES

Expanding the biologist's toolbox with microfabricated sample holders for single objective SPIM and Single Particle Tracking for the characterization of nanomedicines

Elisa Zagato

Thesis submitted to obtain the degree of
Doctor in Pharmaceutical Sciences

Proefschrift voorgedragen tot het bekomen van de graad van
Doctor in de Farmaceutische Wetenschappen

2017/2018

Promoters

Prof. Dr. Kevin Braeckmans

Prof. Dr. Katrien Remaut

Prof. Dr. Kristiaan Neyts

GHENT
UNIVERSITY

Promoters

Prof. Dr. Kevin Braeckmans[1,2]

Prof. Dr. Katrien Remaut[1,3]

Prof. Dr. Kristiaan Neyts[2,4]

[1]*Laboratory of General Biochemistry and Physical Pharmacy, Faculty of Pharmaceutical sciences, Ghent University, Belgium*
[2]*Biophotonics Research Group, Ghent University, Belgium*
[3]*Ghent research group on nanomedicines, Ghent University, Belgium*
[4]*Liquid crystals and Photonics Group, Ghent University, Belgium*

Members of the exam committee

Prof. Dr. Thomas De Beer (chairman)	Universiteit Gent
Prof. Dr. Jo Demeester (secretary)	Universiteit Gent
Prof. Dr. Filip Beunis	Universiteit Gent
Prof. Dr. Winnok De Vos	Universiteit Antwerpen
Prof. Dr. Geert Van Steenberghe	Universiteit Gent
Dr. Hendrik Deschout	University of Gothenburg, Sweden

The author and the promotors give the authorization to consult and to copy parts of this thesis for personal use only. Any other use is limited by the Laws of Copyright, especially to refer to the source whenever results from this thesis are cited.

De auteur en de promotoren geven de toelating dit proefschrift voor consultering beschikbaar te stellen en delen ervan te kopiëren voor persoonlijk gebruik. Elk ander gebruik valt onder de beperkingen van de auteursrecht, in het bijzonder met betrekking tot de verplichting uitdrukkelijk de bron te vermelden bij het aanhalen van resultaten uit dit proefschrift.

TABLE OF CONTENTS

List of abbreviations		1
General Introduction: Aim and Outline		4
Samenvatting		9
Chapter 1	Technical implementation of Light Sheet Fluorescence Microscopy	13
Chapter 2	Microfabricated devices for single objective Single Plane Illumination Microscopy	65
Chapter 3	Single Particle Tracking for studying nanomaterials dynamics: applications and fundamentals in drug delivery	95
Chapter 4	Quantifying the number of nucleic acid therapeutics per nanoparticle by Single Particle Tracking	135
Chapter 5	Broader international context, relevance and future perspectives	165
Summary and General Conclusions		183
Algemene Besluiten		187
Curriculum Vitae		191
Acknowledgement		196

LIST OF ABBREVIATIONS

2PE	Two Photon Excitation
1PE	Single Photon Excitation
AFM	Atomic Force Microscopy
ASLM	Axially Swept Light sheet Microscopy
CARS	Coherent Anti-stokes Raman Spectroscopy
CCM	Cell Colture Medium
CED	Convection-Enhanced Delivery
Ceramide-PEG_{2000}	N-octanoyl-sphingosine-1-[succinyl[methoxy(polyethyleneglycol)2000]
DiASLM	Diagonal ASLM
DoF	Depth of Field
DOPE	1,2-Dioleoyl-sn-glycero-3-phosphoethanolamine
DOTAP	(2,3-Dioleoyloxy-propyl)-trimethylammonium-chloride
DSLM	Digitally Scanned Light sheet Microscopy
DSPE-PEG_{2000}	1,2-Distearoyl-sn-glycero-3-phosphoethanolamine-N-(methoxy(polyethyleneglycol)-2000)
ECS	ExtraCellular Spaces
EGFR	Epidermal growth factor receptor
EPR	Enhanced Permeation and Retention effect
FCS	Fluorescence Correlation Spectroscopy

FoV	Field of View
FRAP	Fluorescence Recovery After Photobleaching
FWHM	Full Width at Half Maximum
HA	Hyaluronic Acid
LNP	Lipid NanoParticle
LPX	Lipoplexes
LSFM	Light Sheet Fluorescence Microscopy
MSD	Mean Squared Displacement
MUM	MUltifocal plane Microscopy
MW	Molecular Weight
NA	Numerical Aperture
NAm	Nucleic acid molecules
NIR	Near Infrared Range
PALM	Photo-Activable Localization Microscopy
pDNA	Plasmid DNA
PEG	Polyethylene glycol
PEI	Polyethylenimine
PIP	Plane Illumination Plug-in
Plasmid/NP ratio	the average number of complexed plasmids for every nanoparticle
PMMA	Poly(methyl methacrylate)
PSF	Point Spread Function
RMS	Root Mean Square deviation

SCAPE	Swept Confocally Aligned Planar Excitation Microscope
SEM	Scanning Electron Microscope
SI	Structured Illumination
siRNA	small interfering RNA
SNR	Signal to Noise Ratio
SoSPIM	Single objective SPIM
SPIM	Single/selective Plane Illumination Microscopy
SPT	Single Particle Tracking
STED	Stimulated Emission Depletion
TIRF (M)	Total Internal Reflection (Microscopy)

GENERAL INTRODUCTION

AIM AND OUTLINE OF THE THESIS

The first decade of the 20th century saw the birth of the very first fluorescence microscope, developed by Otto Heimstaedt and Heinrich Lehmann to study the autofluorescence of bacteria, plant and animal tissues. Little they knew that barely one hundred years later fluorescence microscopy would become a cornerstone of modern biological laboratories and one of biologist's most precious allies. However, progress in fluorescence microscopy didn't happen gradually. The last twenty years have seen a sudden expansion of the field and a blooming of new technologies and illumination modalities. Such a rapid expansion especially favored the life sciences, which greatly benefitted from these advanced techniques and used them to explore the micro- and nano-world. Suddenly, the invisible became visible – chromosomes, organelles, 3D cellular structures – finally enabling the observation of molecular dynamics within the cellular context. As a consequence, these modern times are characterized by a level of collaborations among different branches of science (biology, chemistry, physics, optics, informatics) never seen before. Considerable progress is achieved whenever a close collaboration between these fields is possible. However, increasingly complex instrumentations and techniques require an adequate level of expertise in such fields from the end user as well. Therefore the implementation of a new advanced microscopy technique in a lab or department may require a substantial amount of resources, in terms of funding/money, time and effort to bring the users to the required level of expertise.

Within our work, we aim to bridge the gap between the resources needed to implement a novel, advanced microscopy technique

and the resources available to less-specialized laboratories. Light sheet fluorescence microscopy is a recent technique that enables high resolution 3D imaging of large and small samples for extended periods of time with limited phototoxic effects. However, implementation of the technique in less-specialized laboratories is hindered by its peculiar configuration, the special requirements of its sample holders and the expertise required to assembly the optical path. To address the issue, we aim to develop technology to enable single lens light sheet microscopy that would be relatively simple to implement on existing epi-fluorescent microscopes. In particular, we'll focus on the fabrication of inexpensive mass-producible microfluidic sample holders with integrated optical components that will allow on-chip light sheet illumination. In this approach only a single objective lens is needed to both provide the light sheet illumination and do the fluorescent imaging.

In the second part of the thesis, special attention will be given to another well-known, advanced microscopy method: Single Particle Tracking (SPT). In a pharmaceutical context, SPT has proven to be a precious ally in the development of safe and successful nucleic acid-based therapeutics against genetic diseases. Indeed, to be able to express their therapeutic potential, those nucleic acid-based nanomedicines need to cross several extra- and intra-cellular barriers before reaching their target. Highly sensitive light microscopy techniques, like SPT, are thus necessary for a thorough characterization of nanomedicines as as they travel through those various barriers. The most frequent application is the use of SPT to study nanoparticle mobility in cells and tissues. But SPT can also be used to measure nanoparticle size and concentration in complex biological fluids such as blood. As such SPT is an important tool for in vitro bio-

barrier studies, thus providing important information on the suitability of a particular nanoformulation for *in vivo* applications. Here, we propose to expand the biologist's toolkit by devising a new method to perform additional characterization of nucleic acid-based therapeutics using SPT. We'll exploit the technique to get a new type of information that was inaccessible before, which is the average number of nucleic acid molecules complexed within a nanocarrier, in order to improve complexation protocols and eventually to better understand the relation between nucleic acid content per nanoparticle and its final biological effect.

The **first chapter** presents a review on light sheet fluorescence microscopy, both in its traditional form and according to the latest developments. Special attention is given to how to implement a light sheet microscope in a research lab, both by pointing out the currently commercially available models, as well as by referencing to websites for do-it-yourself assembly of light sheet microscopes and finally by illustrating methodologies to implement light sheet microscopy on standard epi-fluorescent microscope's bodies that are commonly available in biology labs.

The **second chapter** will focus on the design, development and characterization of disposables sample holders to enable light sheet microscopy on epi-fluorescent microscopes. Special attention will be given to strategies that will allow a swift integration of the optical set-up on the microscope and to fabrication methods that may lead to mass-production of the sample holders.

In the **third chapter** single particle tracking SPT is reviewed, describing both fundamental aspects and its applications to gene- and drug-delivery.

Finally, one of the biggest challenge of nucleic acids delivery is the design of nanomaterials that protect their cargo and overcome

the numerous biological barriers our bodies have developed to protect us from external pathogens. A thorough characterization of the interaction between these nanomaterial and their therapeutic cargo is thus of the utmost importance for a rational optimization of the nanomaterial. As such, the **fourth chapter** will describe a SPT-based method to determine the average number of nucleic acids therapeutics complexed with nanoparticles, aimed at providing further fundamental information that will lead to rational optimization of nanocarriers. Finally, in the fifth chapter the broader context is discussed, briefly addressing the development of life-science microscopes and discussing the relevance of the work in this thesis for the field of live-cell imaging. Further improvements are finally discussed to the micromirror sample holders and the SPT-based method for characterization of nanomedicines.

ALGEMENE INLEIDING

DOEL EN STRUCTUUR VAN DE THESIS

Tijdens het begin van de 20ste eeuw werd de allereerste fluorescentie microscoop, ontwikkeld door Otto Heimstaedt en Heinrich Lehmann, gebruikt om de autofluorescentie van bacteriën, plantaardig en dierlijk materiaal te bestuderen. Niemand die toen dacht dat amper honderd jaar later de fluorescentie microscoop in elk modern biologisch laboratorium aanwezig zou zijn en zou uitgroeien tot een van de, door biologen, meest gebruikte techniek. De vooruitgang in fluorescentie microscopie gebeurde echter niet geleidelijk en vooral in de laatste twintig jaar werd een enorme vooruitgang waargenomen met nieuwe technologieën en belichtingsmethoden tot gevolg. De geavanceerde technieken die deze snelle vooruitgang met zich meebracht, waren een zegen voor de levenswetenschappen die deze gebruikten om de micro- en nano-wereld te ontdekken. Hierdoor werd het onzichtbare - chromosomen, organellen, 3D celstructuren – zichtbaar en werd het mogelijk om moleculaire dynamieken binnen een cel te bestuderen. In de laatste jaren geeft de vooruitgang dan ook aanleiding tot nooit eerder geziene samenwerkingen tussen verschillende wetenschappelijke takken (Biologie, chemie, fysica, optica en informatica). Deze nauwe samenwerkingen zorgen ervoor dat steeds meer en diepere inzichten kunnen worden bereikt door gebruik te maken van steeds complexere instrumenten en technieken. Dit heeft echter tot gevolg dat de gebruiker van deze instrumenten een steeds hogere graad aan expertise nodig heeft om deze succesvol te kunnen gebruiken en bijgevolg gaat de implementatie van een nieuwe geavanceerde microscopische techniek in een laboratorium gepaard met de noodzaak voor een substantiële

hoeveelheid middelen wat betreft geld, tijd en inspanningen om mensen op te leiden tot het benodigde niveau van expertise.

In dit onderzoek proberen we de afstand tussen de middelen noodzakelijk om een nieuwe geavanceerde microscopische techniek te implementeren en de middelen beschikbaar in een niet gespecialiseerd laboratorium te verkleinen. De recente techniek “Light sheet fluorescence microscopy” laat toe om hoge resolutie 3D beeldvorming uit te voeren op grote en kleine stalen gedurende een uitgebreide periode met slechts beperkte fototoxische effecten. De implementatie van deze techniek in niet gespecialiseerde laboratoria wordt echter gehinderd door de specifieke configuratie van het instrument, de speciale vereisten voor staalhouders en door de vereiste expertise om het optische pad op te bouwen. Om deze problemen aan te pakken, werd getracht om een technologie te ontwikkelen om “light sheet microscopy”, gebruikmakend van één lens, toe te laten, die relatief makkelijk te implementeren is op reeds bestaande epi-fluorescente microscopen. In het bijzonder werd gewerkt aan de fabricatie van goedkope, in bulk produceerbare, microfluidische staalhouder met geïntegreerde optische componenten die een on-chip light sheet belichting mogelijk maken. Op deze manier is slechts één enkele objectief lens noodzakelijk die gebruikt wordt voor de belichting van het staal alsook voor de fluorescente beeldvorming.
In het tweede deel van dit werk wordt aandacht besteedt aan een andere bekende geavanceerde microscopische techniek namelijk “Single Particle Tracking (SPT)”. In een farmaceutische context, heeft SPT zijn nut reeds bewezen in de ontwikkeling van veilige en succesvolle, op nucleïnezuur gebaseerde, therapeutica tegen genetische ziekten. Opdat deze nucleïnezuur gebaseerde nanomedicijnen hun therapeutische potentieel kunnen bereiken, dienen deze verschillende extra- en intra- cellulaire barrières te overkomen vooraleer ze hun doel bereikt hebben. Bijgevolg zijn

zeer gevoelige microscopische technieken, zoals SPT, noodzakelijk voor een goede studie van de nanomedicijnen op hun weg doorheen deze verschillende barrières. Hiervoor wordt SPT het meest toegepast om de beweeglijkheid van de nanopartikels in cellen en weefsels te bestuderen. SPT kan echter ook gebruikt worden om de grootte van en concentratie aan nanopartikels in complexe biologische vloeistoffen zoals bloed te bepalen. Bijgevolg is SPT ook een belangrijk middel voor in vitro bio-barrière studies en zorgt op deze manier voor belangrijke informatie over de geschiktheid van specifieke nanoformulaties voor in vivo gebruik.Hier zullen we trachten om de beschikbare tools voor een bioloog uit te breiden met een nieuwe methode die toelaat om additionele informatie over nucleïnezuur gebaseerde therapeutica vast te leggen door middel van SPT. Meer bepaald zullen we de techniek gebruiken om informatie, die voorheen niet beschikbaar was, over het gemiddelde aantal gecomplexeerde nucleïnezuur moleculen binnen een nanocarrier vast te leggen. Deze informatie kan op zijn beurt gebruikt worden om complexatie protocols te verbeteren en om de relatie tussen nucleïnezuur inhoud per nanopartikel en het uiteindelijke biologische effect beter te begrijpen.

In het **eerste hoofdstuk** van dit werk wordt een review gemaakt van de “Light Sheet Fluorescence microscopy” voor zowel de traditionele methoden alsook volgens de laatste ontwikkelingen. Extra aandacht wordt besteedt aan hoe een “light sheet” microscoop kan worden geïmplementeerd in een onderzoekslaboratorium. Hierbij worden zowel commercieel beschikbare modellen alsook verschillende websites waarop doe-het-zelf instructies voor het bouwen van een “light sheet” microscoop worden gegeven besproken. Als laatste worden dan verschillende methodes besproken om “light sheet” microscopie uit te voeren op standaard epi-fluorescentie microscopen die beschikbaar zijn in biologische laboratoria. Het **tweede**

hoofdstuk handelt over het ontwerp, de ontwikkeling en karakterisering van wegwerpbare staalhouders die toelaten om "light sheet" microscopie uit te voeren op epi-fluorescentie microscopen. Extra aandacht wordt gegeven aan strategieën die een snelle integratie van de microscopische set-up mogelijk maken en aan fabricage methodes die kunnen leiden tot massaproductie van de staalhouders. In het **derde hoofdstuk** wordt de techniek "Single Particle Tracking (SPT)" toegelicht en worden zowel de fundamentele aspecten alsook de toepassingen voor gen- en geneesmiddelafgifte beschreven. Tot slot is één van de grootste uitdagingen voor nucleïnezuur aflevering het ontwerp van de nanomaterialen die deze beschermen doorheen de verschillende biologische barrières die door ons lichaam ontworpen werden om ons te beschermen van externe pathogenen. Bijgevolg is een uitgebreide karakterisering van de interacties tussen deze nanomaterialen en hun therapeutische inhoud en tussen de nanomaterialen en de barrières van enorm belang in de optimalisatie van deze nanomaterialen. In het **vierde hoofdstuk** zal dan ook een op SPT gebaseerde methode beschreven worden, die gebruikt kan worden om het gemiddelde aantal therapeutsiche nucleïnezuren te bepalen die gecomplexeerd zijn met een nanocarrier. Deze informatie kan dan gebruikt worden voor een verdere optimalisatie van de nanocarrier.

Tot slot wordt in het vijfde hoofdstuk de ontwikkeling van life-science microscopen beschreven en wordt de relevantie van dit project voor beeldvorming van levende cellen besproken. Voorts worden een aantal mogelijke verbeteringen voorgesteld voor zowel de staalhouders als de SPT methode gebruikt om nanomedicijnen te karakteriseren.

CHAPTER **1**

TECHNICAL IMPLEMENTATION OF LIGHT SHEET FLUORESCENCE MICROSCOPY

This chapter is accepted for publication as:

E. Zagato[1,2], T. Brans[1,2], S. De Smedt[1], K. Remaut[1], K. Neyts[2,3], K. Braeckmans[1,2], Technical implementation of Light Sheet Microscopy. *Microscopy Research and Technique*

[1]*Laboratory of General Biochemistry and Physical Pharmacy, Ghent University, Belgium*
[2]*Center for Nano- and Biophotonics, Ghent University, Belgium*
[3]*Liquid crystals and Photonics Group, Ghent University, Belgium*

ABSTRACT Fluorescence-based microscopy is among the most successful methods in biological studies. It played a critical role in the visualization of subcellular structures and in the analysis of complex cellular processes, and it is nowadays commonly employed in genetic and drug screenings. Among the fluorescence-based microscopy techniques, light sheet fluorescence microscopy (LSFM) has shown a quite interesting set of benefits. The technique combines the speed of epi-fluorescence acquisition with the optical sectioning capability typical of confocal microscopes. Its unique configuration allows the excitation of only a thin plane of the sample, thus fast, high resolution imaging deep inside tissues is nowadays achievable. The low peak intensity with which the sample is illuminated diminishes phototoxic effects and decreases photobleaching of fluorophores, ensuring data collection for days with minimal adverse consequences on the sample. It is no surprise that LSFM applications have raised in just few years and the technique has been applied to study a wide variety of samples, from whole organism, to tissues, to cell clusters and single cells. As a consequence, in recent years numerous set-ups have been developed, each one optimized for the type of sample in use and the requirements of the question at hand. Hereby we aim to review the most advanced LSFM implementations in order to assist new LSFM users in the choice of the LSFM set-up that suits their needs best. We also focus on new commercial microscopes and "do-it-yourself" strategies; likewise we review recent designs that allow a swift integration of LSFM on existing microscopes.

INTRODUCTION

Nowadays, fluorescence microscopy has become an important tool for biologists to make sense of the biological world. The ability to conjugate fluorophores with almost any existing molecule, or even to induce cells to produce their own fluorescent proteins, has opened up tremendous possibilities to visualize subcellular structures with high resolution and superior contrast. Total internal refraction fluorescence (TIRF), epi-fluorescence, scanning confocal and spinning disk confocal microscopes are among the most common set-ups, available in almost every research facility that works with cells. Each of these microscope techniques have their assets, but also some limitations. Epi-fluorescence microscopes are well-suited for fast acquisition of dynamics processes, but suffer from low axial resolution and their inability to remove out-of-focus fluorescence. Confocal microscopes fare way better in that respect. While inherently slower, their optical sectioning capability allows for a stunning improvement of contrast and axial resolution compared to widefield epi-fluorescence illumination. However, optical sectioning is achieved by rejecting the out-of-focus light through a single pinhole or a pinhole array. As a consequence, the whole sample has to be irradiated by a high intensity excitation laser beam, leading to a sub-optimal usage of the fluorophore photon budget and increased photo-damage to the sample under observation. TIRF microscopy is gentler towards the specimen, since it stimulates fluorescence only in one plane in the sample of 100-200 nm thickness. Sadly, it's the plane just on top of the coverslip, so that no information whatsoever can be obtained from deeper regions inside the specimen. In recent times a very interesting technique, that combines several of the advantages of the aforementioned systems, has become available to the research

community. This technique is called Light Sheet Fluorescence Microscopy (LSFM), also known as single/selective plane illumination microscopy (SPIM), and enables high resolution, multidimensional (3D+t) imaging of extended 3D samples for extended periods of time with limited phototoxic effects. As explained further in this review, LSFM set-ups vary much from developer to developer due to the specific needs of the sample under observation and the scientific questions being asked. However, with few notable exceptions, they all have in common that they require an objective lens that illuminates a plane in the sample that coincides with the focal plane of the objective lens used for detection, as illustrated in Fig. 1. The sample is usually mounted into a special sample holder compatible with an orthogonal illumination and imaging configuration. Since only the plane under observation is illuminated, out-of-focus excitation is kept at a minimum and high contrast images can be

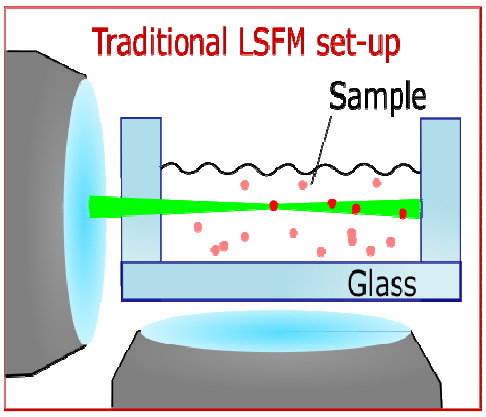

Figure 1: Traditional configuration of objective lenses and the sample in a light sheet fluorescence microscope. A thin plane in the sample is illuminated by an objective lens placed orthogonally with respect to the objective lens used for detection. Such a configuration reduces the background noise and total light exposure of the sample by only illuminating the focal plane of the imaging lens.

acquired at fast rates essentially limited by the speed of the camera. The lower light dose the sample receives, especially when recording 3D images, makes LSFM a gentler and less invasive modality to image photosensitive samples which are prone to photobleaching or phototoxicity. Moreover, thanks to its simple set-up and widefield-like detection, the technique lends itself to be combined with superresolution microscopy (STED/RESOLFT[2-5], PALM /STORM or IML[6-10], SIM[11-13]), techniques based on fluorescence fluctuation (FFS, FCS[14, 15]) as well as other advanced microscopy and spectroscopy techniques (Raman[16], Tomography[17]).

In the last decades, LSFM has been repeatedly put to the test. Although initially developed to study embryonic development[18-23], it has soon found application in the most disparate fields, from developmental biology[24] to marine biology[25]; from single cells to spheroids[26], up till whole organs like heart and vasculature[27, 28], the guts[29], the brain and nervous systems[30-34], the lymph nodes[35], pancreatic islets[36], and even the development of plants[37, 38]. However, despite its demonstrated value for a wide range of applications, a widespread diffusion of LSFM is still lacking. Indeed, while first LSFM instruments are gradually becoming commercialized, in most cases LSFM set-ups are home-built according to a variety of designs depending on the application at hand. Therefore, in this review a succinct overview is provided of the most advanced LSFM modalities with their advantages and disadvantages, aimed at guiding the interested researcher to choose the LSFM set-up that best suits a particular application. In the second part of this review, the focus will be on the commercially available LSFM microscopes and on recent designs that allow swift integration of LSFM on existing microscopes.

PRINCIPLE AND RATIONALE OF LIGHT SHEET FLUORESCENCE MICROSCOPY

The idea behind LSFM is to avoid unnecessary exposure of the sample to potentially toxic laser light by illuminating only a single, thin plane in the sample that coincides with the focal plane of the detection lens (see Fig. 1). Although seemingly harmless, fluorescence microscopy is not completely non-invasive, since prolonged exposure to laser light increase the chance of photodamage in living organisms. Photodamage is mostly due to reactive oxygen species and radicals that are a consequence of photoexcitation. Excited molecules are more reactive than when they are in their ground state and may potentially react with other molecules and produce reactive species that may damage cells. Even at low light intensity, cell homeostasis may be affected, leading to physiological changes. Thus, it is important to use a technique like LSFM that reduces photodamage while still providing useful information about the system under observation. In its traditional configuration[20, 39], an orthogonal light sheet microscope is composed of three distinct components: the excitation arm, the sample holder and the detection arm. The main role of the excitation arm is to shape the laser beam into a light sheet whose thickness essentially determines the optical sectioning capability of the technique. The detection arm determines the lateral and to a large extent the axial resolution as well as the temporal resolution, although in practice the latter is also influenced by the signal to noise ratio, which depends on the intensity of the excitation beam and labeling quality. The combination of the point spread function (PSF) of the illumination and the detection systems, shown in Fig. 2A, leads to an increased axial resolution compared to widefield microscopes. Given the peculiar configuration of LSFM microscopes, special

care must be taken to design a sample holder that places the sample at the required distance between the orthogonal objective lenses, while ensuring sample viability and keeping it stable in position. In the following section the major components of LSFM will be discussed in more detail.

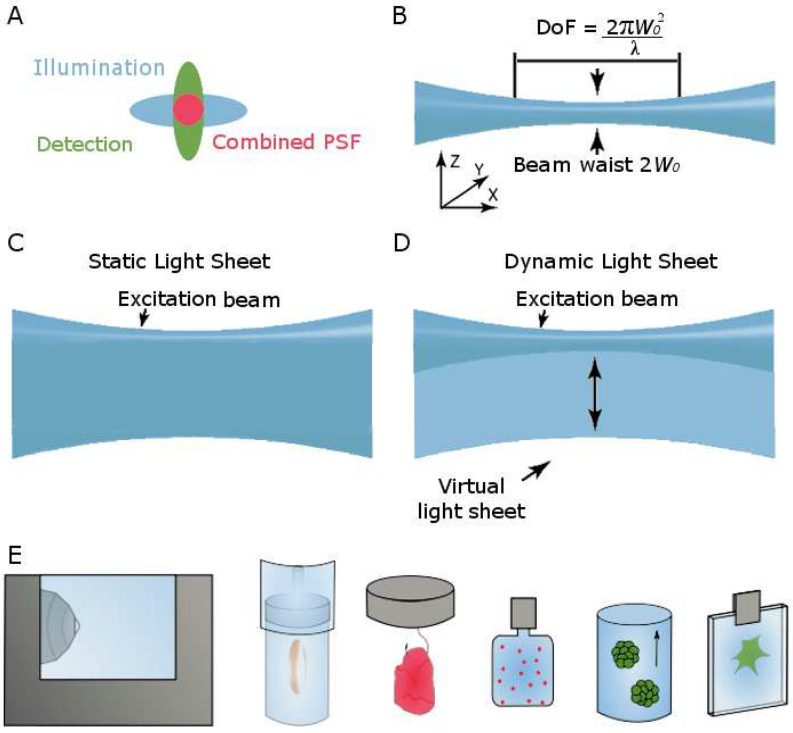

Figure 2. (A) The PSF of an LSFM system is the product of the PSF of the illumination and the detection objective lens. (B) A Gaussian beam is defined by its beam waist W_0 and its depth of field *DoF*. (C) and (D) illustrate a static and dynamic light sheet, respectively. (E) Example of a water-filled chamber (only one of two objective lenses is shown) and its sample holders that are dipped into the water bath. The samples are, respectively, embedded in agarose gel, hooked to the holder, enclosed in a transparent bag, flowing through a channel or adherently attached to a coverslip.

EXCITATION

The excitation light sheet, as shown in Fig. 2C and 2D, may be static or dynamic. A static light sheet is generated by placing a cylindrical lens in the illumination optical path. The set-up is simple and the entire illumination power is spread over the entire field of view, allowing for fast image acquisition. On the contrary, dynamic light sheets, also called digital scanned light sheet microscopy (DSLM), make use of galvanometric mirrors to scan the orthogonal plane with a spherical Gaussian beam so to create a "plane of light"[40]. Dynamic light sheets focus their entire illumination power on a single line and scan the focal plane so as to emulate a light sheet. As a consequence, dynamic light sheets are more homogenous than static ones. In addition, because the illumination is incoherent it is less affected by scatter than static light sheets. As a result, imaging artifacts due to obstacles and denser regions in the sample are reduced, improving the image quality compared to static light sheets[41].

Important characteristics of the light sheet are its beam waist W_0, and the distance over which the beam's thickness remains fairly uniform, called depth of field (*DoF*). Conventional light sheets are created with a Gaussian beam, shown in Fig. 2B, whose *DoF* is proportional to its beam waist. For example, a Gaussian beam with a 1-µm-thick beam waist has a *DoF* of nearly 13 µm at 488 nm wavelength. Gaussian beams are primarily determined by the numerical aperture *NA* of the illumination lens, so that cylindrical lenses with low *NA* are preferred to obtain a light sheet with a large *DoF* at the expense of a lower axial resolution (i.e. larger beam waist) and reduced optical sectioning.

Care must be taken when imaging large and dense samples, to avoid excessive striping artefacts. As clearly shown in Fig. 3, stripes are common in LSFM images. These are caused by all kinds

of obstacles that distort the excitation light beam upon its path through the sample, including opaque regions, scattering structures, and impurities or bubbles in the clearing liquid. Several destriping algorithms have been developed[42-46]. Most of them are designed for light sheets coming only from one side and are not suited for more complex noise patterns[46]. In any case, strategies that avoid stripes formation are to be preferred whenever it is possible. For example, Huisken et al. proved that by quickly tilting or pivoting the beam[19], stripe artifacts and aberrations are reduced and the quality of the image of thick specimens is highly improved.

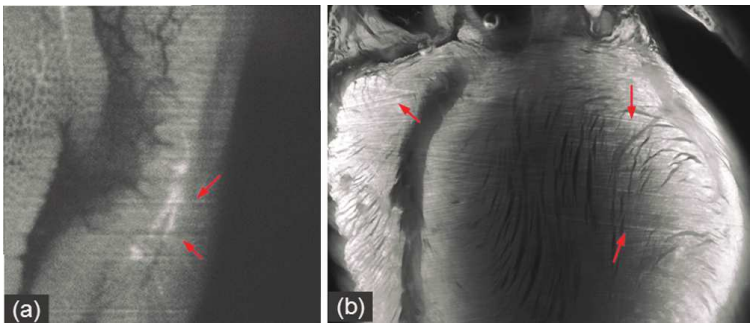

Figure 3. Stripes are a common artefact in LSFM images: (a) a slice of mouse colon imaged with a custom-made unidirectional LSFM system and (b) a slice of mouse heart imaged with a multidirectional LSFM system. The red arrows indicate some prominent stripes. Adapted with permission from Liang et al.[46].

DETECTION

On the detection side, the detection path consist of an imaging objective lens, an emission filter, tube lens and camera. The NA of the imaging objective lens must be carefully considered since it determines the lateral and axial resolution of the image, as shown in Fig. 2A. The effective available resolution in the image is also partially influenced by the spatial and temporal resolution

of the camera, i.e. its pixel density and frame rate. Typically, EMCCD cameras are chosen for their high level of sensitivity that allow faster acquisition times. However, they generally have rather large pixels and, therefore, less spatial sampling and in some cases a limited field of view; instead, modern scientific CMOS cameras are preferred for their improved signal to noise ratio (SNR) detection properties, faster readout and for their high spatial and temporal resolution. Scientific CMOS cameras also may be operated in two data acquisition modes: global shutter, i.e. all the pixels are simultaneously active, and rolling shutter, i.e. only a few adjacent lines are active[47]. As discussed in the section "*the detection pathway"* of this chapter, a clever use of the rolling shutter mode may be beneficial to enhance contrast and increase the image quality.

SAMPLE HOLDER

A LSF microscope is the instrument of choice for long term 3D imaging of live and fixed systems. Although originally implemented in developmental biology, nowadays LSFM applications range from single molecule studies to three dimensional cultures, from fixed and cleared samples to *in vivo* studies. Such a wide range of applications, combined with LSFM unique configuration which makes its implementation on common microscopes challenging, has given rise to a range of atypical, tailor-made sample holders. Well-designed sample holders should fulfill three main requirements[48]. First of all, mechanical stability during imaging is a key feature. The specimen must be well supported to avoid deformation during rotation or sample movements. Second, it is of the utmost importance to employ sample holders that cause minimal light distortion. For example, the materials employed should have a

refractive index as close as possible to the refractive index of the medium in which the sample is embedded. Third, the viability of the specimen is extremely important for long acquisition experiments. Thus the specimen should be well supported and still be able to grow, while at the same time receive the necessary nutrients. Fig. 2E shows the most typical sample holders[48-50]. The most common sample holders position the objective lenses inside a water filled chamber. The sample, typically embryos or cell clusters, is embedded inside a soft gel, usually low-melting agarose or specialized hydrogels, and it is extruded from a capillary inside the chamber. However, care must be taken to monitor the development of the sample, since mechanical forces exerted by the gel are known to be responsible of malformation[51]. Large samples as well as tissues may instead be kept in position by a sterilized hook. Liquid samples like beads in a solvent are best mounted in a transparent, heat sealed plastic bag made from fluorinated poly-ethylene-propylene films[50]. Small cell clusters and spheroids may be pumped through a channel and imaged while they are flowing through the light sheet[52, 53]. Lastly, adherent cells are plated onto small cover glass pieces and positioned in the sample chamber at an angle between the coverslip and the illumination objective lens. It is advisable to not choose an angle of 45° between the coverslip and the illumination objective, since at that angle excitation light reflected by the water/glass interface will reach the camera as well and degrade contrast.

RECENT TECHNOLOGICAL DEVELOPMENTS

A LSFM is the ideal technique to follow fast, dynamic processes that happen in a 3D biological environment. To obtain robust, reliable data, it is crucial that LSFM provides a high

spatiotemporal resolution, ultralow photobleaching rates and an excellent signal to noise ratio SNR. However, imaging large, living specimens using a basic set-up remains challenging. The light sheet has to travel into an inhomogeneous environment with highly absorptive and scattering properties. Not only stripe artifacts due to small regions of higher refraction index are inevitable, but also the SNR can be substantially reduced by out-of-focus fluorescence excited by excitation light scattered in the sample. As a consequence, as the optical path length increases the image quality decreases. In this section we present recent developments to overcome these issues. The most straightforward solution is to collect images of the sample from multiple angles, by simply rotating the sample or by employing multiple objective lenses, and then fuse the collected images together to form a 3D rendering of the sample. Another viable option would be to use a non-diffracting, propagation invariant beam instead of the more typical Gaussian excitation beams. Thanks to their self-healing properties, they can propagate intact deep into scattering samples and increase temporal and spatial resolution. Two photon excitation is also a viable strategy, since it generates a thinner light sheet, avoids unwanted background excitation and reduces photobleaching. Lastly, a thoughtful modification of the detection pathway may increase contrast and acquisition speed.

MULTIVIEW SPIM

Imaging large, living specimens is a tough job due to the highly absorptive and scattering environment in which light has to travel. As Fig. 4A clearly shows, one-sided illumination results in decreasing image quality along the excitation axis due to the deteriorating effect of scattering of the excitation light sheet that

results in out-of-focus fluorescence. These problems may be reduced by so-called multiview sample reconstruction. The idea is to collect multiple image stacks at different angles. If necessary, the image stacks are deconvolved and then fused together to reconstruct a 3D image of the sample. Thanks to multiview reconstruction, the uniformity of the image quality is improved in strongly scattering and absorbing samples, while in transparent samples the axial resolution is strongly enhanced, to the point that the resolution becomes isotropic. Fig. 4 shows the most common configurations that allow multiview reconstruction. In the first SPIM set-up, proposed by Huisken et al.[20], the light sheet is generated inside a buffer-filled chamber. The sample is immersed into the buffer from the top. It can thus be rotated to allow the collection of image stacks from multiple angles on the same sample. Such a system has been used successfully to image fixed *Medaka* and live *Drosophila melanogaster* embryos[20, 54]. However, multiview reconstruction through sample rotation presents several disadvantages[55].

First, due to the difficulties in the precise determination of the axis of rotation relative to the specimen, the images are inherently misaligned. The use of computationally intensive and unreliable image registration algorithms may be necessary to align the images. Second, sample rotation is sometimes slower than the biological dynamics under observation. Lastly, the quality of the image increase with the number of viewing directions. As a consequence, not only the time resolution decreases, but also the sample is exposed to a higher dose of light than in a basic light sheet microscope, increasing photobleaching and phototoxic effects.

The need to collect high SNR images of opaque specimens while retaining its high temporal resolution and low phototoxicity has

led to the development of dual excitation LSFM set-ups. The simpler solution is to add a third objective lens so that the sample can be illuminated from two sides[40], as it was done in mSPIM [19], shown in Fig. 4C. In mSPIM the light sheet is sequentially directed onto the sample from two opposing directions. For faster image acquisition, a fourth lens, used for detection, may be beneficial.

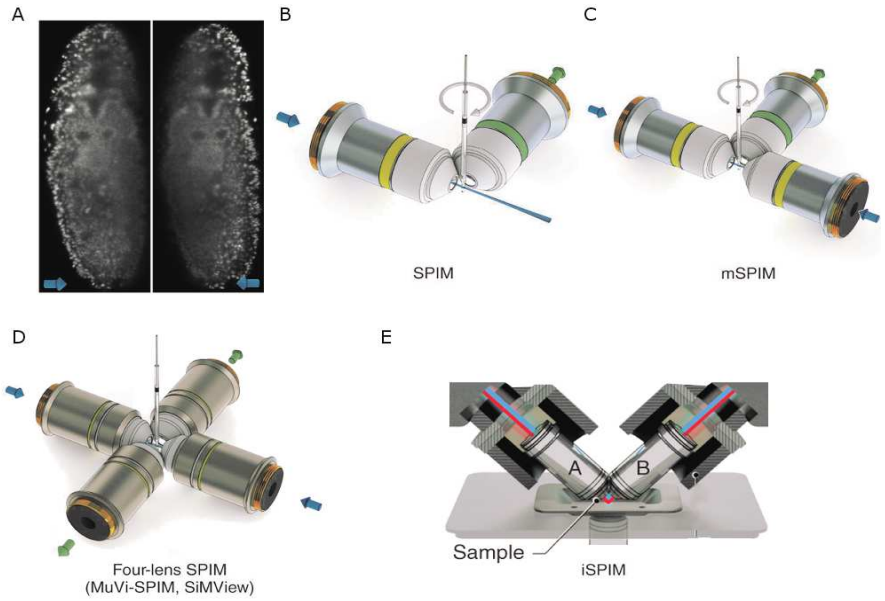

Figure 4. (A) An image of a Drosophila embryo illuminated from the left and from the right. The degradation of the image quality along the illumination direction is evident. Adapted with permission from de Medeiros, et al. [56], licensed under Creative Commons CC-BY 4.0 license (B) A basic SPIM set-up. The sample is rotated to collect multiview images of the specimen, that will be later reconstructed into a 3D figure. (C) In mSPIM two objective lenses provide illumination to the specimen from opposing sides to enhance illumination uniformity. (D) MuVi-SPIM and SiMView systems consist of two lenses used for illumination and two lenses used for detection. (E) Dual inverted SPIM. To achieve isotropic resolution, both lenses are identical and are used alternatively to illuminate and image the sample. Image B,C,D are reprinted by permission from Macmillan Publishers Ltd: NATURE METHODS, from Weber and Huisken [57], copyright 2012.

This set-up is shown in Fig. 4D and is called MuVi-SPIM[55]. The system consists of four objective lenses, two for illumination and two for detection, placed into a fixed geometrical arrangement for multiview data fusion in real time. Both detection objective lenses are focused onto a common focal plane, illuminated alternately by the two dynamic light sheets. Both detection arms are used simultaneously to increase light efficiency. The illumination arms work in an alternated fashion to avoid image blur due to increased scattering coming from two light sheets at the same time. The specimen is positioned in the sample chamber that is moved through the light sheet by a fast piezo stage. While there is no need to rotate the sample, to better resolve small structures, it is recommended to rotate the sample over 90° at least once. Similar to MuVi-SPIM is SiMView[58, 59], a four-armed light sheet microscope which features single photon and multiphoton excitation. Their automated software modules ensure perfect alignment of the light sheets and the detection optics, to increase spatiotemporal resolution. Both mSPIM, MuVi SPIM and SiMView have been used to successfully image, faster than in conventional SPIM, *Drosophila Melanogaster* embryos[55, 56, 58] and live *Zebrafish*[19, 59]. Last but not least, Wu et al. developed a new LSFM with high isotropic spatial resolution in all dimensions[60]. The set-up is built on a dual inverted SPIM (iSPIM) microscope, shown in Fig. 4E. Two objective lenses are placed orthogonally to each other and are both used alternately for illumination and detection. The combination of the two perpendicular views with their self-developed “joint deconvolution method” resulted in an impressive isotropic resolution of 330 nm (NA 0.8), quadrupling the axial resolution as well as improving upon the lateral resolution. The technique retains the LSFM advantages

previously described in this section, but has a faster acquisition speed and presents isotropic resolution.

ENGINEERED LIGHT SHEETS

A key property of LSFM is its excellent optical sectioning ability. Indeed the light sheet thickness, in combination with the NA of the detection lens, determines the axial resolution in the image and its contrast. For conventional light sheets created with Gaussian beams, beam thickness and depth of field are proportional to each other, as previously described. Hence a Gaussian light sheet uniform for several tens of micrometers requires a relatively thick beam waist, which in some application would compromise the axial resolution, expose the sample to unnecessary light irradiation and preclude the application of the technique to sub-cellular studies. Moreover, beams traveling for hundreds of micrometers inside an inhomogeneous environment, such as biological tissues, are usually deformed by obstacles in the light path, with consequences on the image quality. As a consequence, a Gaussian beam is not necessarily the best choice for intracellular studies that require high contrast and high axial resolution over an extended field of view (*FoV*) spanning tens of microns. The ideal light sheet for that kind of application should preferably be consistently thin over the entire specimen. In addition it would be beneficial if the beam has the ability to reform after being partially obstructed (that is, it has "self-

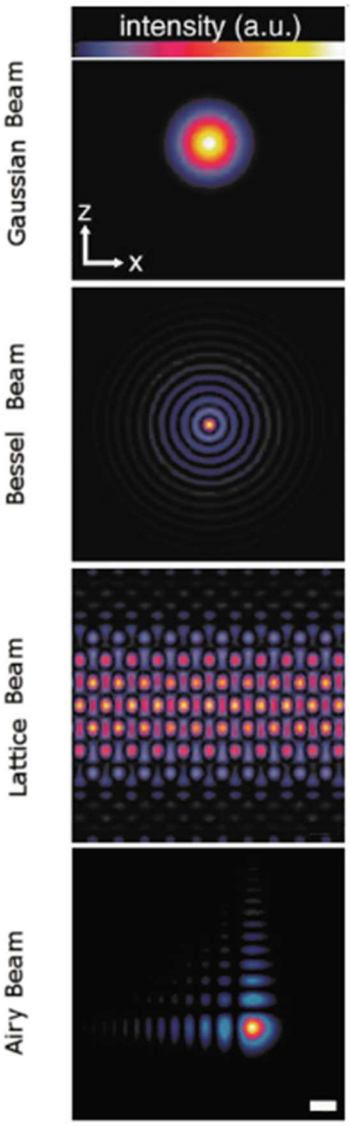

Figure 5. Different beam shapes that have been used to create dynamic light sheets for LSFM. The beam propagates along y. Scale bar 1 µm. Modified from Chen et al. Reprinted with permission from AAAS.

healing" properties) to overcome aberrations induced by imaging deep into tissues. As such it is of interest to look into non-diffracting, propagation-invariant beams. Various reports have emerged over the past few years evaluating Bessel beams[4, 12, 61-67] and Airy beams[68] for LSFM, shown in Fig. 5. Bessel beams are the most used as they are fairly easy to implement. Bessel beams are generated by focusing a Gaussian beam on an axicon lens[64], by using a spatial light modulator[61, 69] or by projecting an annular illumination pattern at the rear pupil of the excitation objective lens[13].

Although Bessel beams have the ability to produce light sheets with a *FoV* 3-5 times longer than a Gaussian *FoV* [13], they suffer from a suboptimal SNR due to the presence of quite pronounced side lobes in the diffraction pattern. While the majority of the beam energy is concentrated in the central peak, a substantial amount of energy still resides in the transversal outer ring structure of Bessel beams. In single photon excitation this means that

substantial fluorescence is coming from above and below the central light sheet.

Thus, when using Bessel beams in LSFM, strategies to remove or suppress side-lobes fluorescent emission are required. The most common strategies make use of confocal scanning detection[62], structured illumination (SI)[11-13, 69] or two-photon excitation 2PE[13, 70-72]. Briefly, in confocal scanning detection mode the image is acquired line-wise.

A single pixel-line records a one-dimensional image at the position of the beam, so that only the part illuminated by the Bessel beam central lobe is recorded. As a consequence, the probability of recording photons emitted in the region illuminated by the side lobes is decreased, providing enhanced contrast and higher axial resolution. High contrast images are thus directly recorded by the camera with no need of image post-processing, as it is the case when using SI. In that case a resolvable multi-harmonic excitation pattern is generated. N such images are then acquired, with the pattern phase in each image shifted by $2\pi/N$. The combined final image detain the strongly modulated signal near the focal plane, while the weak contributions from the out of focus regions are discarded. Both the confocal detection and the SI approaches increase the axial resolution and SNR but at the expense of substantial fluorescent signal rejection (up to 90%)[68] and temporal resolution. The excessive sample irradiation still excites out-of-focus fluorophores, thus spoiling the overall photon budget unnecessarily. Instead, 2PE excitation with Bessel beams offers the possibility to suppress side lobes and effectively provides a thin sheet with no need for out-of-focus light rejection. The disadvantage, however, is that the set-up is more complex. Moreover to image spectrally different fluorophores at the same time it may be necessary to build a second illumination arm to

avoid losing time retuning and realigning the set-up every time a different wavelength is used[13].

The best Bessel-based set-up in terms of spatiotemporal resolution and reduced phototoxicity has been developed by Chen et al.[69]. They used non-diffracting Bessel beams to create a 2D optical lattice which propagates in the sample while keeping its cross-sectional profile unchanged, as seen in Fig. 5. To create the lattice, the laser light is diffracted by a spatial light modulator conjugated with the sample plane, filtered by an annular mask and then focused on the sample by the objective lens. The microscope can be used as a traditional dithered, digitally scanned light sheet microscope or in combination with structured illumination, depending if temporal or axial resolution has priority. Indeed, imaging in dithered mode is 7.5 times faster than in combination with SI, at a comparable SNR, while the axial resolution is only 1.5 times poorer. Although a bigger region of the sample is illuminated compared to traditional Bessel beams, the peak intensity is lower. The lower peak intensity seems linked to the lower phototoxic effects noticed by Chen et al., which managed to collect 1 and 2 order of magnitude more images before noticing phototoxic effects compared to Bessel beams and confocal microscopy, respectively. Reportedly, a major advantage is the acquisition speed, that ranges between 200 to 1000 planes/s in dithered mode, which is one order of magnitude more than with classic Bessel beams. The technique is undoubtedly very effective, but the set-up is quite complex and the use of a SLM reduces the temporal resolution when multicolor imaging is required since the SLM must be rapidly switched and synchronized with every color change[66]. The solution proposed by Zhao et al.[66] is to use a combination of "non-electronic" optical components to create ultrathin Bessel sheets of the same

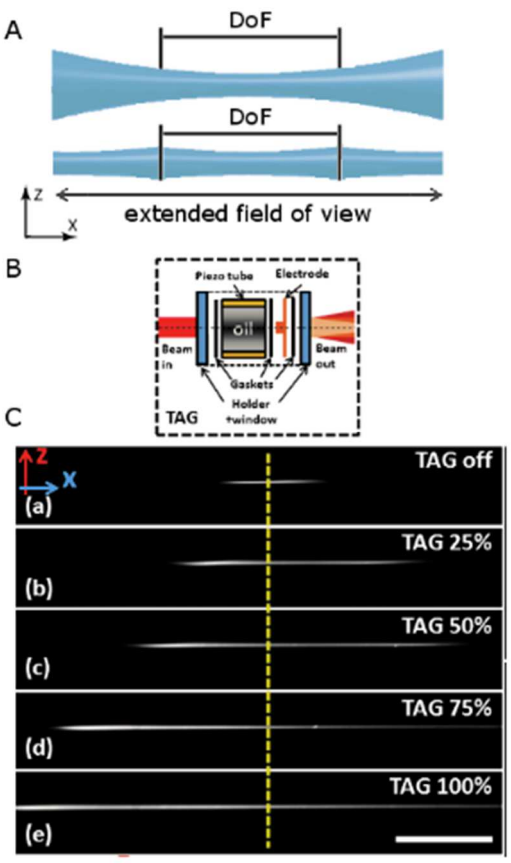

Figure 6. (A) Working principle of tiling. A tiled light sheet can be obtained by considering only the signal that comes from the thinner region of the Gaussian beam. By moving its focus an image with extended field of view is obtained. (B) Scheme of a tunable acoustic gradient index device (TAG), used to scan the focal spot along the illumination axis of the beam. (C) Using the TAG index device, the DoF of the light sheet (a)-(e) can be tailored between 50 µm to 500 µm with constant FWHM of 3 µm. Scale bar: 100 µm. Adapted with permission from Zong at al.[1].

thickness regardless of the input laser light, as long as it is in the visible range. The excitation light passes first through a slit to give it a line-shape, then through an annulus imaged to the back focal plane of the illumination objective. Two combinations of line-thickness and annulus are designed and tested, one optimized to maximize detection efficiency and minimize photobleaching, the other optimized for high resolution.

Another type of self-healing, propagation invariant beam is the Airy beam, shown in Fig. 5. Despite its broad transversal structure, the Airy beam provides high contrast thanks to its asymmetric excitation pattern[68]. A simple deconvolution is able to account for both its broad

main lobe and its curved profile, yielding high contrast and resolution for its entire *FoV*, that is 10 times and 4 times longer than with Gaussian and Bessel beams respectively. Airy beams are usually generated using a SLM, but an approximated Airy beam can also be generated by correctly tilting cylindrical lenses[73].

Despite these many improvements, the quest for ever bigger *FoV* with maximal optical sectioning goes on.

Recently Gao et al.[74, 75] proposed a new technique that gives the possibility to choose the best light sheet required for the experiment while extending its *FoV*. The principle is fairly simple, as shown in Fig. 6.

Instead of generating a large and uniform light sheet, their microscope generates a thinner and shorter light sheet that is moved in multiple positions within the image plane. Only the signal from the center of the light sheet is recorded for every position and large *FoV* image is finally obtained by stitching all those images together.

The microscope is made to be quite versatile: the light sheet is generated by two SLM, one used for the amplitude of the signal, the other to modulate the phase of the beam, that can thus quickly be defocused to move it within the image plane. As a consequence, the microscope can adapt more easily to the type of sample and to the light sheet thickness and *FoV* required since every small change can be implemented in one millisecond. The imaging speed is certainly reduced compared to other LSFM techniques like lattice light sheet or airy beam-based microscopy, but with a smart use of modern days CMOS cameras the "temporal loss" may be quite acceptable for many applications.

A similar approach has been chosen by Zong et al.[1, 76] when they developed their two-photon three-axis digitally scanned light sheet microscope (2P3A-DSLM). They use a tunable acoustic

gradient (TAG) index device, shown in Fig. 6B, to quickly scan the focal spot along the illumination axis and two galvanometric mirrors to scan the focal spot on the focal plane of the detection lens and perpendicularly to that plane. The process is so fast that the temporal resolution is only limited by the detection camera and it can provide sheets with submicrometer thickness and a *FoV* ranging anywhere in between 10x10 μm² and 170x170 μm².

Table 1 presents a summary of light sheet properties discussed in this section.

TABLE 1. LIGHT SHEET CHARACTERISTICS

TYPE BEAM	λ_{ILL}	$NA_{ILL\ LENS}$	LS THICKNESS	FOV	REFERENCE
Gaussian (cyl)	488 nm 543 nm 633 nm	0.16	2-4 μm	N.A.	Pampaloni et al. [41]
Gaussian (DLSM)	488 nm 532 nm	0.42	~2 μm	16 μm	Vettenburg et al. [68]
Bessel	488 nm 532 nm	0.42	~2 μm	42 μm	Vettenburg et al.[68]
Ultrathin Bessel	488 nm 560 nm	0.7	0.6 μm	15 μm	Zhao et al. [66]
Lattice	560 nm	0.55	N.A.	100 μm	Chen et al. [69]
Airy	488 nm 532 nm	0.42	~0.9 μm	346 μm	Vettenburg et al.[68]
2PE Bessel	Near-Infrared	0.5	0.5 μm	60-80 μm	Planchon et al. [13]
(Tiling) Bessel	488 nm 560 nm	0.8	~1.2 μm	200 μm	Fu et al. [74]
2PE 3A-DLSM	680 nm 1080 nm	0.3	~3 μm	Variable (170 μm)	Zong et al. [1]

N.A. = not available

DEEP INTO TISSUES: 2PE MICROSCOPY

Apart from particular beam profiles, 2PE LSFM has particular benefits for imaging deep inside thick tissues and organisms. To achieve 2PE excitation, an infrared laser beam is focused on the sample. Only fluorophores in the regions where there is a high photon density and photon flux are able to absorb two photon at the same time and reach an excited state. As a consequence, the beam results thinner compared to single photon excitation. NIR light interacts less with biological tissues compared to visible light. Therefore, the 2PE light sheet can penetrate at least two times deeper in biological tissues compared to traditional 1PE light sheets, suffers less from scattering effects and better preserves its shape deep inside scattering tissues[77]. Also, NIR light doesn't excite autofluorescence as much as visible light does. On the other side of the coin, a 2PE setup is more complex than a 1PE setup and requires a powerful and costly femtosecond-pulsed laser. As an example, an excitation power of hundreds of mW is necessary to obtain the same signal with 2PE Bessel beams as registered with 1 mW of a 1PE Gaussian beam[72]. At such powers, supra-quadratic absorption processes may induce photodamage of fluorophores and tissues[78].

The advantages of combining 2PE and LSFM may depend on the type of beam shape. A 2PE Gaussian beam which penetrates deep into the sample (>90 μm)[77] has indubitably a better image quality thanks to the higher contrast and the reduced background noise, but it also presents a strongly reduced *FoV* [72]. Reportedly, it is well-suited for imaging inside scattering samples with high resolution and high fluorescent yield[72]. As stated in the previous paragraph, Bessel beams likely benefit the most from 2PE. A recent comparative study shows that 2PE Bessel beams outperform Gaussian beams and 1PE Bessel beams in terms of

contrast, resolution and penetration depth. They also offer a large uniform illumination areas at the expense of a somewhat poorer SNR[67]. 2PE Bessel beam LSFM seem to be the perfect combination for following mildly fast dynamics deep (>150 μm) inside scattering samples for days, since it combines the contrast-enhancing properties of 2PE, the self-healing properties of Bessel beams and the ability of LFSM of reducing light-induced toxicity effects.

2PE LSFM has been successfully employed to image not only embryos and their organs[1, 72, 76, 77, 79, 80] but also subcellular structures and mechanism inside embryos (like pancreatic islets[1], time lapse dynamics of mitochondria[76]) and deep inside highly scattering environments like mouse brain slices[81] and tumor cell clusters[71]. As said, 2PE multicolor imaging is tricky and may potentially lead to cumulative photodamage. Mahou et al.[80] use wavelength mixing to achieve fast multicolor 2PE LSFM. To achieve wavelength mixing, they spatially and temporally overlapped two different pulse trains (800-nm range and 1100-nm range) for the excitation of blue and red fluorophores, respectively. Their spatiotemporal overlap allows the excitation of a third, green fluorophore. Thus they could image in multicolor the beating heart of a zebrafish embryo labeled with CFP, GFP and DsRed (pericardial, myocardial and red blood cells, respectively). Unfortunately, photobleaching of the red fluorophore is enhanced by the light required for excitation of the blue fluorophore (800-nm).

THE DETECTION PATHWAY

In a traditional LSFM setup, the fluorescence detection unit does not differ from the detection unit of a conventional epi-fluorescence microscope. Some recent developments however

have shown that a thoughtful modification of the detection path can enhance LSFM performance in terms of contrast, acquisition speed and spectral resolution. As an example, confocal detection is a useful tool to be added to any digitally scanned light sheet microscope which can be achieved with both an EMCCD [30, 62] or a CMOS camera[47]. Silvestri et al.[30] managed to increase the image contrast obtained using an EMCCD camera in real time with no need of an additional post processing algorithm. A detection de-scanning system is coupled with the digitally scanned light sheet to image the excitation scanning line as a static line in a secondary plane. In this plane a confocal slit is placed, after which a third scanning systems reconstructs the scanned image on the EMCCD camera. On the other hand Baumgart and Kubitscheck [47] chose to exploit the ability of CMOS cameras to address and read out each pixel independently from each other. Thus the camera itself can be used as a slit detector to enhance contrast and the degree of confocality by simultaneously activating only a portion of consecutive pixel lines. A band of consecutive active pixel rows moves across the sensor in sync with the scanning of the illumination beam. The system doesn't require any additional optical or mechanical components, nor any post processing algorithm. Such a simple and clever concept has been revived by Dean et al. in their axially swept light sheet microscope (ASLM)[82] and their diagonally axially swept light sheet microscope (DiASLM)[83]. In their setup instead of a dynamically scanned light sheet they use a cylindrical lens to create a static light sheet. The microscope scans the light sheet in its direction of propagation synchronously with an array of active pixels on the camera. By activating only the pixels that record the in-focus region of the beam, out-of-focus contributions are discarded over an arbitrarily large *FoV*. Each plane is acquired in a single exposure with no

need of deconvolution. Thanks to this method, the relationship between *FoV*, W_0 and axial resolution are decoupled, ensuring high illumination uniformity. Thus high contrast, high resolution images can be acquired over a large *FoV*.

Recording 3D images with LSFM requires the simultaneous movement in *z* of the excitation light sheet and imaging objective lens. To avoid having to move the bulky objective lens up and down, which limits the temporal resolution, recently it was suggested to extend the *DoF* of the detection lens. In that way the excitation light sheet would remain in focus of the objective lens regardless of the light sheet's z-position. It is possible to extend the *DoF* of the detection optics by making use of wavefront coding[79] or by introducing spherical aberrations[84]. The last method is shown in Fig. 7.

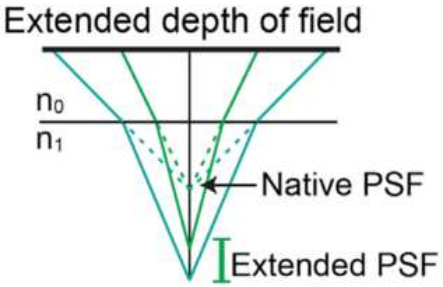

Figure 7. A simple method to extend the depth of field of the detection lens makes use of spherical aberrations cleverly introduced by stratified refractive indexes in front of the detection lens. Reprinted and adapted from Tomer et al. [84], Copyright 2015, with permission from Elsevier.

The only requirement to use wave front coding is to place a suitable phase mask at the exit pupil of the objective lens. All the objects of the sample over the extended DoF are projected to the image plane, thus an appropriate deconvolution is required to reconstruct the final 2D image. A more versatile method to extend the DoF is achieved by placing a block of higher refractive index between the detection lens and the sample. The block introduces

uniform spherical aberrations that induce PSF elongation. The microscope is thus able to scan thousands of volumes per second at 1 mm depth while preserving lateral resolution. Both the "wavefront coding" and the "spherical aberration" approaches are perfectly compatible with Airy beam, lattice and Bessel beams, as well as 2PE and multidirectional LSFM. However, they do suffer from low spectral resolution, as many other microscopy techniques do. Hyperspectral approaches have been recently developed to study the interaction of many components in complex biosystems and have been recently applied to LSFM[85]. The scheme of hyperspectral LSM is presented in Fig. 8 and, as it can be seen, it is applicable only to digitally scanned LSFM. Thanks to a de-scanning mirror and a diffractive unit, for every plane the camera chip records a data cube made of a stack of x, λ data sets. Multi-colors images are then easily obtained by selecting arbitrary, flexible virtual filters. Autofluorescence is thus readily removed or exploited to highlight the structure of the sample. This technique outperforms filter based approaches, not only because of contrast-enhanced detection, but also for its flexibility and its ability to resolve overlapping fluorophores. It's fast since it acquires all the color at once and maintains spatial resolution at a minimal light dose. Such a technique would be beneficial to study the interactions of dozens of components in a sample or to monitor environmental conditions, such as changes

in the pH, as long as fluorophores or dyes sensitive to the environmental change are employed.

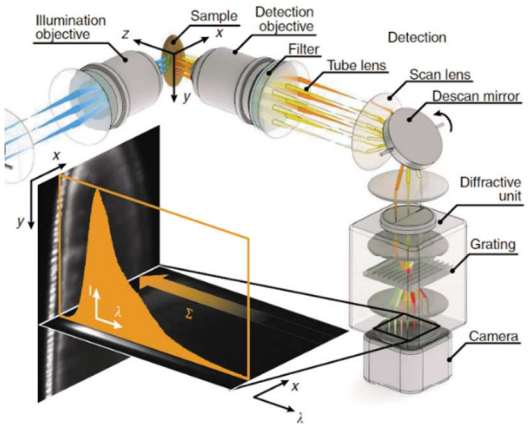

Figure 8. Schematic representation of an hyperspectral LSFM set-up. The light sheet is created by quickly scanning the illumination beam [85] with a scanning mirror. The sample is placed at the intersection of the focal planes of the detection and illumination objective lenses and illuminated with the scanned light sheet. The fluorescence signal is descanned onto a single line with a second scan mirror. A diffractive unit separates the spectral components of the incoming light spatially. On the camera chip, a stack of x, λ-data sets is recorded, resulting in a three-dimensional data cube. Summing over all wavelengths would yield the conventional, single-color image. Obtained by Jahr et al[85] licensed under Creative Commons CC-BY 4.0 license.

WIDESPREAD DIFFUSION OF LSFM

While LSFM is undoubtedly a very valuable addition to the biologist's microscopy toolbox, the advanced configurations discussed above are far from trivial to build and require extensive optics and engineering skills. In order to be truly successful, LSFM should gradually move from the specialized optics laboratory towards user-friendly devices that are available to the broader biological community. Efforts in this direction are ongoing, with construction manuals being made available on the one hand, and first generations of commercial instruments coming to the market on the other hand. In addition, in recent reports concepts are being put forward to implement LSFM on standard microscope bodies.

COMMERCIALLY AVAILABLE MICROSCOPES

In recent years, the LSFM business has expanded enormously. As of January 2015, two such microscopes came to the market. Two years later, already six companies are selling 8 different types of LSFMs, shown in Fig. 9. The first commercialized system is the Lightsheet Z.1, produced by Zeiss. It is based on the set-up introduced by Huisken and Stelzer[20] and it is mainly designed for multiview imaging of large, living specimens, although imaging of cleared specimens is also possible. It is well suited for research in developmental biology and to follow cell dynamics in small model organisms or tissues. The sample, placed vertically into the chamber from above, is illuminated from two sides by a light sheet. The light sheet is rotated to allow fast image recordings from multiple angles, as it is beneficial to increase resolution and information content. The MuVi-SPIM microscope marketed by Luxendo is a valid alternative. Based on the set-up developed by Krzic et al.[55], MuVi-SPIM provides four orthogonal views of the

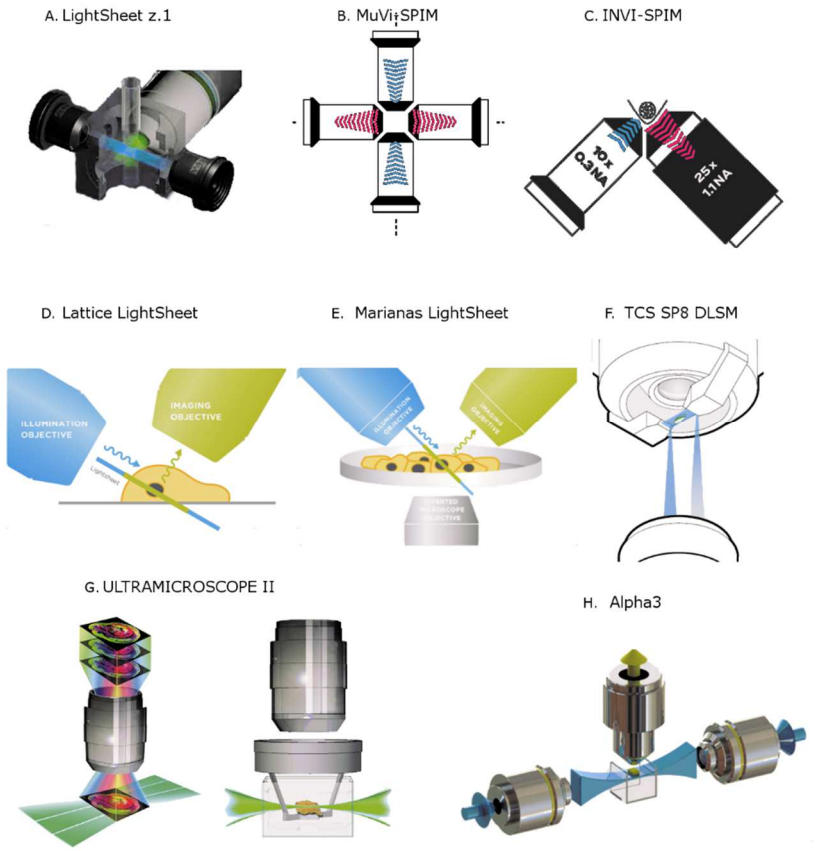

Figure 9. Several commercially available LSFM configurations. A) A detailed view of the sample chamber of the LightSheet z.1 microscope (Zeiss). The sample is placed in the chamber from above and it is illuminated from two opposing sides with light sheet illumination.

Source: *https://www.zeiss.com/microscopy/us/products/imaging-systems/lightsheet-z-1.html* B) Top view of the configuration of objective lenses in a MuVi-SPIM microscope (Luxendo). Illumination is indicated with blue lines, detection with purple lines. Source: *http://luxendo.eu/* C) Side view of the configuration of objective lenses in an InVi-SPIM (Luxendo). Source: *http://luxendo.eu/invi-spim* D) Side view of the objective lenses in the Lattice Lightsheet microscope (3i). The sample is mounted on a round coverslip, placed in water and illuminated by a 0.4 µm thin lattice light sheet. Source: *https://www.intelligent-imaging.com/* E) Marianas Lightsheet (3i)

places a dual inverted SPIM set-up on an inverted live-cell microscope system to allow the combination of multiple imaging modalities. Source: *https://www.intelligent-imaging.com/* F) Close view of the TwinFlect mirror device used in the TCS SP8 Digital Light Sheet microscope (Leica). The laser light is reflected horizontally by two opposing mirrors and imaging is performed through the microscope's objective lens. This configuration allows the implementation of other imaging modalities and techniques. Source: *http://www.leica-microsystems.com/products/confocal-microscopes/details/product/leica-tcs-sp8-dls/* G) Schematic representation of an Ultramicroscope II (LaVisioBioTech). The sample is illuminated from two sides by 6 light sheets whose focus can be rapidly shifted through the sample. Source: *http://www.lavisionbiotec.com/ultramicroscope-ii-technology.html* H) The Alpha[3] microscope (Phaseview) is composed of modular parts that can be separately added to existing microscopes. Source: *http://www.alphalightsheet.com/*

sample with no need for rotation, increasing acquisition speed, long-term stability of the sample and data fusion precision. While MuVi-SPIM is optimized for speed, the InVi-SPIM is more adapted to long-term 3D fluorescent imaging of living specimens. InVi-SPIM is an inverted SPIM microscope with easy access to the sample chamber, that can be customized and autoclaved. It is typically applied on small animal models and mammalian cell culture for 3D reconstruction and tracking of cellular and sub-cellular positions. For large, cleared, fluorescently labeled tissue samples the Ultramicroscope II from LaVisionBioTech, based on the design of Dodt et al.[86], is a viable alternative. Their software is designed to compensate and correct for different refractive indices induced by the clearing reagents. This bidirectional LSFM generates 6 light sheets, 3 per side from different angles, and shift their focus through the sample while imaging. As a result, image acquisition is very fast (100 fps at full frame) and stripes and artifacts are reduced. The light sheet width, thickness and *FoV* are user-defined and can cover large areas of the sample, for a high

degree of flexibility. The Ultramicroscope II has been successfully used for neurobiology applications and to study neovascularization and lymph nodes, as well as developmental steps in animal models, but at cellular resolution since the minimum light sheet thickness is 4 μm, as declared in the online specifications. At present, the only commercially available microscope that provides an uniform light sheet with sub-micrometer thickness is the Lattice LightSheet microscope from 3i (Intelligent Imaging Innovations), based on the set-up of Chen et al.[69].

The creation of a lattice Bessel beam generates a 0.4 μm thin light sheet that extends for 50 μm. The use of a high speed CMOS camera allows collection of images at a 100-500 fps. Samples are simply mounted on a 5 mm round coverslip. It is thus possible to observe with high spatial and temporal resolution cell substructures, cell-cell interaction, single molecule diffusion into spheroids, as well as cell motility in a 3D matrix and embryogenesis.

LSFM can be combined with other microscopy modalities as well. Marianas LightSheet, developed by 3i (Intelligent Imaging Innovations), is one of such developed microscopes. It combines a dual inverted SPIM set-up (see Fig. 4E) with the flexibility of an inverted live-cell microscope system. Spinning disk confocal microscopy and TIRF can be added, as well as the lasers and hardware needed for fluorescence life-time imaging microscopy FLIM or for photomanipulation. The diSPIM set up provides high speed imaging (up to 600 fps) at isotropic resolution. It supports conventional sample holders such as coverslips and petri dishes as well as custom-designed chambers, thus it is adapted to image specimens of various sizes, ranging from single cells to whole organisms. Another example of a LSFM designed to be compatible

with other microscopy modalities is the TCS SP8 Digital Light Sheet microscope from Leica. Thanks to the addition of the TwinFlect mirror device, they turned their confocal platform into a Reflected Digital Light Sheet microscope. In a reflected light sheet microscope a 45° (micro)mirror is placed close to the sample and it is used to reflect the light sheet perpendicular to the detection lens. In the approach chosen by Leica, they make use of two opposing 45° mirrors that are attached to the condenser lens of the diascopic illumination arm. By reflecting and rapidly scanning the laser light coming from the diascopic arm, a light sheet is formed in the sample and imaging is performed through the microscope's objective lens. The same microscope can be combined with stimulated emission depletion STED and coherent anti-stokes raman spectroscopy CARS microscopy, but it is also suitable for FLIM measurements and photoactivated localization microscopy PALM. The sample is mounted in a standard glass bottom dish and embedded in agarose gel. It is mostly used to observe embryogenesis and developmental processes of embryos at a maximum speed of 60 fps, but it is not readily suited for imaging adherent cell cultures. Finally, the Alpha^3 microscope from PhaseView is a modular light sheet microscope designed to be added to existing microscopes. The scanning speed is only limited by the camera rate, thus it can reach 100 fps at full frame with their CMOS camera. The sample is left stationary. It can perform high-speed volumetric imaging of weak fluorescent specimens as well as live imaging of 3D cell cultures.

DO IT YOURSELF LSFM

Apart from buying a ready-made microscope, it is also possible to build a basic LSFM according to detailed instructions. The integrate OpenSPIM hard- and software platform is an open access initiative for building and adapting SPIM technologies. The idea is to make SPIM technology available to the broad scientific community, also to those without an optics background. Thus, a wiki site has been established (http://openspim.org) which contains a list of commercially available parts needed for the set up as well as a few CAD drawing for custom-made parts. Instructions are explained with pictures that show the building procedures step by step and an OpenSPIM/Fiji software package is available with tutorials on how to use the program and to modify the source code. Three basic configurations are described: single sided illumination/single sided detection, double sided illumination/single sided detection and a double sided illumination/double sided detection. The simplest set up fits on an optical breadboard of 30 x 45 cm and uses one laser. It is developed mainly for developmental studies and embryogenesis. The sample is embedded into agarose gel and extruded from a capillary fixed to a 4D positioning systems that can move the sample in an acrylic water-filled chamber. It is of note that from time to time courses are organized by EMBO to learn how to build the OpenSPIM set up.

Alternatively, it is possible to purchase an inverted SPIM set up from ASI and assemble its parts. The company provides all the necessary hardware except for the objective lenses, lasers and cameras. Videos are available with instructions on how to build the set up and align the microscope.

LSFM ON TRADITIONAL EPI-FLUORESCENT MICROSCOPES

The typical design of LSFM with two (or more) perpendicular objective lenses makes that it is not readily compatible with existing microscope bodies, thus hindering its widespread use in the biological sciences. This is why some laboratories have tried to develop solutions to implement LSFM on traditional epi-fluorescence microscope bodies that only make use of a single objective lens.

In 2013, our group proposed microfabricated sample holders that would enable high-resolution light sheet imaging on a traditional epi-fluorescence microscope[87]. The sample holder is a disposable microfluidic chip made of a planar waveguide on a silicium substrate, shown in Fig. 10A. By butt coupling of a single mode optical fiber to the planar waveguide, a 9-µm-thick light sheet illumination could be achieved in the center of the microfluidic channel. The design has proven valuable for single particle tracking in biological fluid and has shown its potential as a diagnostic tool. However, since the light sheet is fixed in the center of the channel, it has limited use for imaging biological samples. A device that is better suited for imaging multi-cellular structures in vitro up until embryos was developed by Guan et al.[88]. Their plane illumination plugin (PIP) device, shown in Fig. 10B, can be mounted directly on the stage of any epi-fluorescence microscope. It consists of a short sliding rail, on which the optical components and a compact laser diode are mounted, and a small chamber in which the sample, placed into a FEP tube, is kept and aligned to the light sheet. The light sheet thickness and *FoV* can be tuned and can range between 5.5 to 10 µm for the beam waist thickness and between hundreds of micron to mm for the *FoV*. Dual illumination is also an option. Key features of this simple, compact add-on are definitely its easy implementation and low

cost (< 500 USD) although it is not suitable for experiments that require high axial resolution.

Another solution that allows light sheet imaging on epi-fluorescent microscopes was presented by Paie et al.[52] who developed an integrated optofluidic device for high throughput analysis of 3D spheroids on chip. Their optofluidic device, schematically depicted in Fig. 10C, consist of a microfluidic channel through which the sample flows at constant speed. An embedded cylindrical lens focuses the laser light, coming from an optical fiber, in the channel and images are collected while the sample flows through the 5.5-μm-thick light sheet. The continuous flow allows imaging of 300-μm spheroids in less than 2 second per sample.

To enable high resolution LSFM on epi-fluorescent microscope, a simple and interesting concept, depicted in Fig. 10D and 10E, is at the base of the so-called Reflected Light Sheet Microscopy, already described above. One possible configuration consists of delivering the light sheet from the opposite direction of the detection lens and making use of a reflective surface close to the sample so as to reflect the light sheet horizontally into the sample. The solution put forward by Gebhardt and colleagues [89] used a tipless AFM cantilever for horizontal reflection of the light sheet beam in adherent cell cultures. They replaced the condenser of the microscope with a vertically mounted high NA objective lens which focused an elliptical Gaussian beam onto the cantilever. The reflected beam generates a submicrometer light sheet, suitable to illuminate single cells as close as 2 μm from the coverslip. Vertical scanning of the sample is achieved by mounting the sample on a x-y-z piezo stage.

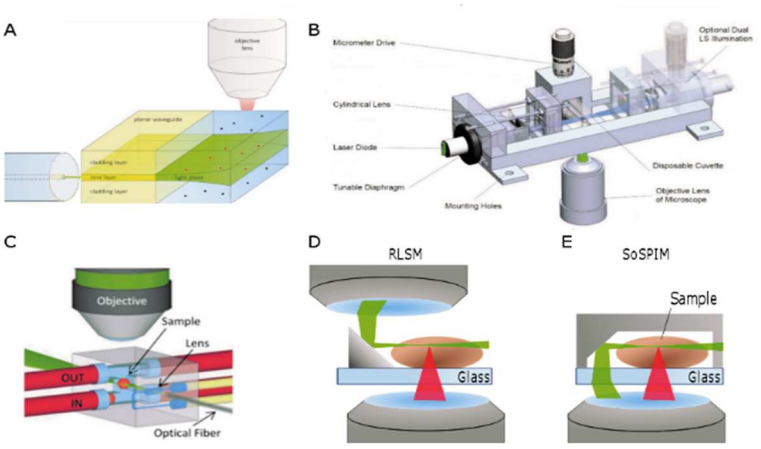

Figure 10. Strategies that integrate LSFM on traditional epi-fluorescence microscopes. (A) Schematic representation of Deschout's sample holder. Through butt-coupling of a single mode fiber, the laser light travels through a planar waveguide and forms a light sheet in the channel. Fluorescent light is collected by an objective lens positioned above or below the sample holder. Adapted from Deschout, Raemdonck, Stremersch, Maoddi, Mernier, Renaud, Jiguet, Hendrix, Bracke, Van den Broecke, Roding, Rudemo, Demeester, De Smedt, Strubbe, Neyts and Braeckmans [87] with permission from The Royal Society of Chemistry. (B) Scheme of PIP device [88]. The device is mounted directly on the microscope body and is already equipped with a compact laser and cylindrical lens. The sample is placed in a disposable cuvette and imaged through the objective lens of the microscope. (C) Optofluidic device for high throughput analysis of spheroids. An embedded, liquid-filled cylindrical lens focuses the laser light coming from an optical fiber into a microfluidic channel. The sample flows at a constant speed through the light sheet, allowing quick scanning of the specimens. Reproduced with permission from Paie, Bragheri, Bassi and Osellame [52], licensed under Creative Commons CC-BY 3.0 license (D) A typical Reflected Light Sheet Microscope (RLSM). The laser beam, coming from a modified condenser, is reflected horizontally on the sample by a 45° mirror. The emitted photons are collected by the objective lens of the microscope. (E) A single-lens variant of RLSM, called SoSPIM. The excitation light is provided through the same objective lens used for detection. The light is reflected horizontally into the sample holder by a microfabricated micromirror.

While a technological feat, this approach requires addition of specially manufactured AFM cantilever holder and separate optics to provide light sheet illumination incident onto the AFM cantilever, all mounted to a fluorescence microscope, which adds another layer of complexity. Similar to this is the design proposed by Greiss et al., who attached a commercially available microprism on a coverslip[10].

A more practical approach would be to provide the light sheet in the sample through the same objective lens that is used for imaging on a fluorescence microscope. Several groups, including ours, developed in parallel microfluidic sample holders with integrated reflective micromirrors which allow horizontal reflection of the excitation light sheet after it passes through the microscope's objective lens[90], as shown in Fig. 10E. The sample holder is placed on a normal epi-fluorescence microscope and a beam-shaping unit is used to provide a sheet of light that emerges from the microscope's standard objective lens. Such a design is compatible with high NA objective lenses and only requires appropriate beam shaping, which can be done before the laser beam is sent into the microscope body. The main differences between the reported devices are to be found in the fabrication process. Galland and coworker's sample holders are made of a UV-curable polymer, index matched with the cell medium, and are obtained through replication from a silicon wafer with tilted microchannel walls prepared by anisotropic wet etching and dry etching. Our group tested an alternative process to fabricate a tilted micromirror, based on polishing of a polyimide wafer at a 45° angle. More information can be found in Chapter 2. The sample holders, made by gluing the polymer based micromirrors, are then successfully replicated to decrease the fabrication costs per sample holder, with no evident loss in optical quality[91].

Meddens et al.[53] chose to house an etched silicon wafer into five layers of PMMA with channels, as seen in Fig. 11.

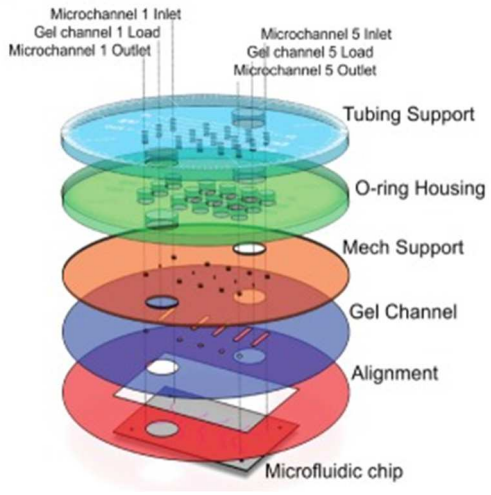

Figure 11. Exploded view of Meddens' chip packaging.

CONCLUSIONS

Nearly two decades after the first modern LSFM microscope was developed, LSFM has become a user-friendly, sample-centered microscopy technique that is already fairly well optimized. The wide variety of set-ups developed in recent years have been designed in response to specific sample needs and the particular scientific questions at hand. Small and fairly transparent model organisms, such as Drosophila Melanogaster or C. Elegans, are now the predominant subject of LSFM research, but it won't be long before larger and more complex organisms are aimed for. Noteworthy is the swept confocally aligned planar excitation microscope (SCAPE), a single-objective LSFM used to image the intact brain of awake behaving mice, and freely moving Drosophila larvae[92].

Integration of LSFM into high-throughput formats is another area of future developments. For instance, drug or genetic screening,

as well as the screening for rare events, could be made possible by the combination of flow-through schemes with automated LSFM imaging. Examples are the development of an open-source platform for high-throughput imaging oriented at drug screening[93] or the integrated optofluidic device for high throughput 3D reconstruction and analysis of spheroids[52]. Also, the combination of LSFM with flow cytometry provides the possibility of imaging cells in high-throughput[94].

The particular arrangement of objective lenses in LSFM requires specialized sample holders, which may pose technical limits to the sample types that can be studied with a particular LSFM configuration. 3D printing may prove useful in the future to more easily develop specific sample holders for particular samples at an acceptable cost. Jeandupeaux and coworkers[95] are taking advantage of the technique by developing a casting kit for the preparation of a hydrogel multisample holder, fully customizable and adaptable to any shape of the sample. 3D micromachining and printing is expected to soon lead to the development of compact LSFM modules and sample holders that should allow a more widespread diffusion of LSFM among the scientific community. Paie's optofluidic device for imaging of spheroids, fabricated by femtosecond laser micromachining, is another example[52].

Some of the compact devices developed to bring light sheet microscopy on traditional microscopes may benefit from the work of Ploschner et al.[96]. They used a spatial light modulator to pre-shape the laser signal in order to obtain a Gaussian or a Bessel light sheet at the distal end of the multi-mode fiber. In order to scan the sample, a series of holographic masks were designed, each of them producing a light sheet in a different plane. Their method produces a 1.2 μm thick light sheet at 50 μm from the

fiber facet. Such a method may one day allow *in vivo* endoscopic imaging deep inside biological tissue, but already at present it could prove useful for on-chip light sheet microscopy.

Lastly, the LSFM technique has great combinatory potential. Optical projection tomography, for example, has been used to generate a transmission contrast image that can provide structural context in large organisms[17, 97], while magnetic resonance imaging MRI has been used to visualize a whole mouse brain while neural stem cell innervation was simultaneously imaged with LSFM[98].

Over time, LSFM has steadily matured and is ready to be applied to the biological questions of this era that more and more require complex cell cultures, tissues and organisms instead of mono-cell cultures. The wide range of set-ups available provide several possibilities for imaging such complex samples with high spatio-temporal resolution. At the same time efforts have been made to provide the scientific communities with a variety of commercialized set-ups, as well as recent designs that allow swift implementation of LSFM on existing microscopes. Certainly, as LSFM will diffuse among research laboratories and research facilities alike, new biological findings are expected to come out thanks to the particular advantages of LSFM that are not offered by any other microscopy modality.

REFERENCES

1. Zong, W.; Chen, X.; Zhao, J.; Zhang, Y.; Fan, M.; Zhou, Z.; Cheng, H.; Sun, Y.; Chen, L. In *Two-photon three-axis digital scanned light-sheet microscopy (2P3A-DSLM)*, CLEO: 2014, San Jose, California, 2014/06/08, 2014; Optical Society of America: San Jose, California, p AW3L.7.
2. Friedrich, M.; Gan, Q.; Ermolayev, V.; Harms, G. S. STED-SPIM: Stimulated emission depletion improves sheet illumination microscopy resolution. *Biophys J* **2011,** *100*, (8), L43-5.
3. Hoyer, P.; de Medeiros, G.; Balazs, B.; Norlin, N.; Besir, C.; Hanne, J.; Krausslich, H. G.; Engelhardt, J.; Sahl, S. J.; Hell, S. W.; Hufnagel, L. Breaking the diffraction limit of light-sheet fluorescence microscopy by RESOLFT. *Proc Natl Acad Sci U S A* **2016,** *113*, (13), 3442-6.
4. Gohn-Kreuz, C.; Rohrbach, A. Light-sheet generation in inhomogeneous media using self-reconstructing beams and the STED-principle. *Opt Express* **2016,** *24*, (6), 5855-65.
5. Scheul, T.; Wang, I.; Vial, J. C. STED-SPIM made simple. *Opt Express* **2014,** *22*, (25), 30852-64.
6. Cella Zanacchi, F.; Lavagnino, Z.; Perrone Donnorso, M.; Del Bue, A.; Furia, L.; Faretta, M.; Diaspro, A. Live-cell 3D super-resolution imaging in thick biological samples. *Nat Methods* **2011,** *8*, (12), 1047-9.
7. Cella Zanacchi, F.; Lavagnino, Z.; Faretta, M.; Furia, L.; Diaspro, A. Light-sheet confined super-resolution using two-photon photoactivation. *PLoS One* **2013,** *8*, (7), e67667.
8. Hu, Y. S.; Zimmerley, M.; Li, Y.; Watters, R.; Cang, H. Single-molecule super-resolution light-sheet microscopy. *Chemphyschem* **2014,** *15*, (4), 577-86.
9. Palayret, M.; Armes, H.; Basu, S.; Watson, A. T.; Herbert, A.; Lando, D.; Etheridge, T. J.; Endesfelder, U.; Heilemann, M.; Laue, E.; Carr, A. M.; Klenerman, D.; Lee, S. F. Virtual-'light-sheet' single-molecule localisation microscopy enables quantitative optical sectioning for super-resolution imaging. *PLoS One* **2015,** *10*, (4), e0125438.
10. Greiss, F.; Deligiannaki, M.; Jung, C.; Gaul, U.; Braun, D. Single-Molecule Imaging in Living Drosophila Embryos with Reflected Light-Sheet Microscopy. *Biophys J* **2016,** *110*, (4), 939-46.
11. Keller, P. J.; Schmidt, A. D.; Santella, A.; Khairy, K.; Bao, Z.; Wittbrodt, J.; Stelzer, E. H. K. Fast, high-contrast imaging of animal development with scanned light sheet-based structured-illumination microscopy. *Nat Meth* **2010,** *7*, (8), 637-642.

12. Zhao, M.; Zhang, H.; Li, Y.; Ashok, A.; Liang, R.; Zhou, W.; Peng, L. Cellular imaging of deep organ using two-photon Bessel light-sheet nonlinear structured illumination microscopy. *Biomed Opt Express* **2014,** *5*, (5), 1296-308.
13. Planchon, T. A.; Gao, L.; Milkie, D. E.; Davidson, M. W.; Galbraith, J. A.; Galbraith, C. G.; Betzig, E. Rapid three-dimensional isotropic imaging of living cells using Bessel beam plane illumination. *Nat Methods* **2011,** *8*, (5), 417-23.
14. Krieger, J. W.; Singh, A. P.; Garbe, C. S.; Wohland, T.; Langowski, J. Dual-color fluorescence cross-correlation spectroscopy on a single plane illumination microscope (SPIM-FCCS). *Opt Express* **2014,** *22*, (3), 2358-75.
15. Chen, X.; Zong, W.; Li, R.; Zeng, Z.; Zhao, J.; Xi, P.; Chen, L.; Sun, Y. Two-photon light-sheet nanoscopy by fluorescence fluctuation correlation analysis. *Nanoscale* **2016,** *8*, (19), 9982-7.
16. Rocha-Mendoza, I.; Licea-Rodriguez, J.; Marro, M.; Olarte, O. E.; Plata-Sanchez, M.; Loza-Alvarez, P. Rapid spontaneous Raman light sheet microscopy using cw-lasers and tunable filters. *Biomed Opt Express* **2015,** *6*, (9), 3449-61.
17. Bassi, A.; Schmid, B.; Huisken, J. Optical tomography complements light sheet microscopy for in toto imaging of zebrafish development. *Development* **2015,** *142*, (5), 1016-20.
18. Huisken, J.; Stainier, D. Y. Selective plane illumination microscopy techniques in developmental biology. *Development* **2009,** *136*, (12), 1963-75.
19. Huisken, J.; Stainier, D. Y. Even fluorescence excitation by multidirectional selective plane illumination microscopy (mSPIM). *Opt Lett* **2007,** *32*, (17), 2608-10.
20. Huisken, J.; Swoger, J.; Del Bene, F.; Wittbrodt, J.; Stelzer, E. H. Optical sectioning deep inside live embryos by selective plane illumination microscopy. *Science* **2004,** *305*, (5686), 1007-9.
21. Udan, R. S.; Piazza, V. G.; Hsu, C. W.; Hadjantonakis, A. K.; Dickinson, M. E. Quantitative imaging of cell dynamics in mouse embryos using light-sheet microscopy. *Development* **2014,** *141*, (22), 4406-14.
22. Weber, M.; Mickoleit, M.; Huisken, J. Multilayer mounting for long-term light sheet microscopy of zebrafish. *J Vis Exp* **2014**, (84), e51119.
23. Lemon, W. C.; Keller, P. J. Live imaging of nervous system development and function using light-sheet microscopy. *Mol Reprod Dev* **2015,** *82*, (7-8), 605-18.

24. Weber, M.; Huisken, J. In vivo imaging of cardiac development and function in zebrafish using light sheet microscopy. *Swiss Med Wkly* **2015,** *145*, w14227.
25. Capoulade, J.; Reynaud, E. G.; Wachsmuth, M., Imaging Marine Life with a Thin Light-Sheet. In *Imaging Marine Life*, Wiley-VCH Verlag GmbH & Co. KGaA: 2013; pp 186-209.
26. Smyrek, I.; Stelzer, E. H. Quantitative three-dimensional evaluation of immunofluorescence staining for large whole mount spheroids with light sheet microscopy. *Biomed Opt Express* **2017,** *8*, (2), 484-499.
27. Trivedi, V.; Truong, T. V.; Trinh le, A.; Holland, D. B.; Liebling, M.; Fraser, S. E. Dynamic structure and protein expression of the live embryonic heart captured by 2-photon light sheet microscopy and retrospective registration. *Biomed Opt Express* **2015,** *6*, (6), 2056-66.
28. Fei, P.; Lee, J.; Packard, R. R.; Sereti, K. I.; Xu, H.; Ma, J.; Ding, Y.; Kang, H.; Chen, H.; Sung, K.; Kulkarni, R.; Ardehali, R.; Kuo, C. C.; Xu, X.; Ho, C. M.; Hsiai, T. K. Cardiac Light-Sheet Fluorescent Microscopy for Multi-Scale and Rapid Imaging of Architecture and Function. *Sci Rep* **2016,** *6*, 22489.
29. Taormina, M. J.; Jemielita, M.; Stephens, W. Z.; Burns, A. R.; Troll, J. V.; Parthasarathy, R.; Guillemin, K. Investigating bacterial-animal symbioses with light sheet microscopy. *Biol Bull* **2012,** *223*, (1), 7-20.
30. Silvestri, L.; Bria, A.; Sacconi, L.; Iannello, G.; Pavone, F. S. Confocal light sheet microscopy: micron-scale neuroanatomy of the entire mouse brain. *Opt Express* **2012,** *20*, (18), 20582-98.
31. Gualda, E. J.; Simao, D.; Pinto, C.; Alves, P. M.; Brito, C. Imaging of human differentiated 3D neural aggregates using light sheet fluorescence microscopy. *Front Cell Neurosci* **2014,** *8*, 221.
32. Wolf, S.; Supatto, W.; Debregeas, G.; Mahou, P.; Kruglik, S. G.; Sintes, J. M.; Beaurepaire, E.; Candelier, R. Whole-brain functional imaging with two-photon light-sheet microscopy. *Nat Methods* **2015,** *12*, (5), 379-80.
33. Keller, P. J.; Ahrens, M. B. Visualizing whole-brain activity and development at the single-cell level using light-sheet microscopy. *Neuron* **2015,** *85*, (3), 462-83.
34. Keller, P. J.; Ahrens, M. B.; Freeman, J. Light-sheet imaging for systems neuroscience. *Nat Methods* **2015,** *12*, (1), 27-9.
35. Abe, J.; Ozga, A. J.; Swoger, J.; Sharpe, J.; Ripoll, J.; Stein, J. V. Light sheet fluorescence microscopy for in situ cell interaction analysis in mouse lymph nodes. *J Immunol Methods* **2016,** *431*, 1-10.

36. Lavagnino, Z.; Dwight, J.; Ustione, A.; Nguyen, T. U.; Tkaczyk, T. S.; Piston, D. W. Snapshot Hyperspectral Light-Sheet Imaging of Signal Transduction in Live Pancreatic Islets. *Biophys J* **2016,** *111*, (2), 409-17.
37. Ovecka, M.; Vaskebova, L.; Komis, G.; Luptovciak, I.; Smertenko, A.; Samaj, J. Preparation of plants for developmental and cellular imaging by light-sheet microscopy. *Nat Protoc* **2015,** *10*, (8), 1234-47.
38. Novak, D.; Kucharova, A.; Ovecka, M.; Komis, G.; Samaj, J. Developmental Nuclear Localization and Quantification of GFP-Tagged EB1c in Arabidopsis Root Using Light-Sheet Microscopy. *Front Plant Sci* **2015,** *6*, 1187.
39. Voie, A. H.; Burns, D. H.; Spelman, F. A. Orthogonal-plane fluorescence optical sectioning: three-dimensional imaging of macroscopic biological specimens. *J Microsc* **1993,** *170*, (Pt 3), 229-36.
40. Keller, P. J.; Schmidt, A. D.; Wittbrodt, J.; Stelzer, E. H. K. Reconstruction of Zebrafish Early Embryonic Development by Scanned Light Sheet Microscopy. *Science* **2008,** *322*, (5904), 1065-1069.
41. Pampaloni, F.; Chang, B. J.; Stelzer, E. H. Light sheet-based fluorescence microscopy (LSFM) for the quantitative imaging of cells and tissues. *Cell Tissue Res* **2015,** *360*, (1), 129-41.
42. Gadallah, F. L.; Csillag, F.; Smith, J. M. Destriping multisensor imagery with moment matching. *International Journal of Remote Sensing* **2000,** *21*, (12), 2505-2511.
43. Fehrenbach, J.; Weiss, P.; Lorenzo, C. Variational algorithms to remove stationary noise: applications to microscopy imaging. *IEEE Trans Image Process* **2012,** *21*, (10), 4420-30.
44. Chang, Y.; Fang, H.; Yan, L.; Liu, H. Robust destriping method with unidirectional total variation and framelet regularization. *Opt. Express* **2013,** *21*, (20), 23307-23323.
45. Münch, B.; Trtik, P.; Marone, F.; Stampanoni, M. Stripe and ring artifact removal with combined wavelet — Fourier filtering. *Opt. Express* **2009,** *17*, (10), 8567-8591.
46. Liang, X.; Zang, Y.; Dong, D.; Zhang, L.; Fang, M.; Yang, X.; Arranz, A.; Ripoll, J.; Hui, H.; Tian, J. Stripe artifact elimination based on nonsubsampled contourlet transform for light sheet fluorescence microscopy. *J Biomed Opt* **2016,** *21*, (10), 106005.
47. Baumgart, E.; Kubitscheck, U. Scanned light sheet microscopy with confocal slit detection. *Opt Express* **2012,** *20*, (19), 21805-14.

48. Guetiérrez-Heredia, L.; Flood, P. M.; Reynaud, E. G., Light Sheet Fluorescence Microscopy: beyond the flatlands In *Current Microscopy Contributions to Advances*

in Science and Technology, A. Méndez-Vilas, E., Ed. Formatex Research Center: 2012; Vol. 2, pp 838-847.

49. Reynaud, E. G.; Peychl, J.; Huisken, J.; Tomancak, P. Guide to light-sheet microscopy for adventurous biologists. *Nat Methods* **2015,** *12*, (1), 30-4.

50. Krieger, J. W.; Singh, A. P.; Bag, N.; Garbe, C. S.; Saunders, T. E.; Langowski, J.; Wohland, T. Imaging fluorescence (cross-) correlation spectroscopy in live cells and organisms. *Nat Protoc* **2015,** *10*, (12), 1948-74.

51. Kaufmann, A.; Mickoleit, M.; Weber, M.; Huisken, J. Multilayer mounting enables long-term imaging of zebrafish development in a light sheet microscope. *Development* **2012,** *139*, (17), 3242-3247.

52. Paie, P.; Bragheri, F.; Bassi, A.; Osellame, R. Selective plane illumination microscopy on a chip. *Lab Chip* **2016,** *16*, (9), 1556-60.

53. Meddens, M. B.; Liu, S.; Finnegan, P. S.; Edwards, T. L.; James, C. D.; Lidke, K. A. Single objective light-sheet microscopy for high-speed whole-cell 3D super-resolution. *Biomed Opt Express* **2016,** *7*, (6), 2219-36.

54. Swoger, J.; Verveer, P.; Greger, K.; Huisken, J.; Stelzer, E. H. Multi-view image fusion improves resolution in three-dimensional microscopy. *Opt Express* **2007,** *15*, (13), 8029-42.

55. Krzic, U.; Gunther, S.; Saunders, T. E.; Streichan, S. J.; Hufnagel, L. Multiview light-sheet microscope for rapid in toto imaging. *Nat Methods* **2012,** *9*, (7), 730-3.

56. de Medeiros, G.; Norlin, N.; Gunther, S.; Albert, M.; Panavaite, L.; Fiuza, U. M.; Peri, F.; Hiiragi, T.; Krzic, U.; Hufnagel, L. Confocal multiview light-sheet microscopy. *Nat Commun* **2015,** *6*, 8881.

57. Weber, M.; Huisken, J. Omnidirectional microscopy. *Nat Meth* **2012,** *9*, (7), 656-657.

58. Tomer, R.; Khairy, K.; Amat, F.; Keller, P. J. Quantitative high-speed imaging of entire developing embryos with simultaneous multiview light-sheet microscopy. *Nat Methods* **2012,** *9*, (7), 755-63.

59. Ahrens, M. B.; Orger, M. B.; Robson, D. N.; Li, J. M.; Keller, P. J. Whole-brain functional imaging at cellular resolution using light-sheet microscopy. *Nat Methods* **2013,** *10*, (5), 413-20.

60. Wu, Y.; Wawrzusin, P.; Senseney, J.; Fischer, R. S.; Christensen, R.; Santella, A.; York, A. G.; Winter, P. W.; Waterman, C. M.; Bao, Z.; Colon-Ramos, D. A.; McAuliffe, M.; Shroff, H. Spatially isotropic four-dimensional

imaging with dual-view plane illumination microscopy. *Nat Biotechnol* **2013,** *31*, (11), 1032-8.
61. Fahrbach, F. O.; Rohrbach, A. A line scanned light-sheet microscope with phase shaped self-reconstructing beams. *Opt Express* **2010,** *18*, (23), 24229-44.
62. Fahrbach, F. O.; Rohrbach, A. Propagation stability of self-reconstructing Bessel beams enables contrast-enhanced imaging in thick media. *Nat Commun* **2012,** *3*, 632.
63. Fahrbach, F. O.; Gurchenkov, V.; Alessandri, K.; Nassoy, P.; Rohrbach, A. Self-reconstructing sectioned Bessel beams offer submicron optical sectioning for large fields of view in light-sheet microscopy. *Opt Express* **2013,** *21*, (9), 11425-40.
64. Gao, L.; Shao, L.; Chen, B. C.; Betzig, E. 3D live fluorescence imaging of cellular dynamics using Bessel beam plane illumination microscopy. *Nat Protoc* **2014,** *9*, (5), 1083-101.
65. Zhang, P.; Phipps, M. E.; Goodwin, P. M.; Werner, J. H. Light-sheet microscopy by confocal line scanning of dual-Bessel beams. *J Biomed Opt* **2016,** *21*, (10), 100502.
66. Zhao, T.; Lau, S. C.; Wang, Y.; Su, Y.; Wang, H.; Cheng, A.; Herrup, K.; Ip, N. Y.; Du, S.; Loy, M. M. Multicolor 4D Fluorescence Microscopy using Ultrathin Bessel Light Sheets. *Sci Rep* **2016,** *6*, 26159.
67. Andilla, J.; Jorand, R.; Olarte, O. E.; Dufour, A. C.; Cazales, M.; Montagner, Y. L.; Ceolato, R.; Riviere, N.; Olivo-Marin, J. C.; Loza-Alvarez, P.; Lorenzo, C. Imaging tissue-mimic with light sheet microscopy: A comparative guideline. *Sci Rep* **2017,** *7*, 44939.
68. Vettenburg, T.; Dalgarno, H. I.; Nylk, J.; Coll-Llado, C.; Ferrier, D. E.; Cizmar, T.; Gunn-Moore, F. J.; Dholakia, K. Light-sheet microscopy using an Airy beam. *Nat Methods* **2014,** *11*, (5), 541-4.
69. Chen, B. C.; Legant, W. R.; Wang, K.; Shao, L.; Milkie, D. E.; Davidson, M. W.; Janetopoulos, C.; Wu, X. S.; Hammer, J. A., 3rd; Liu, Z.; English, B. P.; Mimori-Kiyosue, Y.; Romero, D. P.; Ritter, A. T.; Lippincott-Schwartz, J.; Fritz-Laylin, L.; Mullins, R. D.; Mitchell, D. M.; Bembenek, J. N.; Reymann, A. C.; Bohme, R.; Grill, S. W.; Wang, J. T.; Seydoux, G.; Tulu, U. S.; Kiehart, D. P.; Betzig, E. Lattice light-sheet microscopy: imaging molecules to embryos at high spatiotemporal resolution. *Science* **2014,** *346*, (6208), 1257998.
70. Collier, B. B.; Awasthi, S.; Lieu, D. K.; Chan, J. W. Non-linear optical flow cytometry using a scanned, Bessel beam light-sheet. *Sci Rep* **2015,** *5*, 10751.

71. Fahrbach, F. O.; Gurchenkov, V.; Alessandri, K.; Nassoy, P.; Rohrbach, A. Light-sheet microscopy in thick media using scanned Bessel beams and two-photon fluorescence excitation. *Opt Express* **2013,** *21*, (11), 13824-39.
72. Olarte, O. E.; Licea-Rodriguez, J.; Palero, J. A.; Gualda, E. J.; Artigas, D.; Mayer, J.; Swoger, J.; Sharpe, J.; Rocha-Mendoza, I.; Rangel-Rojo, R.; Loza-Alvarez, P. Image formation by linear and nonlinear digital scanned light-sheet fluorescence microscopy with Gaussian and Bessel beam profiles. *Biomed Opt Express* **2012,** *3*, (7), 1492-505.
73. Yang, Z.; Prokopas, M.; Nylk, J.; Coll-Llado, C.; Gunn-Moore, F. J.; Ferrier, D. E.; Vettenburg, T.; Dholakia, K. A compact Airy beam light sheet microscope with a tilted cylindrical lens. *Biomed Opt Express* **2014,** *5*, (10), 3434-42.
74. Fu, Q.; Martin, B. L.; Matus, D. Q.; Gao, L. Imaging multicellular specimens with real-time optimized tiling light-sheet selective plane illumination microscopy. *Nature Communications* **2016,** *7*, 11088.
75. Gao, L. Extend the field of view of selective plan illumination microscopy by tiling the excitation light sheet. *Opt Express* **2015,** *23*, (5), 6102-11.
76. Zong, W.; Zhao, J.; Chen, X.; Lin, Y.; Ren, H.; Zhang, Y.; Fan, M.; Zhou, Z.; Cheng, H.; Sun, Y.; Chen, L. Large-field high-resolution two-photon digital scanned light-sheet microscopy. *Cell Res* **2015,** *25*, (2), 254-7.
77. Truong, T. V.; Supatto, W.; Koos, D. S.; Choi, J. M.; Fraser, S. E. Deep and fast live imaging with two-photon scanned light-sheet microscopy. *Nat Meth* **2011,** *8*, (9), 757-760.
78. Ji, N.; Magee, J. C.; Betzig, E. High-speed, low-photodamage nonlinear imaging using passive pulse splitters. *Nat Meth* **2008,** *5*, (2), 197-202.
79. Olarte, O. E.; Andilla, J.; Artigas, D.; Loza-Alvarez, P. Decoupled illumination detection in light sheet microscopy for fast volumetric imaging. *Optica* **2015,** *2*, (8), 702-705.
80. Mahou, P.; Vermot, J.; Beaurepaire, E.; Supatto, W. Multicolor two-photon light-sheet microscopy. *Nat Methods* **2014,** *11*, (6), 600-1.
81. Lavagnino, Z.; Sancataldo, G.; d'Amora, M.; Follert, P.; De Pietri Tonelli, D.; Diaspro, A.; Cella Zanacchi, F. 4D (x-y-z-t) imaging of thick biological samples by means of Two-Photon inverted Selective Plane Illumination Microscopy (2PE-iSPIM). *Sci Rep* **2016,** *6*, 23923.

82. Dean, K. M.; Roudot, P.; Welf, E. S.; Danuser, G.; Fiolka, R. Deconvolution-free Subcellular Imaging with Axially Swept Light Sheet Microscopy. *Biophys J* **2015,** *108*, (12), 2807-15.
83. Dean, K. M.; Roudot, P.; Reis, C. R.; Welf, E. S.; Mettlen, M.; Fiolka, R. Diagonally Scanned Light-Sheet Microscopy for Fast Volumetric Imaging of Adherent Cells. *Biophys J* **2016,** *110*, (6), 1456-65.
84. Tomer, R.; Lovett-Barron, M.; Kauvar, I.; Andalman, A.; Burns, V. M.; Sankaran, S.; Grosenick, L.; Broxton, M.; Yang, S.; Deisseroth, K. SPED Light Sheet Microscopy: Fast Mapping of Biological System Structure and Function. *Cell* **2015,** *163*, (7), 1796-806.
85. Jahr, W.; Schmid, B.; Schmied, C.; Fahrbach, F. O.; Huisken, J. Hyperspectral light sheet microscopy. *Nat Commun* **2015,** *6*, 7990.
86. Dodt, H. U.; Leischner, U.; Schierloh, A.; Jahrling, N.; Mauch, C. P.; Deininger, K.; Deussing, J. M.; Eder, M.; Zieglgansberger, W.; Becker, K. Ultramicroscopy: three-dimensional visualization of neuronal networks in the whole mouse brain. *Nat Methods* **2007,** *4*, (4), 331-6.
87. Deschout, H.; Raemdonck, K.; Stremersch, S.; Maoddi, P.; Mernier, G.; Renaud, P.; Jiguet, S.; Hendrix, A.; Bracke, M.; Van den Broecke, R.; Roding, M.; Rudemo, M.; Demeester, J.; De Smedt, S. C.; Strubbe, F.; Neyts, K.; Braeckmans, K. On-chip light sheet illumination enables diagnostic size and concentration measurements of membrane vesicles in biofluids. *Nanoscale* **2014,** *6*, (3), 1741-7.
88. Guan, Z.; Lee, J.; Jiang, H.; Dong, S.; Jen, N.; Hsiai, T.; Ho, C. M.; Fei, P. Compact plane illumination plugin device to enable light sheet fluorescence imaging of multi-cellular organisms on an inverted wide-field microscope. *Biomed Opt Express* **2016,** *7*, (1), 194-208.
89. Gebhardt, J. C.; Suter, D. M.; Roy, R.; Zhao, Z. W.; Chapman, A. R.; Basu, S.; Maniatis, T.; Xie, X. S. Single-molecule imaging of transcription factor binding to DNA in live mammalian cells. *Nature methods* **2013,** *10*, (5), 421-6.
90. Galland, R.; Grenci, G.; Aravind, A.; Viasnoff, V.; Studer, V.; Sibarita, J. B. 3D high- and super-resolution imaging using single-objective SPIM. *Nature methods* **2015,** *12*, (7), 641-4.
91. Zagato, E.; Brans, T.; Verstuyft, S.; van Thourhout, D.; Missinne, J.; van Steenberge, G.; Demeester, J.; De Smedt, S.; Remaut, K.; Neyts, K.; Braeckmans, K. Microfabricated devices for single objective single plane illumination microscopy (SoSPIM). *Opt. Express* **2017,** *25*, (3), 1732-1745.
92. Bouchard, M. B.; Voleti, V.; Mendes, C. S.; Lacefield, C.; Grueber, W. B.; Mann, R. S.; Bruno, R. M.; Hillman, E. M. Swept confocally-aligned planar

excitation (SCAPE) microscopy for high speed volumetric imaging of behaving organisms. *Nat Photonics* **2015,** *9*, (2), 113-119.
93. Gualda, E. J.; Pereira, H.; Vale, T.; Estrada, M. F.; Brito, C.; Moreno, N. SPIM-fluid: open source light-sheet based platform for high-throughput imaging. *Biomed Opt Express* **2015,** *6*, (11), 4447-56.
94. Regmi, R.; Mohan, K.; Mondal, P. P. Light sheet based imaging flow cytometry on a microfluidic platform. *Microscopy Research and Technique* **2013,** *76*, (11), 1101-1107.
95. Jeandupeux, E.; Lobjois, V.; Ducommun, B. 3D print customized sample holders for live light sheet microscopy. *Biochem Biophys Res Commun* **2015,** *463*, (4), 1141-3.
96. Ploschner, M.; Kollarova, V.; Dostal, Z.; Nylk, J.; Barton-Owen, T.; Ferrier, D. E.; Chmelik, R.; Dholakia, K.; Cizmar, T. Multimode fibre: Light-sheet microscopy at the tip of a needle. *Sci Rep* **2015,** *5*, 18050.
97. Mayer, J.; Robert-Moreno, A.; Danuser, R.; Stein, J. V.; Sharpe, J.; Swoger, J. OPTiSPIM: integrating optical projection tomography in light sheet microscopy extends specimen characterization to nonfluorescent contrasts. *Opt Lett* **2014,** *39*, (4), 1053-6.
98. Doerr, J.; Schwarz, M. K.; Wiedermann, D.; Leinhaas, A.; Jakobs, A.; Schloen, F.; Schwarz, I.; Diedenhofen, M.; Braun, N. C.; Koch, P.; Peterson, D. A.; Kubitscheck, U.; Hoehn, M.; Brustle, O. Whole-brain 3D mapping of human neural transplant innervation. *Nat Commun* **2017,** *8*, 14162.

CHAPTER **2**

MICROFABRICATED DEVICES FOR SINGLE OBJECTIVE SINGLE PLANE ILLUMINATION

This chapter is published as:

E. Zagato[1,2], S. Roovers[1,2], T. Brans[1,2], S. Verstuyft[3], D. van Thourhout[3], J. Missinne[4], G. van Steenberge[4], J. Demeester[1], S. De Smedt[1], I. Lentacker[1,2], K. Remaut[1], K. Neyts[1], K. Braeckmans[1,2]. Microfabricated devices for single objective single plane illumination microscopy (SoSPIM). *Opt. Express* **2017,** *25*, (3), 1732-1745.

[1]*Laboratory of General Biochemistry and Physical Pharmacy, Ghent University, Belgium*
[2]*Center for Nano- and Biophotonics, Ghent University, Belgium*
[3]*Photonics Research Group, Department of Information Technology, Ghent University-IMEC, 9000 Gent, Belgium*
[4]*Centre for Microsystems Technology (CMST), Imec and Ghent University, Technologiepark –Zwijnaarde, building 15, Zwijnaarde*
[5]*Liquid crystals and Photonics Group, Ghent University, Belgium*

ABSTRACT Light sheet microscopy is a relatively new form of fluorescence microscopy that is receiving a lot of attention nowadays. The strong points of the technique, such as high signal to noise ratio and its reduced photodamage of fluorescently labelled samples, come from its unique feature to illuminate only a thin plane in the sample that coincides with the focal plane of the detection lens. Typically this requires two closely positioned perpendicular objective lenses, one for detection and one for illumination. Apart from the fact that this special configuration of objective lenses is incompatible with standard microscope bodies, it is particularly problematic for high-resolution lenses which typically have a short working distance. To address these issues we developed sample holders with an integrated micromirror to perform single lens light sheet microscopy, also known as single objective single plane illumination microscopy (SoSPIM). The first design is based on a wet-etched silicon substrate, the second on a microfabricated polished polymer plug. We achieved an on-chip light sheet thickness of 2.3 μm (FWHM) at 638 nm with the polymer micromirror and of 1.7 μm (FWHM) at 638 nm with the silicon micromirror, comparable to reported light sheet thicknesses obtained on dedicated light sheet microscopes. A marked contrast improvement was obtained with both sample holders as compared to classic epi-fluorescence microscopy. In order to evaluate whether this technology could be made available on a larger scale, in a next step we evaluated the optical quality of inexpensive replicas from both types of master molds. We found that replicas from the polished polymer based mold have an optical quality close to that of the master component, while replicas from the silicon based mold were of slightly lower but still acceptable quality. The suitability of the replicated polymer based sample holder for single-lens light sheet

microscopy was finally demonstrated by imaging breast cancer spheroids.

INTRODUCTION

While fluorescence microscopy offers high-contrast imaging in combination with selective labels, exposing biological samples to high intensity excitation light may lead to photobleaching of the fluorophores and induce phototoxicity to the cells or tissue under investigation. This problem is confounded when acquiring a 3D stack of images, which implies that the entire sample is illuminated during the acquisition of each image plane. Light Sheet Fluorescence Microscopy (LSFM) was developed in response to these problems and was elected "Method of the Year 2014" by Nature Methods[1]. In a light sheet fluorescence microscope, two perpendicular objective lenses are used, one for illumination and one for imaging. The illumination objective lens is used to project a thin sheet of excitation light in the sample in such a way that it coincides with the focal plane of the detection objective lens. By restricting excitation of fluorophores to the focal plane, intrinsic optical sectioning of the sample is achieved. To obtain 3D images the sample is moved through the excitation light sheet along the detection optical axis. In this way each plane of the sample is illuminated only once, which reduces photobleaching and phototoxicity issues[2]. When combined with a fast camera, the technique is able to follow dynamic processes that are happening in (relatively) large 3D volumes, like the beating of the heart[3, 4] or the functioning of the brain[5, 6] of zebrafishes and mice, and live formation of spheroids[7]. Two-photon light sheet microscopy has been reported as well for improved imaging depth[8, 9]. However, widespread use of LSFM is hindered due to the fact that it requires two perpendicular objective lenses[10] in close proximity with a dedicated sample holder in between[11, 12]. One problem is that such a configuration is not readily compatible with standard microscope bodies. A

second disadvantage of such a configuration is that spatial constraints prohibit the use of high NA lenses which have short working distances.

In response to this need, microfabricated sample holders have been proposed that would enable high-resolution light sheet imaging in combination with standard microscope bodies[13, 14]. In the design proposed by Deschout et al. the sample holder is a disposable microfluidics chip made of a planar waveguide on a silicium or glass substrate. By butt coupling of a single mode optical fiber to the planar waveguide, a 9-µm-thick light sheet illumination could be achieved in the center of the microfluidic channel. While this sample holder was proven valuable for single particle tracking in biological fluids, it has limited use for imaging biological samples since the position of the light sheet is fixed. A more versatile design was recently proposed by Galland et al., which is based on a microfluidic chip with integrated 45° micromirrors. The chip is placed on a normal epi-microscope and a beam-shaping unit is used to provide a sheet of light that emerges from the microscope's standard objective lens. After reflection on the 45° micromirror a horizontal sheet of light is obtained in the chip that coincides with the imaging focal plane of the same lens. With this configuration they managed to obtain single-lens LSFM images of live embryos and super-resolution images of cell nuclei.

The microfabrication process of the master component for Galland et al.'s micromirror chip is based on sequential anisotropic wet etching and dry etching of a silicon wafer. Here we evaluate a less time consuming and less complex approach based on the polishing of an inexpensive polymer material at a 45° angle. After coating with aluminum or gold, we compare its optical performance to the Si chip according to Galland et al. in

terms of thickness of the reflected light sheet (beam waist), the homogeneity along its optical axis (depth of field) and contrast achieved. Aimed at potential upscaling we additionally evaluated the optical performance of inexpensive replicas from both types of master molds. It is found that replicas from the polished polymer plug perform best and those are finally used for single-lens LSFM imaging of breast cancer cells spheroids as an example application.

CHIP DESIGN AND FABRICATION

As described in more detail in the section "*optical set-up*" of this chapter, the concept relies on the reflection of an elliptical Gaussian beam on a 45° micromirror to create a horizontal light sheet that coincides with the detection focal plane of the objective lens. Given the importance of the beam shape after reflection, we chose to compare two strategies to fabricate the tilted micromirror. In the first strategy, following a previously published method[15], the crystallographic properties of silicon were exploited and the mirror was made chemically flat by means of anisotropic etching. For the second design the micromirror was fabricated by mechanically polishing a polymer sheet at 45 degree, which was then thinned to the required thickness [16]. Subsequently the sheet was coated by either a layer of gold or aluminum, known for their high reflectivity (85% for aluminum and >90% for gold at 45° incidence angle and λ=638 nm). Aimed at upscaling towards inexpensive disposable devices, replicas are made as well by pressing the above mentioned master molds, referred to as "master components", onto a transparent UV-curable polymer material to create a negative stamp. The negative stamp is then pressed on a UV-curable epoxy, cured and subsequently coated with a reflecting layer (Au or Al). In the next

subsections the fabrication process of these different micromirrors is described in detail.

SILICON MICROMIRRORS

The process to fabricate optically flat mirror walls into a silicon wafer consists of three major steps, namely photolithography, etching and cleaning.

The wafer of choice is a thermo-oxidized (100) Si wafer (silicon dioxide layer: 1 μm thick). After initial spin coating of a primer (TI Prime) and the positive photoresist az9260 (MicroChemicals Gmbh, Germany), both followed by a 3 minutes baking step at 110°C, the wafer is covered with a chrome mask, that defines the position of the tilted walls and the channel, and subsequently exposed to UV light (Suss Microtech, Germany) for 200 seconds. The wafer is immersed for 90 s in an aqueous solution consisting of 1 part Developer 400K (MicroChemicals Gmbh, Germany) and 2 parts distilled water in order to remove the UV illuminated regions of the photoresist. In the subsequent etching step, the wafer is placed for 16 min into a buffered 7:1 HF solution (MicroChemicals Gmbh, Germany) that dissolves the unprotected regions of the silicon dioxide and exposes the underlying bare silicon. Next, the wafer is placed for 5 min in an ultrasonic bath filled with acetone to remove the photoresist layer. Then the wafer is put into a stirred KOH bath (KOH/Water/IPA 20/64/16) at 70°C that will selectively remove atoms in the <100> crystal direction, thus etching the channel with tilted walls at approximately 40 μm/hour. A careful monitoring of the etch rate by means of temperature and concentration of the etchant is of the utmost importance since the etch rate can influence the wall roughness. Finally an RCA-1 clean was performed as follows. A solution of 5 parts water, 1 part

27% ammonium hydroxide and 1 part 30% hydrogen peroxide is heated at 70°C, then the wafer is soaked in the solution for 15 min, rinsed with water and put for 5 min into a 5% HCl solution. Fig. 1 shows the end result of this process. In panel A the scheme of the silicon based master mold is portrayed. Panel B and panel C capture a picture of the silicon based master mold and a SEM micrograph of the tilted micromirror.

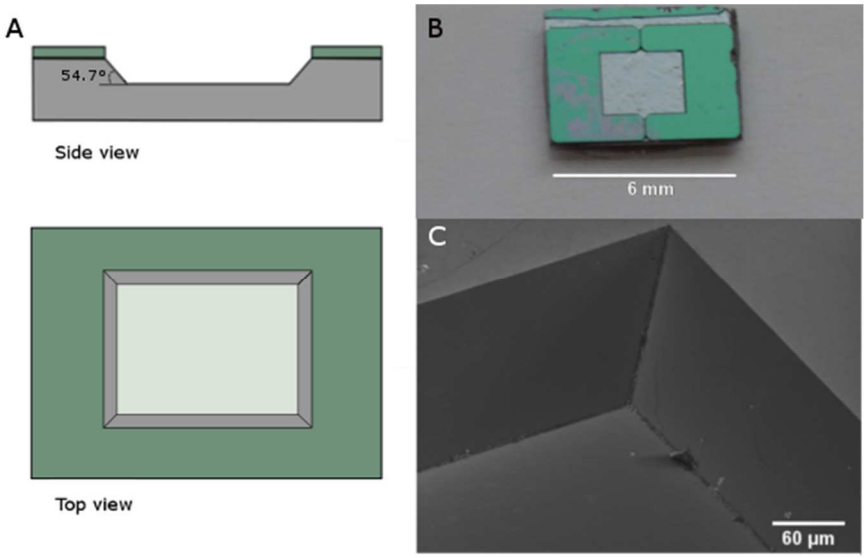

Fig. 1. Master mold with tilted micromirrors fabricated in silicon. (A) Schematic top and side view showing the microcavity with tilted micromirror walls into which the sample can be placed. (B) Top view picture of a microfabricated silicon master mold. (C) SEM micrograph showing the tilted walls of the master mold in one of the corners of the microcavity.

POLYMER MICROMIRRORS

Optically flat tilted surfaces in polyimide (PI) were prepared as described in detail elsewhere[16]. Briefly, a 500-µm-thick flexible PI wafer (OPTIcomp Networks, Inc.) is clamped in a special PMMA device with a 45° trench. The whole device is polished to provide

a 45° polished end facet to the PI foil. Subsequently, the edge defects from the polishing process are eliminated by thinning down the wafer to the desired thickness (200 µm in this case). Afterwards, the wafer is cut into small parts of the desired length and width by a wafer dicer with a diamond coated blade. The tilted end facets are then coated with a 120-nm-thin gold layer by vapor deposition, or with an aluminium layer applied by sputtering. The process yields thin micromirror plugs with an RMS roughness below 20 nm and good control over the angle (± 1 degree), see Fig. 2A and 2C. A simple master mold is created by attaching two opposing mirror plugs to a glass microscope slide, as shown in Fig. 2B.

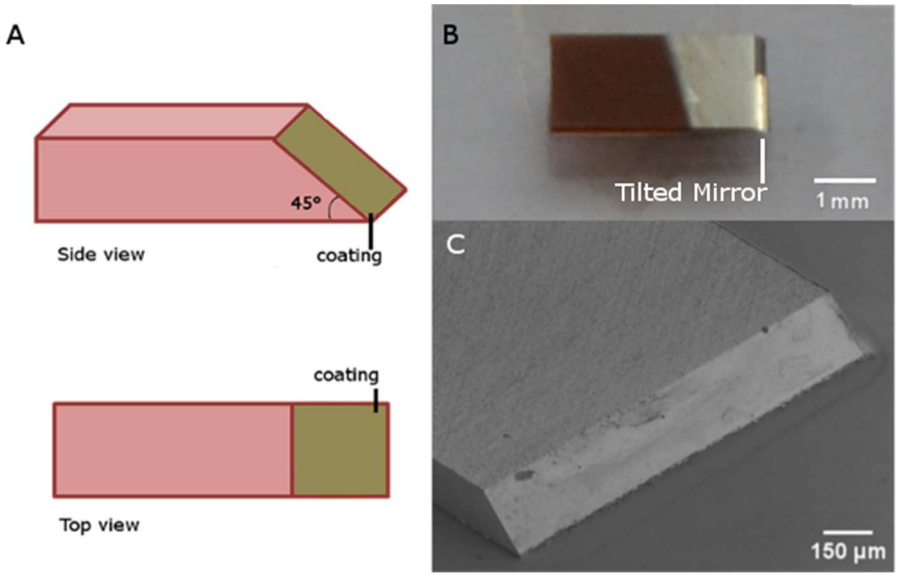

Fig. 2. Master mold with polished tilted micromirrors fabricated in polyimide. (A) Schematic top and side view of the polished polymer plug. (B) A simple master mold is created by gluing two of those polymer plugs, coated with aluminum (or gold), to a microscope slide. The sample can be placed in between the polymer plugs. (C) SEM micrograph of the polished polymer tilted mirror.

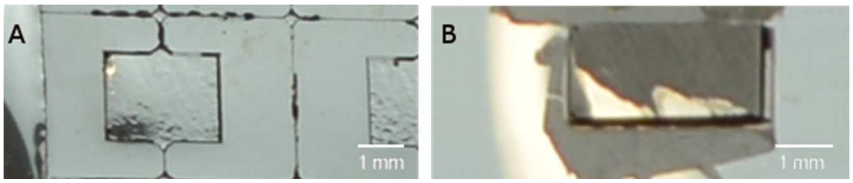

Fig. 3. Replicated sample holders coated with aluminium. (A) Top view of the sample holder replicated from the silicon master mold. (B) Top view of the sample holder replicated from the polymer master mold.

DISPOSABLE REPLICATED SAMPLE HOLDERS

For imaging of biological specimen it is of interest to investigate the optical quality of inexpensive disposable replicas made from the master components. First, the polymer or silicon based master components are covered with a UV-curable, transparent fluorinated molding material (MD700, Solvay Solexis + photoinitiator). Following UV illumination, the polymerized material is easily peeled off from the master components. This stamp is then used to fabricate the actual replicas. To this end, a drop of a UV-curable epoxy (EpoTek OG142-112) is dispensed on a glass slide and the molding stamp is pressed into the drop. Then the epoxy is cured using UV illumination and, after complete hardening, the molding stamp can be peeled-off. This results in epoxy structures with the same topology as the master components. In a final step the replicated micromirrors are coated with a 200 nm reflective layer of either gold (evaporation) or aluminum (sputtering).

OPTICAL SETUP

The excitation light sheet is provided by a laser source (Lasos RLD-638-150, λ: 638 nm, operating at 20 mW). To have full control of the waist, divergence, position and orientation of the light sheet in the measurement chamber, a custom-made beam shaping unit was built as schematically depicted in Fig. 4. After collimation, the beam passes three lenses (section S1) that serve as a variable beam expander. By choosing the appropriate distance between these lenses, the beam width at the back focal plane of the objective can be set, which in turn determines the waist thickness and divergence of the light sheet at the front focal plane of the microscope's objective lens (40x Nikon objective lens, CFI S Plan Fluor Brightfield, NA 0.6). A thin light sheet waist provides better contrast at the expense of more beam divergence and, therefore, a more limited field of view. Being able to choose the waist thickness make the sample holder more versatile and able to switch between observing small cells (thin light sheet and small field of view) and living organism (thicker light sheet and larger field of view).

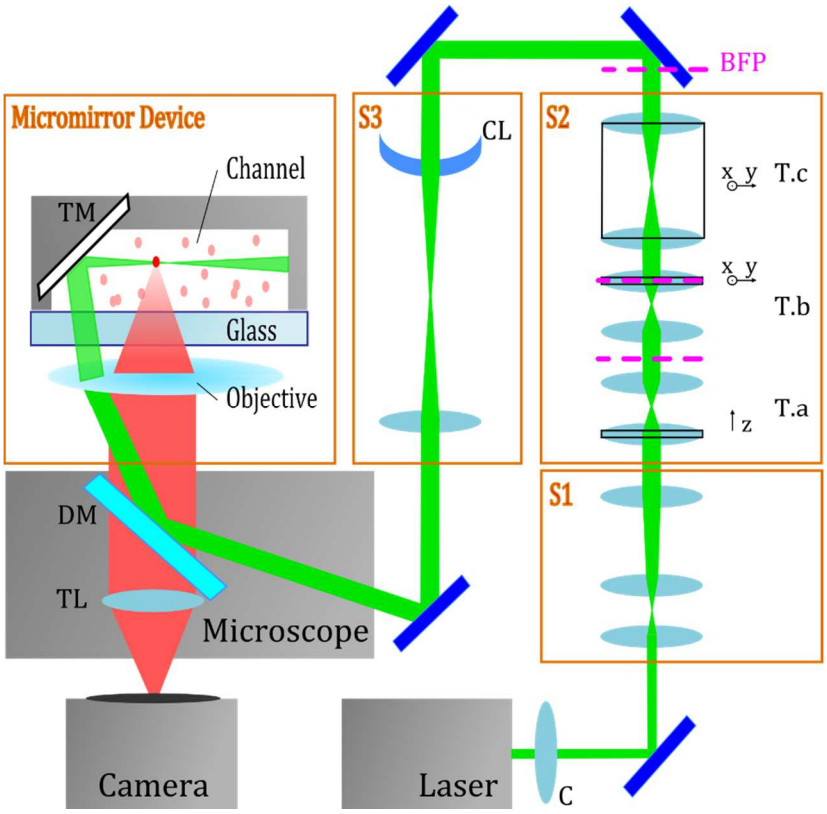

Fig. 4. Single lens light-sheet microscopy is achieved by reflection of an elongated elliptical gaussian beam in a sample holder with integrated microfabricated tilted mirror (TM). After collimation (C), the laser beam passes through a variable beam expander consisting of three lenses (section S1), that allow to adjust the waist thickness and divergence of the light sheet in the channel. The light sheet focus in the sample holder is manipulated independently by the three telescopes (T.a, T.b and T.c) depicted in section S2. The laser beam is shaped into an elliptical Gaussian beam by a telescope in section S3 with a cylindrical back lens (CL). The fluorescent light emitted passes through a dichroic mirror (DM) and is imaged on the camera by a tube lens (TL).

Section S2 consists of three telescopes, each with a specific position with respect to a plane conjugated to the back focal plane

of the microscope objective. Each telescope allows for an independent manipulation of the laser focus at the front focal plane of the objective lens: a translation of the laser focus along the axis of the beam, a lateral translation of the focus and a tilt of the laser beam with respect to the axis of the objective. These manipulations are achieved by respectively axially translating the back lens of the telescope T.a, laterally translating the front lens of T.b and jointly laterally translating both lenses of telescope T.c. After this, the beam passes section S3, consisting of a telescope with a cylindrical back lens. This produces an elliptical Gaussian beam in the focal plane of the objective lens. The laser beam is subsequently coupled into a microscope (Nikon Ti-E) onto which the sample holder with tilted micromirrors is installed. Fluorescence light coming from the sample is collected by the same objective lens and separated from the excitation light by a dichroic mirror. Images are acquired with a digital camera (iXon+, Andor, Belfast, UK).

LIGHT SHEET CHARACTERIZATION AND OPTICAL PERFORMANCE

BEAM CHARACTERIZATION AND CONTRAST USING THE MASTER COMPONENT

A first step in the comparison of the various micromirrors is the characterization of the light sheet beam profile after it is reflected by the micromirrors. At first, we wondered if the type of metal coating (gold applied through evaporation or aluminum applied through sputtering) would influence the optical quality of the reflected beam. The parameters that are of primary interest are the thickness of the light sheet (beam waist) and the homogeneity along its optical axis (effective depth of field). As it is not possible to visualize the light sheet from the side in the sample holders, we replaced the cylindrical lens (see Fig. 4) by a spherical one with the same focal length. In that way the focused beam can be easily visualized from the top through the microscope. A fluorescent solution of 10 μM ATTO647 was used to visualize the focused beam by fluorescence imaging. Another performance indicator is the contrast that is obtained for fluorescent samples. Similar to previous work[13, 17] we used fluorescent nanospheres (Invitrogen, dark red, diameter 100 nm) dispersed in red fluorescent solutions of Cy5 (Mirus Bio LLC, Madison, USA). The concentration of Cy5 was gradually increased to simulate an increasingly higher background intensity. The cylindrical lens was used to create a light sheet in the channel. Time-lapse videos of these samples, were acquired and the contrast was determined for more than 300 of these nanospheres moving within the depth of field region using in-house developed particle tracking software[18].

The contrast C for every nanosphere is calculated from $C = (I - BG)/(I + BG)$, where I is the average intensity of the

nanosphere and BG is the local background intensity calculated along a contour at 4 pixel distance around the edge of the nanosphere. As shown in Fig. 5, neither the beam profile nor the achieved contrast are affected by the metal applied, thus both gold and aluminum can be used.

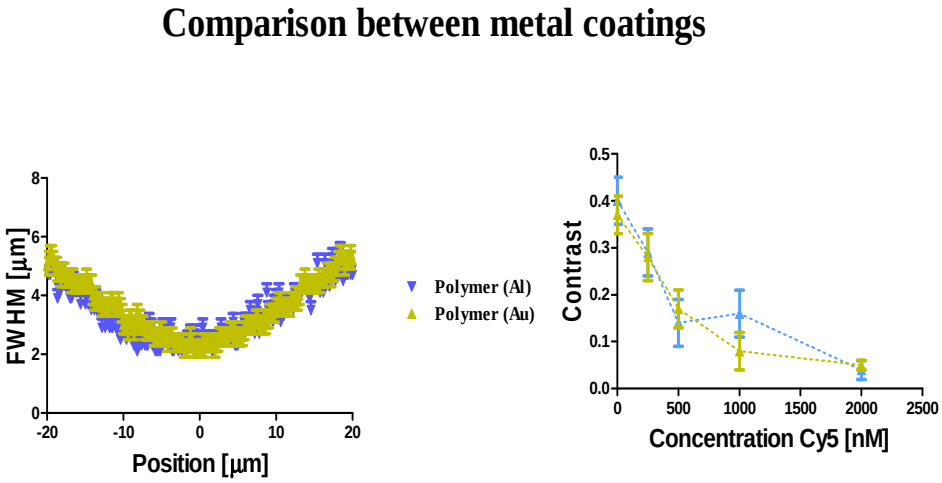

Fig. 5. Influence of metal coating on the beam profile (left) and on the contrast (right). Two polymer master molds were considered, one coated with aluminum through sputtering, the second coated with gold through evaporation. The Full Width at Half Maximum (FWHM) of the focused beam along its optical axis is plotted in the graph. Contrast was determined for fluorescent nanospheres suspended in solutions with increasing concentration of the red fluorescent dye Cy5. Measurements were performed in both molds and compared with normal epi-fluorescence imaging. Neither the beam profile nor the contrast seem effected by the metal used for coating

We first evaluated the optical quality of the reflected beam in both master components. Figs. 6A and 6B show the laser beam reflected from the silicon micromirror and from the polished polymer micromirror, respectively. The Full Width at Half Maximum (FWHM) of the focused beam along its optical axis is

plotted in the graph in Figs. 6C and 6D. We fitted the graph with the equation of propagation

$$W(x) = W_0\sqrt{1+\left(\frac{2x}{DoF_{eff}}\right)^2} \quad (1)$$

with W_0 the FWHM at the beam focus, proportional to the beam waist and DoF_{eff} the effective depth of focus. To properly fit the data, we had to consider the parameters W_0 and DoF_{eff} as independent, meaning that the light sheet profile does not match with perfect Gaussian beam propagation. This is also noticeable from the somewhat asymmetric beam profile in Fig. 6A and 6B. This may be due to aberrations induced by the micromirrors or because of aberrations induced by the fact that the light sheet focus is formed at a longer distance than the objective lens's normal focal plane (infinity corrected objective lens). It can also not be excluded that perhaps the reflected beam is not entirely horizontal in the channel. The focus diameter W_0 is determined as 2.4 ± 0.3 μm for the polished polymer micromirror and 1.6 ± 0.3 μm for the silicon micromirror. The corresponding DoF_{eff} was 19 ± 0.3 μm 10.0 ± 1.0 μm, respectively. Although the performance of both is quite similar, the slightly smaller beam waist with the silicon micromirror is likely due to its surface being more flat than that of the polished micromirror, as can be seen in Figs. 1C and 2C.

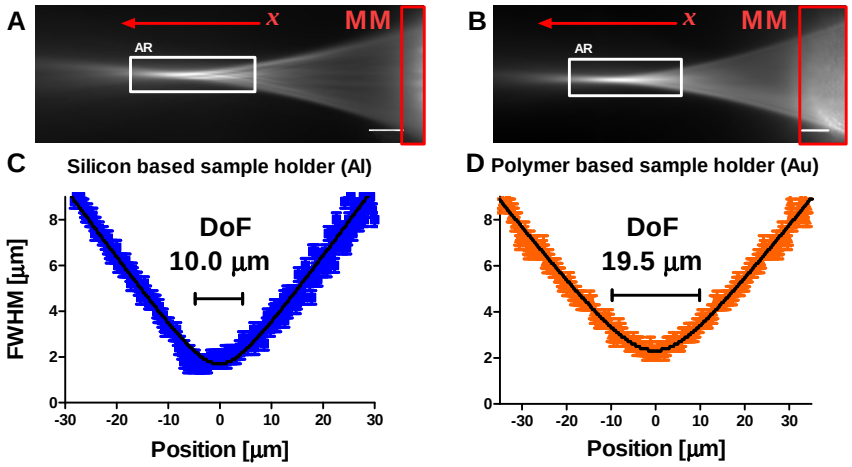

Fig. 6. Characterization of a beam reflected by the tilted micromirror in the silicon based mold (A) and the polymer based mold (B). The beam is imaged by filling the channel in both sample holders with a solution of 10 µM ATTO647. The red rectangles indicate the position where the excitation beam is reflected on the micromirrors (MM) while the white rectangle indicates the analyzed region (AR). The red arrows indicate the direction of the propagation of light. Scale Bar = 16 µm. (C) and (D) The FWHM of the beam was determined along its optical axis in the analyzed region. The beam profile is fitted with Eq. (1) (black line). The silicon based mold had a beam waist of 1.6 ± 0.3 µm (FWHM) and a DoF of 10.0 ± 1.0 µm. The polished polymer chip was found to have a beam waist of 2.4 ± 0.3 µm (FWHM) and a depth of focus (DoF) of 19 ± 0.3 µm.

The average contrast values are plotted in Fig. 7 as a function of Cy5 concentration. It is to be noted that more and more nanospheres become indistinguishable from the background as the concentration of Cy5 increases. The contrast for those invisible particles is put to zero in the calculation of the average contrast values. Thus, the average contrast was calculated presuming the same number of particles as registered in the

videos without Cy5. The results in Fig. 7 are compared with the contrast values of the same nanospheres imaged with a home-build epi-fluorescent microscope[18]. The contrast obtained using light sheet illumination with the silicon- or the polymer- based mold is at least two times higher compared to epi-fluorescence microscopy.

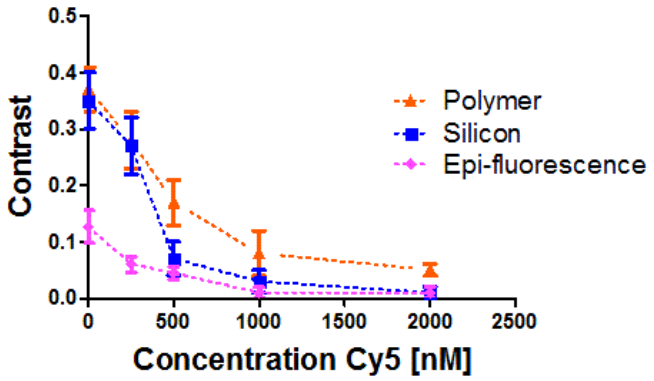

Fig. 7. Contrast comparison between light sheet illumination in the master component and epi-fluorescence illumination. Contrast was determined for fluorescent nanospheres suspended in solutions with increasing concentration of the red fluorescent dye Cy5. Measurements were performed in both molds and compared with normal epi-fluorescence imaging.

BEAM CHARACTERIZATION AND CONTRAST IN THE REPLICATED SAMPLE HOLDERS

As described previously, the silicon and polymer based sample holders are replicated in a UV-curable epoxy. The replicated sample holders, coated with aluminium, are tested and their performance in terms of beam profile and contrast achieved are compared to the performances of their master component in Fig. 8. Replicas from the silicon based mold show a rather asymmetric profile, see Fig. 8C. The minimal FWHM W_0 is 2.6 ± 0.3 μm, that is, replicas from the silicon based mold have a beam waist about 1.5 times wider than the beam waist of the master component. At the same time the DoF_{eff} enlarged slightly from 10.0 to 12.0 ± 0.5 μm. Replicas from the polymer based mold are found to have more regular beam profiles, see Fig. 8D. Their W_0, 1.9 ± 0.3 μm for the aluminium coated micromirror, is slightly better than the master component, which was 2.4 ± 0.3 μm. Correspondingly the DoF_{eff} decreased slightly from 19 to 17.3 ± 1.1 μm. This improvement could be due to small roughness's present in the master component that are smoothed out in the replication process. As a consequence, the contrast of replicated sample holders based on the silicon master mold in Fig. 8E is worse compared to the contrast observed in the silicon based master mold, while the contrast measured in the replicated sample holder based on the polymer master mold shown in Fig. 8F is comparable to the contrast measured in the polymer based master mold.

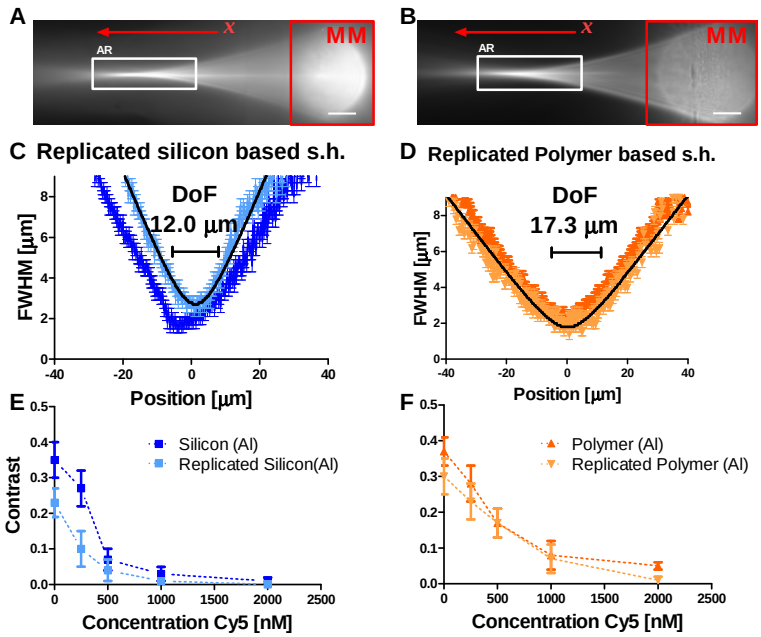

Fig. 8. Characterization of a beam in disposable sample holders replicated from the silicon (A) and polymer (B) based master mold. The beam is imaged by filling the channel in both sample holders with a solution of 10 µM ATTO647. The red rectangles indicate the position where the excitation beam is reflected on the micromirrors (MM) while the white rectangle indicates the analyzed region (AR). The red arrows indicate the direction of propagation of the light. Scale Bar = 16 µm. (C, D) The FWHM of the beam was determined along its optical axis in the analyzed region indicated in figure A and B. The beam profile is fitted with the Eq. (1) (black line). The FWHM profile of the beam imaged using the replicated sample holder is compared to the profile obtained from the master components. The sample holder replicated from the silicon based master component was found to have a beam waist of 2.6 ± 0.3 µm (FWHM) and a depth of focus (DoF) of 12.0 ± 0.5 µm. The sample holder replicated from the polished polymer master component had a beam waist of 1.9 ± 0.3 µm (FWHM) and a DoF of 17.3 ± 1.1 µm. (E and F) Comparison between contrast measured in the replicated sample holders and in the master components of fluorescent nanospheres suspended in solutions with increasing concentration of Cy5.

IMAGING OF SPHEROIDS

Following the successful fabrication and evaluation of the replicated polymer based sample holder, we finally demonstrate that it can be used for light sheet microscopy. An eGFP positive MCF-7 human breast cancer cell line was kindly provided by prof. dr. Olivier De Wever, Ghent University, Belgium. These human breast cancer cells were grown adherently until they reached 70% confluency, after which they were trypsinised and kept in suspension for 72h at 37°C, 5% CO_2 under constant gyratory shaking (70 rpm) to allow spheroid formation. The spheroids were then placed into the replicated sample holder and imaged in light sheet mode, shown in Fig. 9. The fluorescence that is back-reflected by the tilted mirror towards the camera is removed by cropping of the images so that the tilted mirror is no longer visible. The spheroid was imaged from bottom to top by moving the objective lens downward in 1 μm steps. This changes the incidence position of the illumination beam on the micromirror, so that the z-position of the horizontal light sheet in the microchannel is also changed. It is to be noted that this procedure also causes a lateral shift of the light sheet focus, which is compensated by appropriately adjusting the T.a telescope shown in Fig. 4. The difference in contrast is remarkable in comparison with standard epi-fluorescent microscopy. In light sheet mode it is possible to identify single cells and their positions throughout the spheroid while this is not possible in the epi-fluorescence images. It demonstrates that high-quality light sheet imaging is possible with our sample holders replicated from the polymer master component.

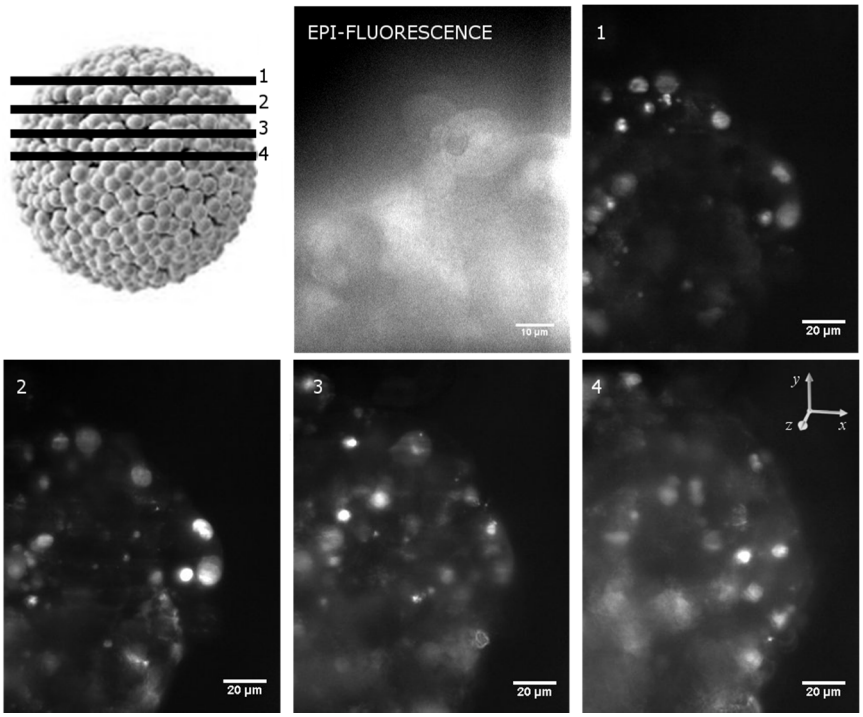

Fig. 9. Images of MCF-7 human breast cancer spheroids at different planes. Cells were imaged from bottom to top and the z-planes were 1 µm apart.

DISCUSSION AND CONCLUSION

In recent years, the interest of the scientific community in light sheet microscopy has steadily increased and the field has seen rise in applications [7, 19, 20]. However, in its typical configuration LSFM relies on at least two objective lenses that are placed orthogonally close to one another. For objective lenses with long working distances this is not a problem, but naturally this means that the numerical aperture, and therefore resolution, is limited. Therefore, for high resolution imaging, other solutions are required. In addition, such an orthogonal double lens configuration is not easily compatible with standard microscopy

bodies, thus hindering its widespread use in the biological community.

One solution consists of delivering the light sheet from the opposite direction of the detection lens and making use of a reflective surface close to the sample so as to reflect the light sheet horizontally into the sample. Leica, for instance, uses this approach in its commercial light sheet microscope. On an inverted microscope, they make use of two opposing 45° mirrors that are attached to the condenser lens of the diascopic illumination arm. For light sheet imaging, the sample is mounted in hydrogel on a petri dish and the 45° mirrors are lowered so that they are placed around the gel-mounted sample. Laser light is coupled into the diascopic illumination arm and is reflected horizontally. By rapid scanning of the laser beam in one direction, a light sheet is emulated in the sample and imaging is realized through the microscope's objective lens. While this configuration is well suited for imaging larger organisms, like e.g. C. Elegans, it is not readily suited for imaging adherent cell cultures. An alternative solution was put forward by Gebhardt and his colleagues [21] who used a tipless AFM cantilever for horizontal reflection of the light sheet beam in adherent cell cultures. It allowed the use of high numerical aperture lenses and consequently the generation of a submicrometer light sheet, apt to illuminate single cells as close as 2 μm from the coverslip. While a technological feat, this approach requires addition of specially manufactured AFM cantilever holder and separate optics to provide light sheet illumination incident onto the AFM cantilever, all mounted to a fluorescence microscope, which adds another layer of complexity.

A more practical approach would be to provide the light sheet in the sample through the same objective lens that is used for

imaging on a fluorescence microscope. In 2013 our group demonstrated on-chip single lens light sheet imaging by making use of a microfluidic chip with an integrated planar waveguide [13]. Excitation light was delivered into the chip by butt coupling of a fiber coupled laser to the planar waveguide. The excitation light then emerges as a wide but thin sheet of light in the measurement microchannel. While the contrast enhancement was shown to be beneficial for accurate nanoparticle tracking in suspension, the general use of this device for imaging purposes is limited due to the light sheet being fixed in space. Galland et al. instead recently developed microfluidic sample holders with integrated reflective micromirrors which allow horizontal reflection of the excitation light sheet after it passes through the microscope's objective lens [14]. Such a design is compatible with high NA objective lenses and only requires appropriate beam shaping, which can be done before the laser beam is sent into the microscope body. The sample holders are made of a UV-curable polymer, index matched with the cell medium, and are obtained through replication from a silicon wafer with tilted microchannel walls prepared by anisotropic wet etching and dry etching.

Here we evaluated if a less complicated approach could be used to fabricate micromirrors. The process starts from an inexpensive PI wafer which is polished at 45°, cut in smaller parts and attached to a microscope slide. We achieved an on-chip light sheet thickness of 2.3 µm (FWHM) at 638 nm for the polymer micromirrors, which was slightly worse than the 1.7 µm (FWHM) at 638 nm for micromirrors prepared in silicon by anisotropic wet etching. However, the optical quality of replicated sample holders was better for those prepared from the polymer master mold as compared to those prepared from the silicon master mold. This shows that our approach based on an inexpensive polished

polymer plugs is very well suited for upscaling of sample holders with integrated micromirrors for single-lens LSFM. The suitability of those replicated sample holders for LSFM microscopy was demonstrated by imaging breast cancer spheroids.

Such disposable sample holders with integrated micromirrors allow single-lens light sheet microscopy on chip. As it only requires minor modifications in the light path between the laser and the microscope body, the technique can be readily implemented on any research grade epi-fluorescent microscope and should allow the transfer of this technology to less specialized laboratories.

In summary, we proposed and tested a different approach to fabricate sample holders with integrated micromirrors for single-lens light sheet microscopy. The master mold obtained by polishing of an inexpensive polymer wafer was compared to a previously reported master mold obtained by anisotropic Si etching. While the optical quality of the Si master mold was slightly better than that of the polished polymer wafer, replica's from the latter made from UV-curable epoxy turned out to have the best performance. The usability of those replicas was demonstrated by capturing high-quality images of human cancer spheroids. Taken together our work shows that single lens LSFM has the potential to become an accessible imaging modality that is compatible with standard fluorescence microscopes available in most cell biology labs.

APPENDIX

Fabrication procedure of the silicon based master mold

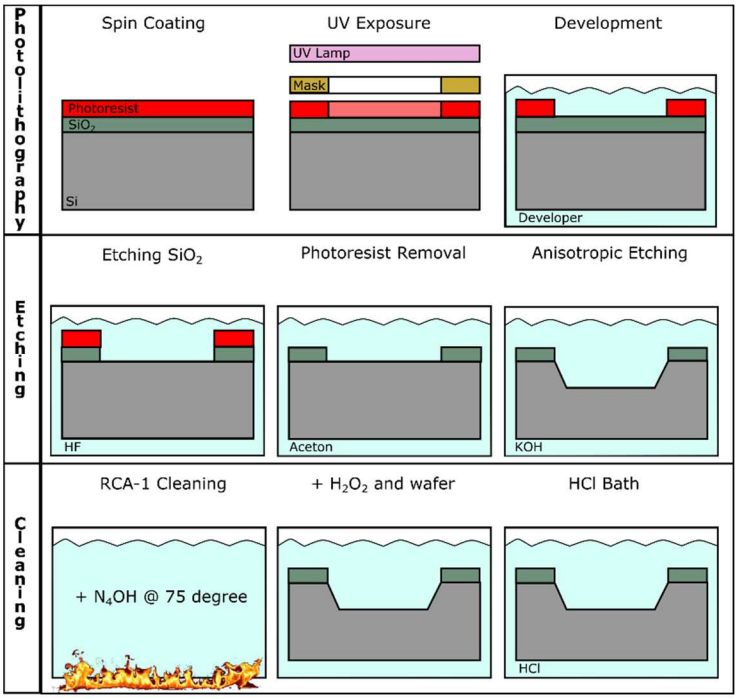

Fig. 1 SI Fabrication procedure of the silicon based master mold. The process is divided in three parts, namely photolithography, etching and cleaning. A thermo-oxidized wafer (silicon dioxide layer: 1 µm thick) is spin coated with a primer and subsequently with a positive photoresist, both followed by a 3 minutes baking step at 110°C. Afterwards, the wafer is covered with a chrome mask, that defines the position of the tilted walls and the channel, and subsequently exposed to UV light for 200 seconds. The wafer is immersed for 90 s in an aqueous solution consisting of 1 part Developer 400K and 2 parts distilled water in order to remove the UV illuminated regions of the photoresist. In the subsequent etching step, the wafer is placed for 16 min into a buffered 7:1 HF solution that dissolves the unprotected regions of the silicon dioxide and exposes the underlying bare silicon. Next, the wafer is placed for 5 min in an

ultrasonic bath filled with acetone to remove the photoresist layer. Then the wafer is put into a stirred KOH bath (KOH/Water/IPA 20/64/16) at 70°C that will selectively remove silicon in the <100> crystal direction, thus etching the channel with tilted walls at approximately 40 µm/hour. A careful monitoring of the etch rate by means of temperature and concentration of the etchant is of utmost importance since the etch rate can influence the wall roughness. Finally an RCA-1 clean was performed as follows. A solution of 5 parts water, 1 part 27% ammonium hydroxide and 1 part 30% hydrogen peroxide is heated at 70°C, then the wafer is soaked in the solution for 15 min, rinsed with water and put for 5 min into a 5% HCl solution

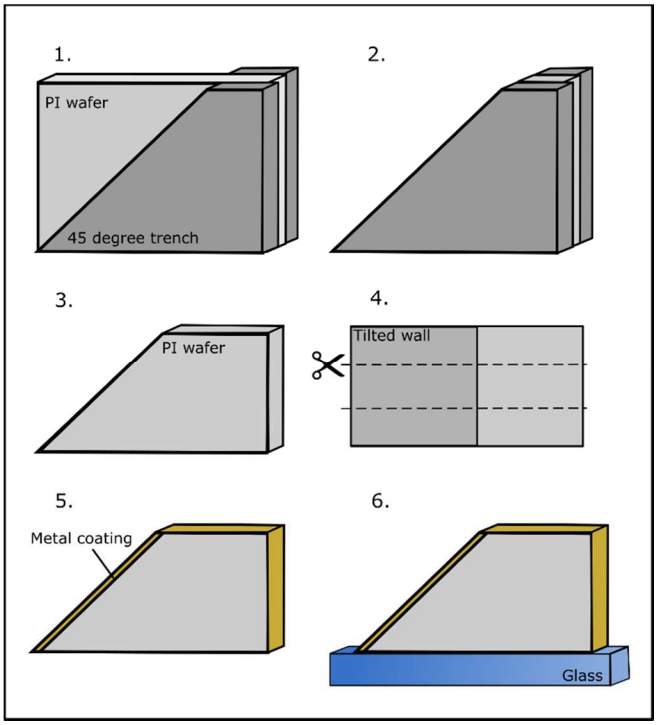

Fig. 2 SI. Fabrication procedure of the polymer-based master mold. 1. A 500-µm-thick flexible PI wafer is clamped in a special PMMA device with a 45° trench. 2. The device is polished to provide a 45° polished end facet to the PI wafer. 3. The wafer is polished and thinned down at both sides to the desired thickness. This step also removes unwanted edge defects. 4. The wafer is cut

into small parts of the desired length and width by a wafer dicer with a diamond coated blade. 5. The tilted end facets are then coated with a 120-nm-thin gold layer by vapor deposition, or with an aluminum layer applied by sputtering. 6. The polymer plug is now ready to be glued to a microscopy slide.

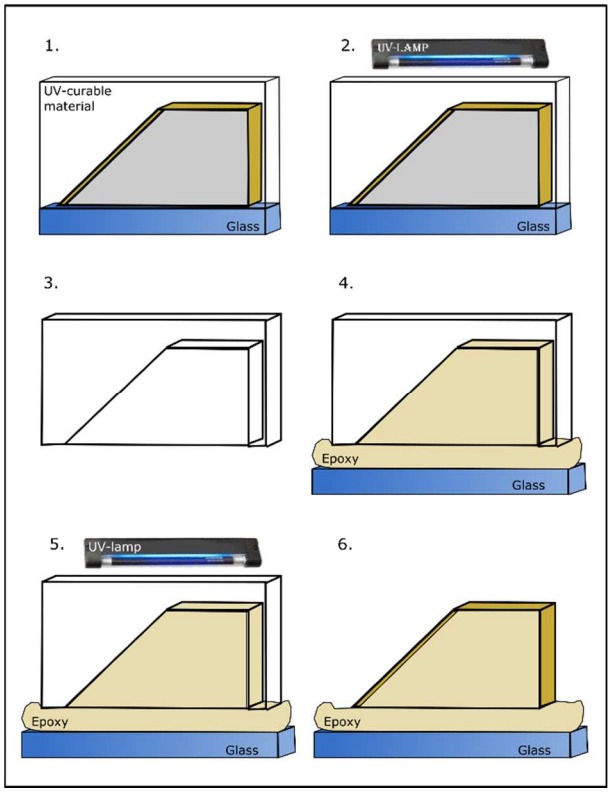

Fig. 3 SI. Schematic overview of the replication process. 1. The polymer or silicon based master components are covered with a UV-curable, transparent fluorinated molding material. 2. The molding material is polymerized by UV illumination. 3. The polymerized mold is easily peeled off from the master component. 4. The material is used as a stamp to fabricate the actual replicas. A drop of a UV-curable epoxy is thus dispersed on a glass slide and the molding stamp is peeled off. 6. The replicated micromirrors are coated with a 200 nm reflective layer of either gold (evaporation) or aluminum (sputtering).

REFERENCES

1. Method of the Year 2014. *Nat Meth* **2015,** *12*, (1), 1-1.
2. Huisken, J.; Stainier, D. Y. Selective plane illumination microscopy techniques in developmental biology. *Development* **2009,** *136*, (12), 1963-75.
3. Mickoleit, M.; Schmid, B.; Weber, M.; Fahrbach, F. O.; Hombach, S.; Reischauer, S.; Huisken, J. High-resolution reconstruction of the beating zebrafish heart. *Nature methods* **2014,** *11*, (9), 919-22.
4. Trivedi, V.; Truong, T. V.; Trinh le, A.; Holland, D. B.; Liebling, M.; Fraser, S. E. Dynamic structure and protein expression of the live embryonic heart captured by 2-photon light sheet microscopy and retrospective registration. *Biomed Opt Express* **2015,** *6*, (6), 2056-66.
5. Vladimirov, N.; Mu, Y.; Kawashima, T.; Bennett, D. V.; Yang, C. T.; Looger, L. L.; Keller, P. J.; Freeman, J.; Ahrens, M. B. Light-sheet functional imaging in fictively behaving zebrafish. *Nature methods* **2014,** *11*, (9), 883-4.
6. Bouchard, M. B.; Voleti, V.; Mendes, C. S.; Lacefield, C.; Grueber, W. B.; Mann, R. S.; Bruno, R. M.; Hillman, E. M. C. Swept confocally-aligned planar excitation (SCAPE) microscopy for high-speed volumetric imaging of behaving organisms. *Nat Photon* **2015,** *9*, (2), 113-119.
7. Pampaloni, F.; Richa, R.; Ansari, N.; Stelzer, E. H. K., Live Spheroid Formation Recorded with Light Sheet-Based Fluorescence Microscopy. In *Advanced Fluorescence Microscopy: Methods and Protocols*, Verveer, J. P., Ed. Springer New York: New York, NY, 2015; pp 43-57.
8. Cella Zanacchi, F.; Lavagnino, Z.; Faretta, M.; Furia, L.; Diaspro, A. Light-Sheet Confined Super-Resolution Using Two-Photon Photoactivation. *PloS one* **2013,** *8*, (7), e67667.
9. Lavagnino, Z.; Sancataldo, G.; d'Amora, M.; Follert, P.; De Pietri Tonelli, D.; Diaspro, A.; Cella Zanacchi, F. 4D (x-y-z-t) imaging of thick biological samples by means of Two-Photon inverted Selective Plane Illumination Microscopy (2PE-iSPIM). *Scientific reports* **2016,** *6*, 23923.
10. Krzic, U.; Gunther, S.; Saunders, T. E.; Streichan, S. J.; Hufnagel, L. Multiview light-sheet microscope for rapid in toto imaging. *Nat Meth* **2012,** *9*, (7), 730-733.
11. Reynaud, E. G.; Peychl, J.; Huisken, J.; Tomancak, P. Guide to light-sheet microscopy for adventurous biologists. *Nat Meth* **2015,** *12*, (1), 30-34.
12. Ritter, J. G.; Veith, R.; Veenendaal, A.; Siebrasse, J. P.; Kubitscheck, U. Light sheet microscopy for single molecule tracking in living tissue. *PloS one* **2010,** *5*, (7), e11639.

13. Deschout, H.; Raemdonck, K.; Stremersch, S.; Maoddi, P.; Mernier, G.; Renaud, P.; Jiguet, S.; Hendrix, A.; Bracke, M.; Van den Broecke, R.; Roding, M.; Rudemo, M.; Demeester, J.; De Smedt, S. C.; Strubbe, F.; Neyts, K.; Braeckmans, K. On-chip light sheet illumination enables diagnostic size and concentration measurements of membrane vesicles in biofluids. *Nanoscale* **2013**.
14. Galland, R.; Grenci, G.; Aravind, A.; Viasnoff, V.; Studer, V.; Sibarita, J. B. 3D high- and super-resolution imaging using single-objective SPIM. *Nature methods* **2015,** *12*, (7), 641-4.
15. Franssila, S., Anisotropic Wet Etching. In *Introduction to Microfabrication*, John Wiley & Sons, Ltd: 2010; pp 237-254.
16. Bosman, E.; Van Steenberge, G.; Milenkov, I.; Panajotov, K.; Thienpont, H.; Bauwelinck, J.; Van Daele, P. Fully Flexible Optoelectronic Foil. *Selected Topics in Quantum Electronics, IEEE Journal of* **2010,** *16*, (5), 1355-1362.
17. Ritter, J. G.; Veith, R.; Siebrasse, J. P.; Kubitscheck, U. High-contrast single-particle tracking by selective focal plane illumination microscopy. *Optics express* **2008,** *16*, (10), 7142-52.
18. Braeckmans, K.; Buyens, K.; Bouquet, W.; Vervaet, C.; Joye, P.; De Vos, F.; Plawinski, L.; Doeuvre, L.; Angles-Cano, E.; Sanders, N. N.; Demeester, J.; De Smedt, S. C. Sizing nanomatter in biological fluids by fluorescence single particle tracking. *Nano Lett* **2010,** *10*, (11), 4435-42.
19. Ahrens, M. B.; Orger, M. B.; Robson, D. N.; Li, J. M.; Keller, P. J. Whole-brain functional imaging at cellular resolution using light-sheet microscopy. *Nat Methods* **2013,** *10*, (5), 413-20.
20. Jemielita, M.; Taormina, M. J.; Burns, A. R.; Hampton, J. S.; Rolig, A. S.; Guillemin, K.; Parthasarathy, R. Spatial and Temporal Features of the Growth of a Bacterial Species Colonizing the Zebrafish Gut. *mBio* **2014,** *5*, (6).
21. Gebhardt, J. C.; Suter, D. M.; Roy, R.; Zhao, Z. W.; Chapman, A. R.; Basu, S.; Maniatis, T.; Xie, X. S. Single-molecule imaging of transcription factor binding to DNA in live mammalian cells. *Nature methods* **2013,** *10*, (5), 421-6.

CHAPTER 3

SINGLE PARTICLE TRACKING FOR STUDYING NANOMATERIAL DYNAMICS: APPLICATIONS AND FUNDAMENTALS IN DRUG DELIVERY

This chapter is published as:

E. Zagato[1,2], K. Forier[1,2], T. Martens[1,2], K. Neyts[2,3], J. Demeester[1], S. De Smedt[1], K. Remaut[1], K. Braeckmans[1,2] . Single-particle tracking for studying nanomaterial dynamics: applications and fundamentals in drug delivery. *Nanomedicine (Lond)* **2014,** *9*, (6), 913-27.

[1]*Laboratory of General Biochemistry and Physical Pharmacy, Ghent University, Belgium*
[2]*Center for Nano- and Biophotonics, Ghent University, Belgium*
[5]*Liquid crystals and Photonics Group, Ghent University, Belgium*

ABSTRACT Many macromolecular therapeutics could potentially treat genetic disorders and cancer. They have however not reached the clinical stage yet due to a lack of suitable carriers that can bring the therapeutics from the administration site to the subcellular site in target cells. One of the reasons that is hindering the development of such carriers is the limited knowledge of their transport dynamics and intracellular processing. Single Particle Tracking (SPT) microscopy, thanks to its single molecule sensitivity and its broad applicability, has found its entry in the field of drug delivery to get an answer to these questions. This review aims to introduce the fundamentals of SPT to the drug delivery community and highlight the most recent discoveries obtained with SPT in the field of drug delivery.

INTRODUCTION

Many macromolecular therapeutics based on nucleic acids show potential for the treatment of a wide variety of genetic disorders, viral infections and cancer[1]. Despite recent successes[2, 3], the delivery of drug and/or nucleic acid material inside target cells is still a challenging task. Naked nucleic acids are often prone to degradation and require to be incorporated into a nanocarrier system[4]. This nanocarrier has to cross the many different biological barriers illustrated in figure 1 before releasing its cargo at the intended (subcellular) site[1]. First, it should be able to find its way in the body to the target cell, then it has to enter inside this cell and all along protect its cargo until it reaches the desired subcellular compartment, being the cell nucleus, as in the case of plasmid DNA delivery, or the cytoplasm, as in the case of small interfering RNA.

One of the major difficulties in the development of a safe and successful nanocarrier is the limited knowledge about the extra- and intra- cellular processing of such nanoparticles[5]. This is partly due to the strong dependence of cellular uptake mechanisms on the cell type and partly due to the insufficient knowledge of the physicochemical and biophysical properties of a nanoparticle when it interacts with a complex biological environment, such as the cytosol[5, 6].

Highly sensitive, advanced light microscopy techniques are thus necessary to study the intracellular, as well as the extracellular, processes[6-8]. Amongst those, Fluorescence recovery after photobleaching (FRAP), fluorescence correlation spectroscopy (FCS) and Single Particle Tracking (SPT) have proven particularly useful in the field of drug delivery[6]. FRAP, however, requires a high and uniform nanoparticle concentration with good control

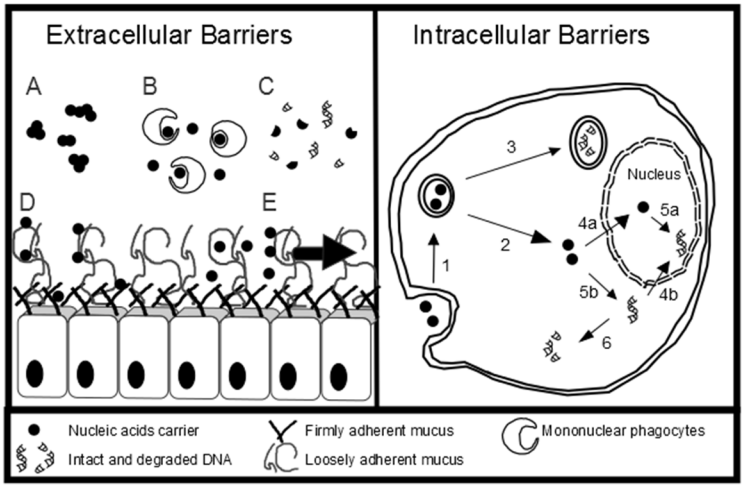

Figure 1: Schematic representation of the biological barriers a nucleic acid-based nanomedicine may encounter. **Extracellular Barriers**: upon administration, the nanomedicine will interact with biological fluids, like blood and intraperitoneal fluids, full of salts, proteins and phagocytes. As a consequence, the nanomedicine may form aggregates (A), be removed from circulation (B) or lose its cargo before it reaches the cells of interest (C). Moreover, many surfaces inside the body are covered by mucus. Thus, the nanomedicine must avoid to be trapped into the mucin mesh (D) and must reach the delivery site before it is removed by the mucus clearance mechanism (E). **Intracellular Barriers**: after reaching the delivery site, the nanomedicine must cross the cell membrane and enter inside the cell via endocytosis (1). The nanomedicine should then be able to escape from the endosome and reach the perinuclear region (2) before it is degraded (3). Once in the perinuclear region, it may enter inside the nucleus (4a) and there release its cargo (5a) or release its cargo in the cytoplasm (5b) where it will most likely be degraded by nucleases (6) if it doesn't enter inside the nucleus (4). Thanks to SPT, it is now possible to monitor the aggregation of nanoparticles in biological fluids [9-11] and their concentration [12, 13]. SPT has been widely used to study the mobility of nanoparticles in mucus [14-16] and vitreous humour[17, 18] and to study the intracellular pathway used by the nanomedicines [19-22].

of the photobleached area, which can be problematic when working in thick light scattering tissues. FCS can deal with lower concentrations but depends on careful calibration of the detection volume, which is difficult to do in biological tissues. Moreover, both FRAP and FCS provide ensemble average measurements based on the signal from a large number of particles. Thus, rare stochastic events are easily missed. On the contrary, SPT can monitor the movement and obtain mobility information of individual nanoparticles.

In the context of nanomedicine research SPT is sometimes referred to as Multiple Particle Tracking (MPT) to underscore the fact that multiple nanoparticles are tracked simultaneously. As illustrated in figure 2, SPT tracks the movement of fluorescently labeled particles in a (biological) sample. From the analysis of the trajectories, one can obtain information about the particles and their interaction with the surrounding environment[7, 8]. SPT also allows to study the porosity and microrheological properties of materials. For instance, the microviscosity and pore dimensions of tissues like vitreous, mucus and brain extracellular space have been investigated by SPT[18, 23, 24], and information on the interaction of the particles with these tissues led to the optimization of their surface chemistry[9, 14, 17, 25]. When both the particles and the intracellular components of interest are labeled with spectrally different labels, co-localization studies can reveal the intracellular trafficking of the nanoparticle[21, 26, 27], correlate their type of motion with the structures of the cytoskeleton responsible for the motion[28, 29] and spot the bottlenecks of the process[30].

SPT is thus able to study single molecule dynamic behavior in real-time with nanometer spatial resolution. A downside of SPT

is that it requires a low concentration of particles and that extensive image processing is needed to extract the data.

This review will be divided in two parts. First, the most recent applications of SPT to drug delivery will be discussed, from nanoparticle dynamics in extracellular matrices like blood and mucus to transport across the cell membrane and through the intracellular compartments. In a second part, an introduction will be given on the fundamentals of SPT aimed at making this technique more accessible to the non-specialist.

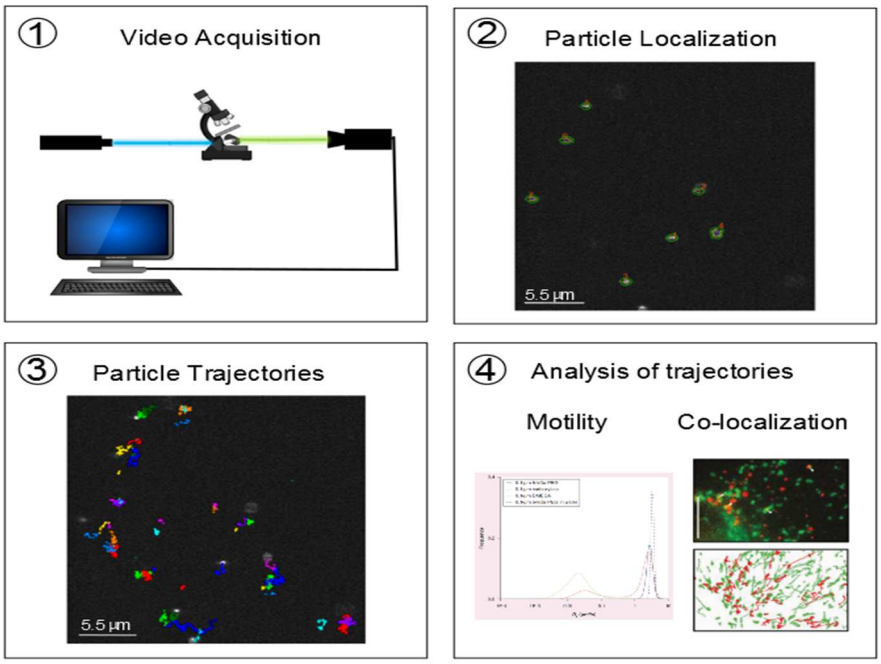

Figure 2: Scheme of an SPT experiment. After recording a suitable amount of SPT time-lapse videos, software processing is used to localize the particle center positions in every frame to obtain the trajectories of the recorded particles. These trajectories hold information on the motion of the particles, such as the diffusion coefficient, velocity, or, in a multicolor configuration, the interaction between the particles and another biological constituent (e.g. endosomes). The figure is partly adapted with permission from Forier et al.[14].

APPLICATIONS OF SPT

Originally applied to study protein membrane dynamics, the use of SPT in the last decade has extended to the study of many aspects in drug delivery: from nanoparticle and drug characterization in biological fluids (plasma, blood, intraperitoneal fluid)[9, 10, 31], over nanoparticle studies in complex extracellular matrices (lung and cervical mucus, vitreous humor, brain extracellular space)[14, 16-18, 24, 32, 33], to studies of intracellular trafficking[21, 30]. A detailed overview for each of those applications is given below.

EXTRACELLULAR ENVIRONMENT

Before a therapeutic drug reaches its target cell, it must be administered. The usual administration routes, depending on the target tissue, are: intravenous, oral, pulmonary and ocular administration. For specific cancer types, for example peritoneal carcinomatosis, also intraperitoneal delivery is being explored[34]. Depending on the delivery route chosen, the drug formulations will have to overcome different extracellular environments (see Fig. 1). The nanomedicines should typically remain highly mobile and should protect the encapsulated therapeutics while avoiding immune-responses by the organism. This is not an easy task as many surfaces inside the body are covered by mucus, a biological film that has evolved to entrap foreign pathogens and exogenous particles. Also, the circulatory system itself is packed with mononuclear phagocytes and serum nucleases ready to destroy exogenous nanoparticles and nucleic acids. Furthermore, the high concentration of salt and proteins present in blood and mucus can significantly destabilize the carrier and its load[1], causing loss of therapeutic efficiency, reduced cellular uptake[35], the formation of a protein corona that may lead to altered surface properties and

targeting[36] as well as unwanted aggregation[6]. It is thus fundamental to study the physicochemical behavior of the nanomedicine in these environments.

Intravenous administration

SPT was recently shown by our group to be the first technique that can monitor concentration and aggregation of fluorescently labeled nanoparticles in undiluted biological fluids like plasma and whole blood[9, 10, 13, 31]. To allow more precise concentration measurements of biological particles in body fluid, our group recently developed a method to calculate the concentration of freely diffusing monodisperse[13, 37] and polydisperse[38] nanoparticles from their diffusion coefficient.

The first version of our concentration method was used by Naeye et al. while testing the hemocompatibility of dextran nanogels loaded with small interfering RNA (siRNA), a down regulator of mRNA translation, in human plasma and blood[10]. Naeye et al. quantified the percentage of nanogels interacting with blood cells by measuring through SPT the concentration of free diffusing nanogels in blood and in plasma. They discovered that the percentage of nanogels not bound to blood cells or platelets increases with increasing nanogel concentration, suggesting that blood cells quickly saturate. They also used SPT to monitor potential aggregation between siRNA dextran nanogels in human plasma and blood. In another study Braeckmans et al. used SPT to compare the aggregation behavior of cationic DOTAP:DOPE liposomes in undiluted serum, plasma and whole blood, finding that aggregation of the particles in whole blood was worse as compared to plasma and serum[9]. These results underline the necessity to test the stability of the particles directly in the relevant biofluid, rather than derived or diluted components, and that shielding the dextran nanogels as well as DOTAP:DOPE

nanoparticles with a sufficiently dense polyethylene glycol (PEG) coating is necessary to prevent their aggregation.
Following their example, Filipe at al. monitored the behavior of fluorescently labeled subvisible IgG aggregates formed by heat stress or pH-shift in buffer and in serum[11]. They showed that aggregates mostly in the sub-micron range, formed by pH-shifts, tend to form larger aggregates after 24 h incubation, while aggregates mostly in the sub-micron range, formed by heat stress, remain stable. This finding stresses the importance to find analytical strategies to monitor aggregation in undiluted body fluids.

Brain-targeted administration

Delivering substances to the cells of the brain is no easy task. The blood-brain barrier is a well-known impediment for the delivery of therapeutics in the brain parenchyma [39]. Nowadays, methods to improve drug penetration into brain tissues exploit the enhanced permeation and retention (EPR) effect, typical of blood vessel disrupted by tumors or inflammations, or make use of a minimally invasive therapeutic procedure, like localized convection-enhanced delivery (CED), to directly infuse drugs and drug-loaded nanoparticles into the brain. These strategies however may become ineffective if the drug-loaded nanoparticles cannot pass through the brain's extracellular space (ECS) and reach the desired target cells. Previously, Thorne et al. reported the dimension of rat cortical ECS pores to be less than 64 nm[40]. However a recent study, conducted by observing the mobility of polystyrene nanoparticles densely coated with 5 kDa PEG chains by SPT, shows that nearly 30% of pores in human, rat and mouse brain are bigger than 100 nm and that densely coated nanoparticles as big as 114 nm can rapidly penetrate into human and rat brain tissue[24]. These results underline the importance of

defining the critical particle characteristics that will allow a greater dispersion of drug into the brain and a higher drug-loading efficiency.

Oral, Pulmonary and Vaginal administration

Sometimes it is preferential to deliver the therapeutics directly to the gastrointestinal, respiratory or vaginal tracts[41, 42]. In this case the nanoparticles have to pass through the layer of mucus which lines these mucosal membranes. Mucus consists of cross-linked mucin fibers coated with a complex array of proteoglycans and forms a highly heterogeneous mesh[43]. This mucus barrier is at present the main obstacle to the treatment of various mucosal diseases, including cystic fibrosis and inflammatory diseases of the gastrointestinal and vaginal tracts[43, 44]. The difficulties for the delivery of therapeutic drugs to the cells underlying the viscous and sticky mucus layers are usually aggravated by the rapid mechanism of mucus clearance which removes the therapeutic drugs from the delivery site within minutes or hours[15]. Many efforts are put into engineering muco-inert nanoparticles that can penetrate this formidable barrier[15, 45]. SPT is a valuable and powerful tool to study the mobility of various fluorescently labeled nanoparticles into mucus samples. Studies using fluorescently labeled nanomedicines have proven to be instrumental in determining the optimal physicochemical characteristics for mucus-penetrating nanoparticles[14, 16, 32, 44]. For pulmonary therapy, the particles must be smaller than 200 nm and densely coated with low MW (between 2 and 5 kDa) PEG chains. For vaginal administration, particles as big as 500 nm in diameter can diffuse rapidly into the mucosal layers, provided that they are densely coated with low MW PEG chains[25, 32]. Such nanoparticles will be able to resist binding via hydrophobic, cationic and hydrogen bonding interactions and to pass through

the pores of the mucin mesh. It has been suggested that the major protection mechanism of the mucus relies mostly upon mucoadhesion rather than on steric obstruction[23]. Moreover, the vaginal mucus structure has been shown to adapt to environmental changes, e.g. by shrinking the pore size in presence of non-ionic detergents[23] or a high concentration of hydrophobic particles[25]. This suggests that the pore size of the vaginal mucus may be altered for therapeutic or prophylactic purposes by topical administration of surface-active agents. The size of the pores has been calculated from SPT measurement by fitting the transport rates of various sized PEG-coated polystyrene particles to an obstruction-scaling model[16, 23, 46].

Ocular administration

Many chronic and progressive eye disorders affecting the retina may benefit from nanomedicines or gene therapy[47]. From the drug delivery point of view however, the eye is shielded from systemic circulation by the blood-retina barrier and from the outside by the corneal epitelium, both limiting the accessibility of intravenously injected or topically applied macromolecular compounds, respectively. Administration directly in the ocular environment is therefore currently the method of choice, not in the least because it is easily accessible and lacks systemic spread due to both ocular barriers. Intravitreal injection delivers the nanomedicines in the central part of the eye, the vitreous humor, a hydrated biogel composed of mostly hyaluronic acid (HA) and collagen. For the nanomedicines to effectively reach the retina, located at the periphery of the eye, the nanoparticles should remain mobile in this vitreous gel. It has been shown before that the vitreal network poses a significant barrier for the mobility of nanoparticles[48, 49]. Not surprisingly, SPT has been recently used to relate optimal intravitreal mobility to the ideal characteristics

of drug- and gene-loaded nanoparticles in the vitreous of the eye[17, 18]. As a matter of fact, SPT is one of the few techniques that allow imaging of nanoparticles directly inside intact vitreous, permitting to get information of their behavior with minimum artifacts. The ideal drug- or gene- carrier targeted to retinal cells must have a high mobility in the intact vitreous body, while keeping the interaction with the other vitreal components to a minimum. Recently our group developed a robust assay to evaluate and compare intravitreal mobility of nanoparticles in the intact vitreous body. Our studies[17], confirmed by the results obtained by Xu et al.[18], show that cationic nanoparticles are mostly immobilized in vitreous, while a negatively charged and hydrophilic surface should promote optimal intravitreal mobility to nanoparticles in the submicron range.

INTRACELLULAR TRAFFICKING

Once the nanomedicine particle carrier reaches its target cell, it needs to be internalized and reach the intended subcellular target site (see Fig. 1). As still relatively little is known about the uptake and intracellular processing of nanoparticles, efficient and specific intracellular delivery of therapeutic agents remains a major issue. Research in the last decade has clearly demonstrated that endosomal uptake and the subsequent trafficking of nanoparticles through endosomal compartments is a complex process that depends on many parameters, including the type of nanoparticle (chemical composition, charge, size, surface functionalization etc.)[50, 51], cell type[5, 52], cell cycle[53] and surface adsorbed proteins (the so-called protein corona)[35, 36]. Consequently, more and more it is being appreciated that a detailed understanding of their intracellular processing is needed for rational optimization of their structure and composition[1, 5, 7, 8,

[51, 54-56]. In recent years, SPT has proven to be an efficient and reliable tool to characterize and evaluate the intracellular processing of nanomedicines, as discussed below.

Biophysical analysis of intracellular nanoparticle mobility

SPT is used extensively to study the behavior of nanoparticles in the cell and to probe the local environment surrounding the nanoparticle. The most common type of mobility analysis is based on the nanoparticle's mean square displacement (MSD, see technical part for more details) that can reveal if its motion is hindered by obstacles, if it is confined into a sub-compartment or if it is enhanced by some mechanism of active transport. One common concern when designing new nanomedicine carriers involves the use of a PEG coating. It is believed that PEG coating may protect the particle from degradation by nucleases and acts as a steric barrier that prevents particles from adsorbing to intracellular components.

Suh and co-workers demonstrated that adding 3.2 kDa PEG chains to 100 nm model polystyrene nanoparticles microinjected in the cytoplasm doubles both the percentage of particles that exhibit free diffusion and their average transport rate at long time scales[57]. Kim and co-workers compared the cellular uptake and intracellular mobility of highly compacted DNA nanoparticles with two different molecular weights of PEG, 10 kDa and 5 kDa[20]. They found no difference between the two formulations and suggest to use the lower molecular weight to reduce the mucoadhesivity of the particles in the context of cystic fibrosis treatment.

Engineering nanoparticles that easily enter the cell and possibly circumvent the degradative pathway is a way to improve the transfection efficiency. Functionalization of nanoparticles with ligands for targeting receptors is a strategy to influence

internalization. Trafficking of three different formulations based on linear PEI, one of which targeted to EGFR, was observed in EGFR overexpressing carcinomas cells. EGFR targeting leads to faster and more efficient internalization compared with untargeted particles[29]. Many trajectories could be divided in three phases of motion, all characterized by changes in particle motion and instantaneous velocity. The corresponding movements were correlated with the retrograded actin flow (phase 1), or were typical of nanomedicines located into endosomes transported along microtubules (phase 3), thus confirming the key role played by actin filaments and microtubules in the uptake and intracellular transport of nanomedicine particles, such as PEI/DNA complexes[28].

Particle size influences the delivery route taken, too. While particles bigger than 40 nm are quickly trapped inside lysosomes, sub-25 nm polymeric particles were found to cross the cytoplasm inside non-degradative vesicles that rapidly localize to the periphery of the cell nucleus[58]. Lai and co-workers saw that the motion of vesicles was similar for both pathways, although vesicles from the non-degradative pathway were on average slower than the vesicles from the degradative pathway. Thus they stayed in the perinuclear region for longer times, possibly enhancing the concentration of particles delivered near the nucleus[19]. It has been suggested, based on the limited mobility of DNA in the cytoplasm[59], that delivery of genes close to the nucleus could enhance gene transfection efficiency, although it remains a matter of debate as direct experimental evidence is missing[56].

Analysis of co-localization with endosomal compartments

In the past 10 years, many studies have focused on unraveling the endocytic pathways through which nanomedicines enter cells[54,

[55]. In contrast, it is only in the last few years, thanks to improved live cell imaging methods, that the first studies have emerged (including a pioneering study from the promoter's group) that shed more insight into the intracellular trafficking of nanomedicines[21, 22, 30, 60]. In a multicolor configuration, SPT can provide information on the mobility of each spectrally distinct compound as well as the potential interaction between both compounds. One common strategy is to label endogenous particles, like marker proteins of a selected type of endosome, with an EGFP construct, and label exogenous particles, like the nanomedicine of interest, with a fluorophore that emits in the far red region of the spectrum. A lot of information about the exact endocytic pathway and the intracellular processing can be extracted by quantifying the percentage of particles that are co-localized with the labeled marker protein.

Sahay et al, for example, were able to examine the cellular uptake of siRNA delivered in lipid nanoparticles (LNP) and spot the main bottlenecks of the process[30]. Their analysis shows that the main obstacle for an efficient gene silencing with LNP carrier is the weak endosomal escape.

Similar difficulties were found by Sandin and co-workers[22] and Suh and co-workers[60]. They used live-cell multicolor confocal microscopy and SPT to follow their nanoparticles from the point of internalization to their transfer into late endosomes and lysosomes. Despite the sensitivity of the technique and its ability to observe rare events, like the transfer of the nanoparticles from one endocytic vesicle to another, they could not spot escaping events from the endosomes. In our own group dual color SPT was used to study in detail the trafficking of bioreducible gene polyplexes in retinal pigment epithelium cells. The postendocytic trafficking profile, shown in figure 3, indicates that these cationic

bioreducible polyplexes undergo flotillin-mediated endocytosis or Rab5-mediated endocytosis and are then transferred to late endosomes and lysosomes. The study shows that the polyplexes are still present inside lysosomes and flotillin-coated vesicles after 24 h. Since the trapped particles don't contribute to transfection, this study highlights the importance to study endosomal sorting as it plays a major role in determining the efficacy of intracellular drug release.

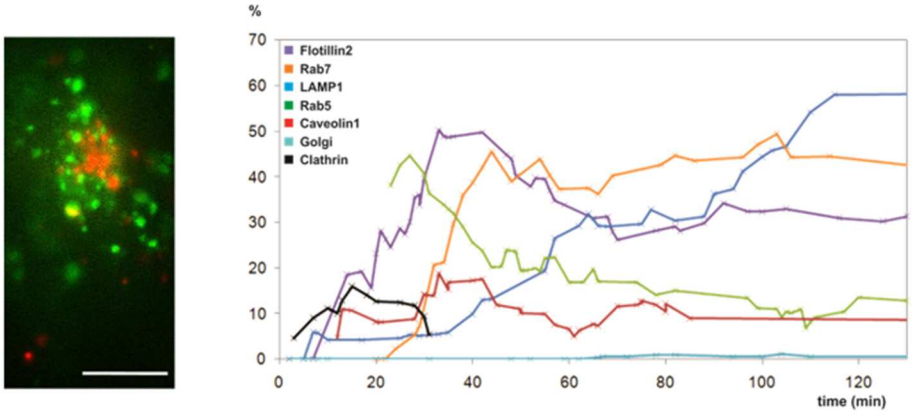

Figure 3: Map of the postendocytic trafficking profile of cationic polyplexes complexed with pDNA in ARPE-19 cells. On the left, an ARPE-19 cell with EGFP-labeled endosomes and Cy5-labeled polyplexes is shown. Scale bar is 10 μm. On the left, the percentage of co-localization of the polyplexes with many type of endosomal vesicles is shown in function of time. The figure is adapted with permission from Vercauteren et al[21]. Copyright 2011 American Chemical Society.

TUTORIAL – THE BASICS OF SPT

SPT is a technique that was developed in the early nineties, and, from its initial implementation, has revolutionized cell studies. Nowadays there are many possibilities linked to it. The quality of the results depends on the best match between optical instrumentation, fluorescent probes and the algorithms used for particle localization, calculation of trajectories and mobility analysis.

The aim of this section is to give an overview of the technical possibilities of SPT and to guide the reader towards the most appropriate experimental conditions and methods of data analysis. We will start with a discussion of the most fundamental aspect of SPT, being the localization of particles, and then explain the experimental conditions and data analysis methods that lead to an optimal localization precision.

PARTICLE LOCALIZATION

The most fundamental aspect of SPT is the localization of particles. Once the particle locations are known, trajectories can be calculated and mobility analysis can be performed. Having acquired SPT movies, the first step is to identify the particles by means of image processing software. Typically this involves removing image background as much as possible to improve the particle contrast. This may be accomplished by using an appropriate filter, such as an unsharp filter or a Gaussian spatial filter[61]. The result is an image where particles appear bright against a much darker background. The particles are then analyzed with an appropriate algorithm to determine their position with nanometer precision. The main methods for calculating the particle position are cross-correlation[62, 63], fitting of a 2D Gaussian function [7, 62] and centroid identification[62]. Cross-

correlation algorithms are based on relative changes in position from one frame to the next and perform well with particles bigger than the illumination wavelength. For smaller objects, Gaussian fitting and centroid identification performs better. While Gaussian fitting performs better with immobilized or slowly diffusing particles, in a recent study it is shown that the centroid algorithm is more robust when particles are moving during the image capture, as is generally the case for SPT experiments[64].
It has been shown that the precision with which stationary particles can be localized with the centroid algorithm can be calculated from:

$$\sigma_C = F\left\{\frac{s_0^2\left(1+\frac{z_{lim}^2}{3z_0^2}\right)+\frac{a^2}{12}}{N} + \frac{81\pi b^2\left(s_0^2\left(1+\frac{z_{lim}^2}{3z_0^2}\right)+\frac{a^2}{12}\right)^2}{4a^2N^2}\right\} \quad (1)$$

z_{lim} is the position along the optical axis in which the particle becomes undetectable[64]. Eq. (1) shows there are basically three major contributions to the localization precision: i) the number of photons *N* collected per particle, ii) the contribution *b* from the background and iii) the image pixel size *a*. Below, it will be discussed how each of those factors can be optimized to obtain optimal localization precision.

Maximizing the number of photons

In order to be able to determine the particle position with good accuracy and precision, the fluorescent probes must emit a large number of photons for the whole duration of the video recording. As a consequence, a good fluorescent probe for SPT should have a high quantum yield of fluorescence emission and a high photostability to ensure acquisition of long and precise trajectories. Furthermore, the label should be as small as possible.

An interesting trick to minimize photobleaching of the fluorescent probe is to use stroboscopic illumination to illuminate the sample only when the camera is actively recording a frame of the video, while the illumination is switched off during the read-out time of the camera.

Many types of probes have been used in SPT in the context of nanomedicine research, including fluorescent proteins, small organic fluorophores, inorganic semiconductors (quantum dots)[65], noble metal nanoclusters[65] and inorganic nanoparticles[65, 66].

Fluorescent proteins have the major advantage of being genetically engineered to be incorporated into specific subcellular structures. This is of interest to study the co-localization of nanomedicine drug delivery systems with specific GFP-tagged intracellular organelles. They suffer, however, from a relatively low molecular brightness and fast photobleaching rates, which makes tracking of molecules labeled with a single fluorescent protein a challenging task. Tracking organelles labeled with multiple copies of fluorescent proteins is very well possible, though[21].

Organic dyes are mostly used to label nanomedicine particles or their cargo. Typically, they are brighter and more photostable than fluorescent proteins, although they also may photobleach if exposed to high laser power. This can be balanced by incorporating a sufficient number of labels, but one should perform proper control experiments to make sure that the labels do not influence the nanoparticle's physicochemical properties.

Inorganic semiconductors instead have the advantage of being more resistant to photobleaching and, therefore, are better suited for long term tracking[65-67]. However, they suffer from blinking due to which trajectories are truncated and their surface needs an

amphiphilic coating in order to be used for biological applications. In addition, currently there is no established general method for labeling of subcellular structures in living cells with quantum dots as they are quite large compared to organic dyes and cannot penetrate through the plasma membrane[68].
Recently, single walled carbon nanotubes (SWNTs)[65, 69], noble metal nanoclusters[65] and fluorescence nanodiamonds (FNDs)[70] have been used for SPT. These new probes should be more photostable with limited toxic effects to cells. One advantage is that their emission can be tuned to the near-infrared range[71] which is useful to image deeper inside tissues.

Minimizing background contribution

The type of illumination that is used to excite the fluorophores can improve contrast and minimize background noise substantially. Epi-fluorescence microscopy, confocal microscopy and total internal reflection fluorescence microscopy (TIRFM), explained in figure 4, have been used the most for SPT[66, 72]. Epi-fluorescence, TIRFM and spinning disk confocal microscopy all make use of a fast sensitive camera, like an EMCCD or a CMOS camera and are as such adapted to follow fast processes. Epi-fluorescence microscopy is the simplest configuration and the most commonly used. It suffers, however, from background noise and low contrast due to out-of-focus fluorescence. Confocal illumination and detection can reduce the background noise and increase contrast considerably. Images in the traditional laser scanning confocal microscopes are formed by a sequential pixel by pixel scanning process, due to which artifacts may be introduced in the apparent particle trajectories. Furthermore, the signal to noise ratio (SNR) is rather low at high frame rates due to the low quantum efficiency of the photomultiplier tubes that are typically used as detectors. For observing fast particle dynamics,

spinning disk confocal microscopy is more suited as it combines confocality with fast imaging and a high SNR since CCD cameras with high quantum efficiency and on-chip signal amplification can be used. For membrane studies, TIRF microscopy is the method of choice. In a TIRF microscope, the light is totally reflected at the interface between two media of different refractive index (usually, a glass substrate and a cell). The evanescent wave that is formed at the boundary cannot penetrate deep in the sample but only excites the fluorophores in a thin layer of about 200 nm near the interface. Although this results in excellent contrast and reduction of out-of-focus fluorescence, the technique is inherently limited to studying processes close to the coverslip, such as the dynamics of plasma membrane components.

An interesting alternative method that was suggested for imaging fast events deep inside living cells, where the signal to noise ratio is low, is light sheet illumination. In light sheet illumination a thin plane is illuminated in the sample that coincides with the focal plane of the detection objective lens. In this way, the sample regions above and below the focal plane are not illuminated and cannot contribute to the background signal. Combined with a fast sensitive CMOS or EMCCD camera, it facilitates the acquisition of images with high contrast up to 200 μm inside living tissue[73-75].

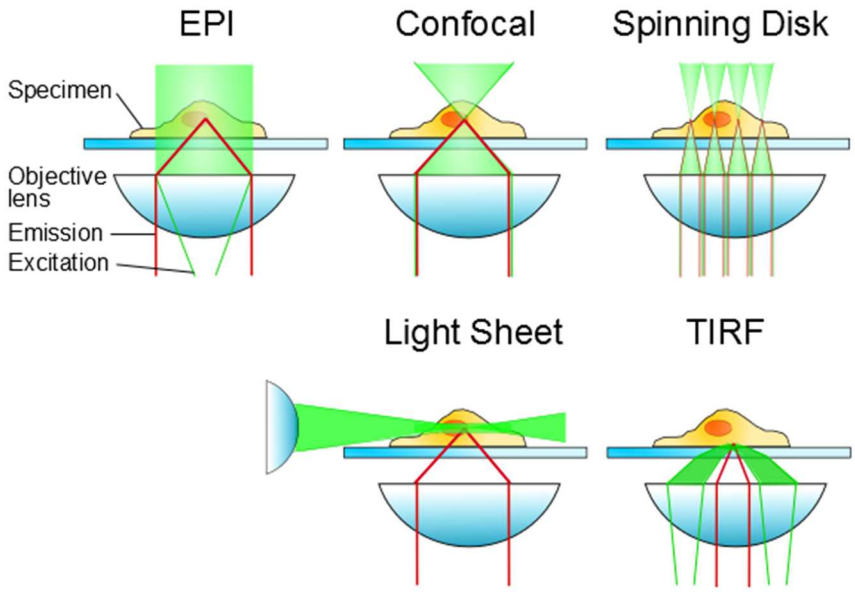

Figure 4: Example of the most common illumination strategies for SPT. The simplest to set up is epi-illumination, but it has the highest background noise due to out-of-focus light. Traditional confocal illumination reduces the background noise, but it is rather slow. Spinning disk confocal microscopy combines fast image acquisition with excellent detection sensitivity when combined with an EMCCD or CMOS camera. TIRF reduces the background noise enormously, but excitation is limited to a few 100 nm above the coverslip. Lastly, light sheet microscopy facilitates the acquisition of images deep inside living tissue by increasing contrast and limiting photobleaching.

Selecting an appropriate pixel size

As mentioned, the image pixel size influences the localization precision, with smaller pixels leading to better precision. Indeed, smaller pixels lead to a better sampling of the particle image so that its center can be determined more precisely. However, pixels should not be too small either. The smaller the image pixel size, the less photons will fall onto a single pixel, leading to a low SNR.

Following the Nyquist criterion, as a rule of thumb the pixel size should be 2-3 times smaller than the radius of the point spread function PSF (that is, the width of the image of a subresolution particle). Using a high-resolution objective lens (e.g. NA 1.4) this means a pixel size of 80-120 nm. The microscope magnification thus needs to be adapted to the physical size of the pixels on the detector. This allows the collection of a sufficient amount of photons per pixel to limit the influence of detector noise, while increasing the precision with which the photons can be localized.

Dealing with particle motion during image capture

In order to obtain an image, the detector needs to collect photons for a certain time, which we refer to as the image acquisition time. If a particle moves during this time, which is to be expected in SPT experiments, the shape of its image can be altered, as illustrated in figure 5. For diffusing particles, the deformation of the particle image is dependent on the diffusion coefficient of the particle and on the image acquisition time, which results in a modified version of eq. (1) to calculate the localization precision[64]. As is to be expected, the more the particle moves during image acquisition, the worse the localization precision will be. Of equal importance is the finding that the popular Gaussian fitting algorithm does not perform reliably in this case, due to the asymmetric shape of the particle's image. Instead, the centroid algorithm performs very well since it does not depend on a particular predefined shape of the particle image.

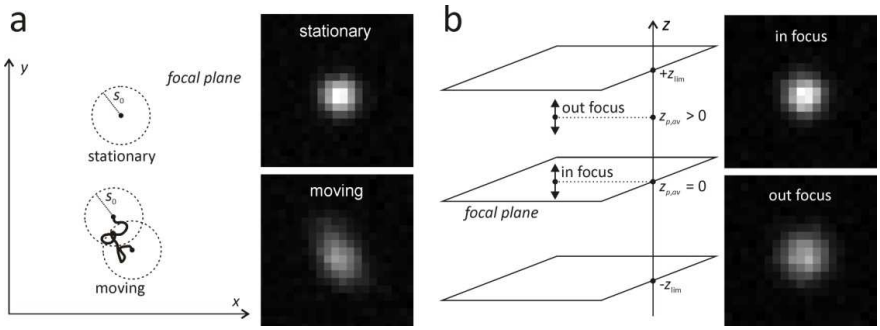

Figure 5: Effect of motion during image acquisition on the particle point spread function PSF. Image (a) illustrates how lateral movement parallel to the focal plane modify the PSF of a particle, making it more difficult to localize the center. S_0 is the standard deviation of the stationary PSF, as approximated by a Gaussian. Image (b) illustrates how axial movement perpendicular to the focal plane influences the PSF. The PSF of the particle out of focus has a higher standard deviation than the PSF of the particle in focus. Copyright Wiley-VCH Verlag GmbH & Co. KGaA. Reproduced with permission from Deschout et al.[64].

TRAJECTORY ANALYSIS

To construct trajectories, the simplest and computationally fastest algorithm is the nearest neighbor algorithm[76]. It simply connects positions of particles that are closest to each other in subsequent frames, if these positions are within a plausible distance. Some more advanced methods were proposed to address particular issues, such as blinking of quantum dots[63]. Most methods require low particle density to have unambiguous particle correspondence, thus limiting the amount of data collected per experiment and rendering the capture of rare events less likely. When a high density of particles is required, a multiple-hypothesis tracking method can solve problems related to particle overlap and disappearance. This method constructs all

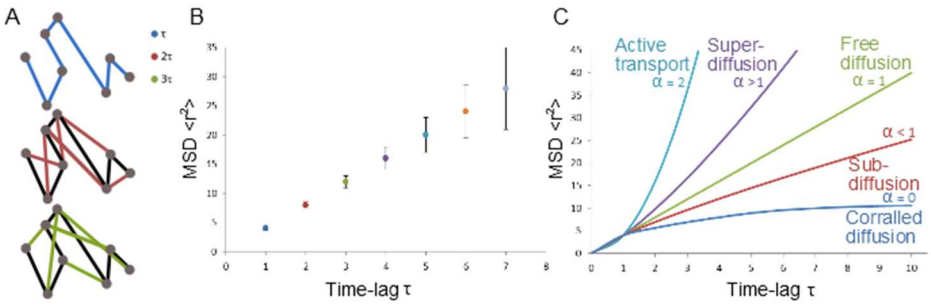

Figure 6: Mean square displacement. (A) a trajectory showing the distance between two points that are one frame apart, i.e. a time-lag τ (blue), two frames (time-lag 2τ (red)), three frames (time-lag 3τ (green)). (B)For each time-lag the mean square displacement can be calculated, which is graphically represented in a MSD vs. time-lag plot. Note that the error increases with increasing the time lag, because there are less data points from which the average value is calculated. (C) The MSD vs. time-lag plot can be used to discriminate between different types of motion.

the possible trajectories in the movie and chooses the largest non-conflicting set of trajectories as the final solution[77]. As the interaction between a nanoparticle and the surrounding environment influences the motion of the particle, the analysis of its trajectory can reveal essential aspects of this interaction. Trajectory analysis is mostly done in terms of the mean square displacement (MSD), which is the average of the square distances between any pair of points in a trajectory that are a time-interval τ apart, referred to as the time-lag. Evaluation of the MSD as a function of time-lag τ reveals the mode of motion of the particle, as shown in figure 6. For a particle undergoing free diffusion the MSD is a linear function of τ [8, 64]:

$$MSD = 4D\tau - 4/3\, D\, \Delta t + 4\sigma^2 \qquad (2)$$

where D is the diffusion coefficient of the particle, Δt is the image exposure time and σ is the localization precision and depends from the algorithm used. Thus, τ is the time interval between frames and is the sum of the image exposure time Δt and the camera read-out time. Fitting Eq. (2) to the experimental MSD data can yield the diffusion coefficient D of the particle. Note that, with increasing τ, less data points are available within the trajectory. For example, look at the trajectory shown in Fig. 6A: seven data points (blue lines) are available when we consider one time lag τ, but when we consider two time lags or three (2τ and 3τ) the number of data points decreases to six and five (red lines and green lines), respectively. As the uncertainty of the calculated MSD increases with increasing time-lag due to the decrease in data points, it is recommended to either include only 25% of time-lags into the fitting or to perform a weighted fit. The more positions the trajectory contains, the more precise the analysis will be. As a consequence, the camera exposure time and the time interval between the camera frames need to be accurately chosen to find a balance between capturing photons, limiting motion blur and sampling of the particle motion. Although a theoretical framework was developed by our group that allows to optimize the localization precision (i.e. balancing photon collection and motion blur[64]) to the best of our knowledge there is no complete theory available at this time that also includes the effect on trajectory sampling.

As a last remark, note that the localization precision σ itself depends on the image acquisition time and on the diffusion coefficient of the particle[64].

If the particles are diffusing in a purely viscous liquid, the size of the particle can be determined from the diffusion coefficient using the Stokes-Einstein-Sutherland equation[78]. Conversely, if

the size of the particle is known, the microviscosity of the environment can be determined from the instantaneous diffusion coefficient.

Types of motion different from pure Brownian motion can happen in an environment where boundaries, obstacles or active forces are present. Particles moving in the cytoplasm and continuously bouncing against obstacles, or undergoing binding-unbinding events, will show anomalous subdiffusion. Particles that are actively transported give rise to anomalous super-diffusion. In both cases the MSD versus τ can be described by Forier et al.[14]:

$$MSD = \Gamma\tau^{\alpha} - \tfrac{1}{3}\Gamma'\Delta t + 4\sigma^{2} \qquad (3)$$

with $\Gamma = \Gamma' = 4D\tau^{1-\alpha}$. However, since in many experiments $\Delta t \ll \tau$, the motion of the particle during the image acquisition time is considered Brownian and $\Gamma' = 4D$ by approximation. The anomaly parameter α is a measure for the mode of diffusion: for free diffusion $\alpha = 1$, while $\alpha < 1$ and $\alpha > 1$ represent anomalous sub- and super-diffusion, respectively[79]. Corralled motion occurs when a particle is trapped in a confined space, leading to a constant MSD at longer time-lags (Fig. 6C).

Correlation between trajectories can be used to investigate interparticle interactions. For instance, recently we developed a new method based on correlated trajectories to quantify co-localization/interaction of spectrally different particles[21, 26]. By scanning for periods of correlation within trajectories of spectrally different particles, time-dependent interactions can be investigated.

NEW DEVELOPMENTS

Single particle tracking is traditionally performed in a two dimensional fashion, however most biological processes occur in three dimensions inside potentially anisotropic environments. In such a case, 2D tracking can lead to artifacts, misleading results and underestimation of the diffusion coefficient [80]. There are two approaches to 3D SPT:

- *The "ex post facto"* approach, in which data from a region of interest is collected in three dimensions and the particle trajectories are reconstructed afterwards;
- *The feedback loop* approach, in which a single particle is followed in real time and kept in focus using a feedback loop.

The "*ex post facto*" approach uses a scanning confocal microscope to collect several z-stacks of the region where the particle is moving [7, 27]. This approach has the ability to track more than one particle at a time but at the expense of temporal resolution. It is thus recommended to use this method preferably while imaging slowly moving particles.

Orbital tracking is an example of the feedback loop approach. It is based on confocal microscopy but the focus of the laser beam monitor the regions above and below the focal plane to record the particle position and keep the particle near the focal plane using a feedback loop[80, 81].

Another example of the feedback loop approach is the possibility to reconstruct the particle axial position from the shape of the particle point spread function (PSF). Multifocal plane microscopy (MUM) and bifocal imaging for example collect two or more image planes, at least one above and one below the plane of interest, and calculate the particle axial position by the shape of

the PSF[82-84]. This information is then used to keep the particle in focus through a feedback loop. Another possibility is to introduce an optical element, like a weak cylindrical lens or a spatial light modulator, to shape the PSF in order to break its axial symmetry. The introduction of a weak cylindrical lens in front of an EMCCD camera transforms the circular PSF in an elliptical PSF whose ellipticity and orientation varies according to the particle's axial position[75, 85]. More complicated PSF shapes may be engineered as well, as did Thompson and coworkers by using a double-helix PSF to localize and track dim single emitters[86].

An interesting method to track particle in 3D is digital holographic microscopy (DHM)[87]. This technique allows to simultaneously size and track individual spherical particles with a precision of 1 nm in the focal plane and 10 nm along the optical axis. DHM works with particles of similar size as the wavelength of light and requires minimal instrumental calibration, while offering high acquisition speed, high localization precision and a very large depth of focus. Thanks to recent advances, it is nowadays possible to image gold nanoparticles in living cells with DHM[88].

CONCLUSION

Single Particle Tracking has shown to be an interesting technique in the field of nanomedicine mediated drug delivery. Although mainly limited to a relatively limited number of specialized labs until now, suitable microscopy instrumentation and software packages that are becoming commercially available will bring this technique within reach of drug delivery groups that are not necessarily specialists on advanced microscopy techniques. The exemplary studies reported by pioneering groups will be more and more performed as standard assays for obtaining a better understanding of the physicochemical properties of

nanomedicine formulations in the intended biological environment. This includes studying aggregation in biofluids, studying their transport properties in extracellular media, and studying their intracellular trafficking in target cells. This widespread use will then in turn lead to a more rational development of nanoscopic drug delivery systems.

On the technical side, more exotic illumination schemes such as light sheet microscopy, along with continuous improvements in fluorescent labeling strategies, will help to improve the contrast and the detection sensitivity. Spinning disk microscopy, swept field microscopy and light sheet microscopy should pave the way to achieving 3D tracking of multiple particles. The combination of SPT and super resolution microscopy techniques, like photoactivated localization microscopy (PALM) and image correlation spectroscopy (ICS), will certainly extend its applicability to experiments where a high density of particles is unavoidable[27, 89].

REFERENCES

1. Remaut, K.; Sanders, N. N.; De Geest, B. G.; Braeckmans, K.; Demeester, J.; De Smedt, S. C. Nucleic acid delivery: Where material sciences and bio-sciences meet. *Mat Sci Eng R* **2007,** *58*, (3-5), 117-161.
2. Konstan, M. W.; Davis, P. B.; Wagener, J. S.; Hilliard, K. A.; Stern, R. C.; Milgram, L. J.; Kowalczyk, T. H.; Hyatt, S. L.; Fink, T. L.; Gedeon, C. R.; Oette, S. M.; Payne, J. M.; Muhammad, O.; Ziady, A. G.; Moen, R. C.; Cooper, M. J. Compacted DNA nanoparticles administered to the nasal mucosa of cystic fibrosis subjects are safe and demonstrate partial to complete cystic fibrosis transmembrane regulator reconstitution. *Human gene therapy* **2004,** *15*, (12), 1255-69.
3. Farjo, R.; Skaggs, J.; Quiambao, A. B.; Cooper, M. J.; Naash, M. I. Efficient non-viral ocular gene transfer with compacted DNA nanoparticles. *PloS one* **2006,** *1*, e38.
4. Lechardeur, D.; Sohn, K. J.; Haardt, M.; Joshi, P. B.; Monck, M.; Graham, R. W.; Beatty, B.; Squire, J.; O'Brodovich, H.; Lukacs, G. L. Metabolic instability of plasmid DNA in the cytosol: a potential barrier to gene transfer. *Gene therapy* **1999,** *6*, (4), 482-97.
5. Vercauteren, D.; Rejman, J.; Martens, T. F.; Demeester, J.; De Smedt, S. C.; Braeckmans, K. On the cellular processing of non-viral nanomedicines for nucleic acid delivery: mechanisms and methods. *Journal of controlled release : official journal of the Controlled Release Society* **2012,** *161*, (2), 566-81.
6. Braeckmans, K.; Buyens, K.; Naeye, B.; Vercauteren, D.; Deschout, H.; Raemdonck, K.; Remaut, K.; Sanders, N. N.; Demeester, J.; De Smedt, S. C. Advanced fluorescence microscopy methods illuminate the transfection pathway of nucleic acid nanoparticles. *J Control Release* **2010,** *148*, (1), 69-74.
7. Ruthardt, N.; Lamb, D. C.; Brauchle, C. Single-particle tracking as a quantitative microscopy-based approach to unravel cell entry mechanisms of viruses and pharmaceutical nanoparticles. *Molecular therapy : the journal of the American Society of Gene Therapy* **2011,** *19*, (7), 1199-211.
8. Huang, F.; Dempsey, C.; Chona, D.; Suh, J. Quantitative nanoparticle tracking: applications to nanomedicine. *Nanomedicine* **2011,** *6*, (4), 693-700.
9. Braeckmans, K.; Buyens, K.; Bouquet, W.; Vervaet, C.; Joye, P.; De Vos, F.; Plawinski, L.; Doeuvre, L.; Angles-Cano, E.; Sanders, N. N.; Demeester, J.; De Smedt, S. C. Sizing nanomatter in biological fluids by fluorescence single particle tracking. *Nano Lett* **2010,** *10*, (11), 4435-42.

10. Naeye, B.; Deschout, H.; Roding, M.; Rudemo, M.; Delanghe, J.; Devreese, K.; Demeester, J.; Braeckmans, K.; De Smedt, S. C.; Raemdonck, K. Hemocompatibility of siRNA loaded dextran nanogels. *Biomaterials* **2011,** *32*, (34), 9120-7.
11. Filipe, V.; Poole, R.; Oladunjoye, O.; Braeckmans, K.; Jiskoot, W. Detection and characterization of subvisible aggregates of monoclonal IgG in serum. *Pharmaceutical research* **2012,** *29*, (8), 2202-12.
12. Deschout, H.; Raemdonck, K.; Stremersch, S.; Maoddi, P.; Mernier, G.; Renaud, P.; Jiguet, S.; Hendrix, A.; Bracke, M.; Van den Broecke, R.; Roding, M.; Rudemo, M.; Demeester, J.; De Smedt, S. C.; Strubbe, F.; Neyts, K.; Braeckmans, K. On-chip light sheet illumination enables diagnostic size and concentration measurements of membrane vesicles in biofluids. *Nanoscale* **2013**.
13. Roding, M.; Deschout, H.; Braeckmans, K.; Rudemo, M. Measuring absolute number concentrations of nanoparticles using single-particle tracking. *Phys Rev E Stat Nonlin Soft Matter Phys* **2011,** *84*, (3 Pt 1), 031920.
14. Forier, K.; Messiaen, A. S.; Raemdonck, K.; Deschout, H.; Rejman, J.; De Baets, F.; Nelis, H.; De Smedt, S. C.; Demeester, J.; Coenye, T.; Braeckmans, K. Transport of nanoparticles in cystic fibrosis sputum and bacterial biofilms by single-particle tracking microscopy. *Nanomedicine (Lond)* **2013,** *8*, (6), 935-49.
15. Lai, S. K.; Wang, Y. Y.; Hanes, J. Mucus-penetrating nanoparticles for drug and gene delivery to mucosal tissues. *Advanced drug delivery reviews* **2009,** *61*, (2), 158-71.
16. Suk, J. S.; Lai, S. K.; Wang, Y. Y.; Ensign, L. M.; Zeitlin, P. L.; Boyle, M. P.; Hanes, J. The penetration of fresh undiluted sputum expectorated by cystic fibrosis patients by non-adhesive polymer nanoparticles. *Biomaterials* **2009,** *30*, (13), 2591-7.
17. Martens, T. F.; Vercauteren, D.; Forier, K.; Deschout, H.; Remaut, K.; Paesen, R.; Ameloot, M.; Engbersen, J. F.; Demeester, J.; De Smedt, S. C.; Braeckmans, K. Measuring the intravitreal mobility of nanomedicines with single-particle tracking microscopy. *Nanomedicine* **2013**.
18. Xu, Q.; Boylan, N. J.; Suk, J. S.; Wang, Y. Y.; Nance, E. A.; Yang, J. C.; McDonnell, P. J.; Cone, R. A.; Duh, E. J.; Hanes, J. Nanoparticle diffusion in, and microrheology of, the bovine vitreous ex vivo. *Journal of controlled release : official journal of the Controlled Release Society* **2013,** *167*, (1), 76-84.
19. Lai, S. K.; Hida, K.; Chen, C.; Hanes, J. Characterization of the intracellular dynamics of a non-degradative pathway accessed by polymer

nanoparticles. *Journal of controlled release : official journal of the Controlled Release Society* **2008,** *125*, (2), 107-11.
20. Kim, A. J.; Boylan, N. J.; Suk, J. S.; Lai, S. K.; Hanes, J. Non-degradative intracellular trafficking of highly compacted polymeric DNA nanoparticles. *Journal of controlled release : official journal of the Controlled Release Society* **2012,** *158*, (1), 102-7.
21. Vercauteren, D.; Deschout, H.; Remaut, K.; Engbersen, J. F.; Jones, A. T.; Demeester, J.; De Smedt, S. C.; Braeckmans, K. Dynamic colocalization microscopy to characterize intracellular trafficking of nanomedicines. *ACS nano* **2011,** *5*, (10), 7874-84.
22. Sandin, P.; Fitzpatrick, L. W.; Simpson, J. C.; Dawson, K. A. High-speed imaging of Rab family small GTPases reveals rare events in nanoparticle trafficking in living cells. *ACS nano* **2012,** *6*, (2), 1513-21.
23. Lai, S. K.; Wang, Y. Y.; Hida, K.; Cone, R.; Hanes, J. Nanoparticles reveal that human cervicovaginal mucus is riddled with pores larger than viruses. *Proceedings of the National Academy of Sciences of the United States of America* **2010,** *107*, (2), 598-603.
24. Nance, E. A.; Woodworth, G. F.; Sailor, K. A.; Shih, T. Y.; Xu, Q.; Swaminathan, G.; Xiang, D.; Eberhart, C.; Hanes, J. A dense poly(ethylene glycol) coating improves penetration of large polymeric nanoparticles within brain tissue. *Science translational medicine* **2012,** *4*, (149), 149ra119.
25. Lai, S. K.; O'Hanlon, D. E.; Harrold, S.; Man, S. T.; Wang, Y. Y.; Cone, R.; Hanes, J. Rapid transport of large polymeric nanoparticles in fresh undiluted human mucus. *Proceedings of the National Academy of Sciences of the United States of America* **2007,** *104*, (5), 1482-1487.
26. Deschout, H.; Martens, T.; Vercauteren, D.; Remaut, K.; Demeester, J.; De Smedt, S.; Neyts, K.; Braeckmans, K. Correlation of Dual Colour Single Particle Trajectories for Improved Detection and Analysis of Interactions in Living Cells. *International Journal of Molecular Sciences* **2013,** *14*, (8), 16485-16514.
27. Dupont, A.; Stirnnagel, K.; Lindemann, D.; Lamb, D. C. Tracking image correlation: combining single-particle tracking and image correlation. *Biophysical journal* **2013,** *104*, (11), 2373-82.
28. Bausinger, R.; von Gersdorff, K.; Braeckmans, K.; Ogris, M.; Wagner, E.; Brauchle, C.; Zumbusch, A. The transport of nanosized gene carriers unraveled by live-cell imaging. *Angewandte Chemie* **2006,** *45*, (10), 1568-72.
29. de Bruin, K.; Ruthardt, N.; von Gersdorff, K.; Bausinger, R.; Wagner, E.; Ogris, M.; Brauchle, C. Cellular dynamics of EGF receptor-targeted

synthetic viruses. *Molecular therapy : the journal of the American Society of Gene Therapy* **2007,** *15*, (7), 1297-305.
30. Sahay, G.; Querbes, W.; Alabi, C.; Eltoukhy, A.; Sarkar, S.; Zurenko, C.; Karagiannis, E.; Love, K.; Chen, D.; Zoncu, R.; Buganim, Y.; Schroeder, A.; Langer, R.; Anderson, D. G. Efficiency of siRNA delivery by lipid nanoparticles is limited by endocytic recycling. *Nature biotechnology* **2013,** *31*, (7), 653-8.
31. Filipe, V.; Poole, R.; Kutscher, M.; Forier, K.; Braeckmans, K.; Jiskoot, W. Fluorescence single particle tracking for the characterization of submicron protein aggregates in biological fluids and complex formulations. *Pharmaceutical research* **2011,** *28*, (5), 1112-20.
32. Wang, Y. Y.; Lai, S. K.; Suk, J. S.; Pace, A.; Cone, R.; Hanes, J. Addressing the PEG mucoadhesivity paradox to engineer nanoparticles that "slip" through the human mucus barrier. *Angewandte Chemie* **2008,** *47*, (50), 9726-9.
33. Suh, J.; Dawson, M.; Hanes, J. Real-time multiple-particle tracking: applications to drug and gene delivery. *Advanced drug delivery reviews* **2005,** *57*, (1), 63-78.
34. Hallaj-Nezhadi, S.; Dass, C. R.; Lotfipour, F. Intraperitoneal delivery of nanoparticles for cancer gene therapy. *Future Oncology* **2012,** *9*, (1), 59-68.
35. Guarnieri, D.; Guaccio, A.; Fusco, S.; Netti, P. Effect of serum proteins on polystyrene nanoparticle uptake and intracellular trafficking in endothelial cells. *J Nanopart Res* **2011,** *13*, (9), 4295-4309.
36. Salvati, A.; Pitek, A. S.; Monopoli, M. P.; Prapainop, K.; Bombelli, F. B.; Hristov, D. R.; Kelly, P. M.; Aberg, C.; Mahon, E.; Dawson, K. A. Transferrin-functionalized nanoparticles lose their targeting capabilities when a biomolecule corona adsorbs on the surface. *Nature nanotechnology* **2013,** *8*, (2), 137-43.
37. Roding, M.; Deschout, H.; Braeckmans, K.; Rudemo, M. Measuring absolute nanoparticle number concentrations from particle count time series. *J Microsc* **2013,** *251*, (1), 19-26.
38. Roding, M.; Deschout, H.; Braeckmans, K.; Sarkka, A.; Rudemo, M. Self-calibrated concentration measurements of polydisperse nanoparticles. *J Microsc* **2013,** *252*, (1), 79-88.
39. Wohlfart, S.; Gelperina, S.; Kreuter, J. Transport of drugs across the blood-brain barrier by nanoparticles. *Journal of controlled release : official journal of the Controlled Release Society* **2012,** *161*, (2), 264-73.
40. Thorne, R. G.; Nicholson, C. In vivo diffusion analysis with quantum dots and dextrans predicts the width of brain extracellular space.

Proceedings of the National Academy of Sciences of the United States of America **2006,** *103*, (14), 5567-72.
41. Roy, I.; Vij, N. Nanodelivery in airway diseases: challenges and therapeutic applications. *Nanomedicine* **2010,** *6*, (2), 237-44.
42. Georgiades, P.; Pudney, P. D.; Thornton, D. J.; Waigh, T. Particle tracking microrheology of purified gastrointestinal mucins. *Biopolymers* **2013**.
43. Cone, R. A. Barrier properties of mucus. *Advanced drug delivery reviews* **2009,** *61*, (2), 75-85.
44. Ensign, L. M.; Schneider, C.; Suk, J. S.; Cone, R.; Hanes, J. Mucus penetrating nanoparticles: biophysical tool and method of drug and gene delivery. *Advanced materials* **2012,** *24*, (28), 3887-94.
45. Ensign, L. M.; Cone, R.; Hanes, J. Oral drug delivery with polymeric nanoparticles: the gastrointestinal mucus barriers. *Advanced drug delivery reviews* **2012,** *64*, (6), 557-70.
46. Amsden, B. An Obstruction-Scaling Model for Diffusion in Homogeneous Hydrogels. *Macromolecules* **1999,** *32*, (3), 874-879.
47. Naik, R.; Mukhopadhyay, A.; Ganguli, M. Gene delivery to the retina: focus on non-viral approaches. *Drug Discovery Today* **2009,** *14*, (5–6), 306-315.
48. Koo, H.; Moon, H.; Han, H.; Na, J. H.; Huh, M. S.; Park, J. H.; Woo, S. J.; Park, K. H.; Kwon, I. C.; Kim, K.; Kim, H. The movement of self-assembled amphiphilic polymeric nanoparticles in the vitreous and retina after intravitreal injection. *Biomaterials* **2012,** *33*, (12), 3485-93.
49. Peeters, L.; Sanders, N. N.; Braeckmans, K.; Boussery, K.; Van de Voorde, J.; De Smedt, S. C.; Demeester, J. Vitreous: a barrier to nonviral ocular gene therapy. *Investigative ophthalmology & visual science* **2005,** *46*, (10), 3553-61.
50. Rejman, J.; Oberle, V.; Zuhorn, I. S.; Hoekstra, D. Size-dependent internalization of particles via the pathways of clathrin- and caveolae-mediated endocytosis. *The Biochemical journal* **2004,** *377*, (Pt 1), 159-69.
51. Adler, A. F.; Leong, K. W. Emerging links between surface nanotechnology and endocytosis: impact on nonviral gene delivery. *Nano today* **2010,** *5*, (6), 553-569.
52. Dobay, M. P.; Schmidt, A.; Mendoza, E.; Bein, T.; Radler, J. O. Cell type determines the light-induced endosomal escape kinetics of multifunctional mesoporous silica nanoparticles. *Nano letters* **2013,** *13*, (3), 1047-52.

53. Kim, J. A.; Aberg, C.; Salvati, A.; Dawson, K. A. Role of cell cycle on the cellular uptake and dilution of nanoparticles in a cell population. *Nature nanotechnology* **2012,** *7*, (1), 62-8.
54. Iversen, T. G.; Skotland, T.; Sandvig, K. Endocytosis and intracellular transport of nanoparticles: Present knowledge and need for future studies. *Nano today* **2011,** *6*, (2), 176-185.
55. Hofmann, D.; Mailander, V. Pharmacology of nanocarriers on the microscale: importance of uptake mechanisms and intracellular trafficking for efficient drug delivery. *Nanomedicine* **2013,** *8*, (3), 321-3.
56. Nguyen, J.; Szoka, F. C. Nucleic Acid Delivery: The Missing Pieces of the Puzzle? *Accounts Chem Res* **2012,** *45*, (7), 1153-1162.
57. Suh, J.; Choy, K. L.; Lai, S. K.; Suk, J. S.; Tang, B. C.; Prabhu, S.; Hanes, J. PEGylation of nanoparticles improves their cytoplasmic transport. *International journal of nanomedicine* **2007,** *2*, (4), 735-41.
58. Lai, S. K.; Hida, K.; Man, S. T.; Chen, C.; Machamer, C.; Schroer, T. A.; Hanes, J. Privileged delivery of polymer nanoparticles to the perinuclear region of live cells via a non-clathrin, non-degradative pathway. *Biomaterials* **2007,** *28*, (18), 2876-2884.
59. Rehman, Z.; Zuhorn, I. S.; Hoekstra, D. How cationic lipids transfer nucleic acids into cells and across cellular membranes: recent advances. *Journal of controlled release : official journal of the Controlled Release Society* **2013,** *166*, (1), 46-56.
60. Suh, J.; An, Y.; Tang, B. C.; Dempsey, C.; Huang, F.; Hanes, J. Real-time gene delivery vector tracking in the endo-lysosomal pathway of live cells. *Microscopy research and technique* **2012,** *75*, (5), 691-7.
61. Lakadamyali, M.; Rust, M. J.; Babcock, H. P.; Zhuang, X. Visualizing infection of individual influenza viruses. *Proceedings of the National Academy of Sciences of the United States of America* **2003,** *100*, (16), 9280-5.
62. Cheezum, M. K.; Walker, W. F.; Guilford, W. H. Quantitative comparison of algorithms for tracking single fluorescent particles. *Biophysical journal* **2001,** *81*, (4), 2378-88.
63. Bachir, A. I.; Durisic, N.; Hebert, B.; Grutter, P.; Wiseman, P. W. Characterization of blinking dynamics in quantum dot ensembles using image correlation spectroscopy. *J Appl Phys* **2006,** *99*, (6).
64. Deschout, H.; Neyts, K.; Braeckmans, K. The influence of movement on the localization precision of sub-resolution particles in fluorescence microscopy. *J Biophotonics* **2012,** *5*, (1), 97-109.

65. Li, W.; Liu, R.; Wang, Y.; Zhao, Y.; Gao, X. Temporal Techniques: Dynamic Tracking of Nanomaterials in Live Cells. *Small* **2013,** *9*, (9-10), 1585-1594.
66. Zhou, X.; Wang, L. Uses of single-particle tracking in living cells. *Drug discoveries & therapeutics* **2010,** *4*, (2), 62-9.
67. Chang, J. C.; Rosenthal, S. J. Real-time quantum dot tracking of single proteins. *Methods in molecular biology* **2011,** *726*, 51-62.
68. Delehanty, J. B.; Mattoussi, H.; Medintz, I. L. Delivering quantum dots into cells: strategies, progress and remaining issues. *Analytical and bioanalytical chemistry* **2009,** *393*, (4), 1091-105.
69. Strano, M. S.; Jin, H. Where is it heading? Single-particle tracking of single-walled carbon nanotubes. *ACS nano* **2008,** *2*, (9), 1749-52.
70. Fu, C.-C.; Lee, H.-Y.; Chen, K.; Lim, T.-S.; Wu, H.-Y.; Lin, P.-K.; Wei, P.-K.; Tsao, P.-H.; Chang, H.-C.; Fann, W. Characterization and application of single fluorescent nanodiamonds as cellular biomarkers. *Proceedings of the National Academy of Sciences* **2007,** *104*, (3), 727-732.
71. He, X.; Gao, J.; Gambhir, S. S.; Cheng, Z. Near-infrared fluorescent nanoprobes for cancer molecular imaging: status and challenges. *Trends in molecular medicine* **2010,** *16*, (12), 574-83.
72. Brandenburg, B.; Zhuang, X. Virus trafficking - learning from single-virus tracking. *Nature reviews. Microbiology* **2007,** *5*, (3), 197-208.
73. Ritter, J. G.; Veith, R.; Siebrasse, J. P.; Kubitscheck, U. High-contrast single-particle tracking by selective focal plane illumination microscopy. *Optics express* **2008,** *16*, (10), 7142-52.
74. Ritter, J. G.; Veith, R.; Veenendaal, A.; Siebrasse, J. P.; Kubitscheck, U. Light sheet microscopy for single molecule tracking in living tissue. *PloS one* **2010,** *5*, (7), e11639.
75. Spille, J. H.; Kaminski, T.; Konigshoven, H. P.; Kubitscheck, U. Dynamic three-dimensional tracking of single fluorescent nanoparticles deep inside living tissue. *Optics express* **2012,** *20*, (18), 19697-707.
76. Schiffmann, D. A.; Dikovskaya, D.; Appleton, P. L.; Newton, I. P.; Creager, D. A.; Allan, C.; Nathke, I. S.; Goldberg, I. G. Open microscopy environment and findspots: integrating image informatics with quantitative multidimensional image analysis. *BioTechniques* **2006,** *41*, (2), 199-208.
77. Jaqaman, K.; Loerke, D.; Mettlen, M.; Kuwata, H.; Grinstein, S.; Schmid, S. L.; Danuser, G. Robust single-particle tracking in live-cell time-lapse sequences. *Nature methods* **2008,** *5*, (8), 695-702.

78. Sutherland, W. LXXV. A dynamical theory of diffusion for non-electrolytes and the molecular mass of albumin. *Philosophical Magazine Series 6* **1905,** *9*, (54), 781-785.
79. Metzler, R.; Klafter, J. The random walk's guide to anomalous diffusion: a fractional dynamics approach. *Physics Reports* **2000,** *339*, (1), 1-77.
80. Katayama, Y.; Burkacky, O.; Meyer, M.; Brauchle, C.; Gratton, E.; Lamb, D. C. Real-time nanomicroscopy via three-dimensional single-particle tracking. *Chemphyschem : a European journal of chemical physics and physical chemistry* **2009,** *10*, (14), 2458-64.
81. Levi, V.; Ruan, Q.; Gratton, E. 3-D particle tracking in a two-photon microscope: application to the study of molecular dynamics in cells. *Biophysical journal* **2005,** *88*, (4), 2919-28.
82. Toprak, E.; Balci, H.; Blehm, B. H.; Selvin, P. R. Three-dimensional particle tracking via bifocal imaging. *Nano letters* **2007,** *7*, (7), 2043-5.
83. Prabhat, P.; Gan, Z.; Chao, J.; Ram, S.; Vaccaro, C.; Gibbons, S.; Ober, R. J.; Ward, E. S. Elucidation of intracellular recycling pathways leading to exocytosis of the Fc receptor, FcRn, by using multifocal plane microscopy. *Proceedings of the National Academy of Sciences of the United States of America* **2007,** *104*, (14), 5889-94.
84. Ram, S.; Prabhat, P.; Chao, J.; Ward, E. S.; Ober, R. J. High accuracy 3D quantum dot tracking with multifocal plane microscopy for the study of fast intracellular dynamics in live cells. *Biophysical journal* **2008,** *95*, (12), 6025-43.
85. Huang, B.; Wang, W.; Bates, M.; Zhuang, X. Three-dimensional super-resolution imaging by stochastic optical reconstruction microscopy. *Science* **2008,** *319*, (5864), 810-3.
86. Thompson, M. A.; Lew, M. D.; Badieirostami, M.; Moerner, W. E. Localizing and tracking single nanoscale emitters in three dimensions with high spatiotemporal resolution using a double-helix point spread function. *Nano letters* **2010,** *10*, (1), 211-8.
87. Lee, S. H.; Roichman, Y.; Yi, G. R.; Kim, S. H.; Yang, S. M.; van Blaaderen, A.; van Oostrum, P.; Grier, D. G. Characterizing and tracking single colloidal particles with video holographic microscopy. *Optics express* **2007,** *15*, (26), 18275-82.
88. Warnasooriya, N.; Joud, F.; Bun, P.; Tessier, G.; Coppey-Moisan, M.; Desbiolles, P.; Atlan, M.; Abboud, M.; Gross, M. Imaging gold nanoparticles in living cell environments using heterodyne digital holographic microscopy. *Optics express* **2010,** *18*, (4), 3264-3273.

89. Uphoff, S.; Reyes-Lamothe, R.; Garza de Leon, F.; Sherratt, D. J.; Kapanidis, A. N. Single-molecule DNA repair in live bacteria. *Proceedings of the National Academy of Sciences of the United States of America* **2013,** *110*, (20), 8063-8.

CHAPTER 4

QUANTIFYING THE AVERAGE NUMBER OF NUCLEIC ACID THERAPEUTICS PER NANOPARTICLE BY SINGLE PARTICLE TRACKING MICROSCOPY

This chapter is submitted for publication as:

E. Zagato[1,2], L. Vermeulen[1,2], H. Dewitte[1,2], G. Van Imschoot[3], R. E. Vandenbroucke[3], J. Demeester[1] , S. De Smedt[1], K. Neyts[2,3], K. Remaut[1], K. Braeckmans[1,2]. Quantifying the number of nucleic acid therapeutics per nanoparticle by Single Particle Tracking.

[1]*Laboratory of General Biochemistry and Physical Pharmacy, Ghent University, Belgium*
[2]*Center for Nano- and Biophotonics, Ghent University, Belgium*
[3] *VIB, Center for Inflammation Research, Department of Biomedical Molecular Biology, Ghent University, Belgium*
[4]*Liquid crystals and Photonics Group, Ghent University, Belgium*

ABSTRACT Nucleic acid biopharmaceuticals are being investigated as potential therapeutics. They need to be incorporated into a bio-compatible carrier so as to overcome several biological barriers. Rational development of suitable nanocarriers requires high quality characterization techniques. While size, concentration and stability can be very well measured these days, even in complex biological fluids, a method to accurately quantify the number of nucleic acid therapeutics encapsulated in nanocarriers is still missing. Here we present a method, based on concentration measurements with Single Particle Tracking microscopy, with which it is possible to directly measure the number of plasmid DNA molecules per nanoparticle, referred to as the plasmid/NP ratio. Using DOTAP:DOPE liposomes as model carrier, we demonstrate the usefulness of the method by investigating the influence of various experimental factors on the plasmid/NP ratio. We find that the plasmid/NP ratio is inversely proportional with the size of the pDNA and that the plasmid/NP decreases when lipoplexes are prepared at lower concentrations of pDNA and nanocarrier, with values ranging from 6.5 to 3 plasmid/NP. Furthermore, the effect of pre- and post-PEGylation of lipoplexes was examined, finding that pre-PEGylation results in a decreased plasmid/NP ratio, while post-PEGylation did not alter the plasmid/NP ratio. These proof-of-concept experiments show that Single Particle Tracking offers an extension of the nanoparticle characterization toolbox, and is expected to aid in the efficient development of nanoformulations for nucleic acids based therapies.

INTRODUCTION

Nucleic acid biopharmaceuticals present a tremendous potential for treatment of life-threatening and incurable diseases. DNA vaccines, siRNA and gene–based treatments are attracting an ever-growing interest, although delivering these nucleic acid molecules to the desired cells is not an easy task. The human body has evolved to resist against organisms whose main purpose is to insert nucleic acids into the cells of our body. To reach the desired target the therapeutic nucleic acids need to overcome numerous *in vivo* extracellular and intracellular barriers. Just to name a few, they have to cross multiple tissues (mucus and extracellular matrices), evade the immune system, remain intact in a nuclease rich environment, reach the target cell and enter the cytoplasm or nucleus[1]. To be able to survive such a long and perilous journey, therapeutic nucleic acids require a safe, biocompatible carrier that protects and delivers them to the target cells. As a consequence, over time studies focusing on engineering gene delivery systems have increased exponentially. Liposomes, cationic polymers, nanogels, inorganic and magnetic particles, as well as cell penetrating peptides have been studied at length[1-5]. During development they are thoroughly characterized in terms of size, surface charge, stability and tendency to adsorb proteins.
A typical route to incorporate nucleic acid molecules (NAm) into nanocarriers is by electrostatic complexation. Cationic carriers are mixed with the negatively charged nucleic acids at a certain charge ratio to form stable complexes. While the charge ratio between both is easily calculated, typically it is not known how many nucleic acid copies are present per nanoparticle. Yet, even at a fixed charge ratio, it is quite plausible that differences in the complexation conditions, such as the volume in which the complexes are prepared, may introduce differences on the loading

degree per nanoparticle, which in turn may influence the final effectivity of the nanoformulation. Being able to know and consequently manipulate the number of therapeutic molecules per carrier may prove beneficial for rational optimization of the preparation method to ensure maximal effectivity. However, determining the number of NAms copies in nanoparticles is not easily accomplished. One strategy based on single molecule photobleaching has been proposed[6, 7], but it requires a very low background noise and single fluorophore detection sensitivity. Moreover, care must be taken to ensure that every nucleic acid molecule is labeled with one and only one fluorophore, next to the fact that this method is only suited for a very small number of cargo molecules per NP as bleach steps of individual fluorophores have to be resolved. Indeed, for larger numbers of molecules these small changes in fluorescence intensity will drown in the overall shot noise.

To address this need, here we propose a new approach to determine the number of DNA copies in nanoparticles. It is based on single particle tracking (SPT) microscopy[8] with which nanoparticle number concentrations can be accurately determined[9-13]. In brief, the Brownian motion of individual nanoparticles is imaged, and the frequency of entering and leaving the focal plane is used as a fundamental metric from which the absolute nanoparticle number concentration can be determined. In this paper, we demonstrate that by making use of SPT concentration measurements it is possible to determine the number of DNA copies per nanoparticle as follows. As a first step, the pDNA number concentration of a pDNA solution is measured, which can be done either by SPT or by classic absorbance measurements. The pDNA is subsequently mixed with the carrier material to form nanocomplexes. Next, the number concentration

of the formed DNA-carrier complexes is measured with SPT. Upon full complexation of the pDNA, the ratio of the two quantities gives the average number of plasmids for every nanoparticle, referred to in this paper as the plasmid/NP ratio.
To demonstrate the proof-of principle, we focus on cationic DOTAP:DOPE liposomes as carriers for pDNA complexation, which have been frequently evaluated for gene therapy in the past two decades[14-16]. The interested reader is referred to excellent reviews for more information on this carrier system for gene therapy [17, 18] We use the described SPT methodology to investigate how pDNA size, lipoplex (LPX) charge ratio and concentration at which LPX are prepared influence the number of pDNA copies per lipoplex. Also, on the carrier side, we investigate the influence of pre- or post-PEGylation of the lipoplexes on the number of pDNA copies per nanoparticle. Taken together we demonstrate that SPT concentration measurements present a unique method to precisely determine the number of plasmids per nanoparticle for a given nanoformulation. This new type of information is expected to contribute to the rational optimization of gene complexes for improved gene delivery.

MATERIALS AND METHODS

PREPARATION OF LIPOSOMES

(2,3-Dioleoyloxy-propyl)-trimethylammonium-chloride,DOTAP, and 1,2-Dioleoyl-sn-glycero-3-phosphoethanolamine, DOPE, were purchased from Corden Pharma LLC (Liestal, Switzerland). 1,2-Distearoyl-sn-glycero-3-phosphoethanolamine-N-methoxy (polyethyleneglycol)-2000) (DSPE-PEG_{2000}) and N-octanoyl-sphingosine-1-[succinyl[methoxy(polyethyleneglycol)2000]] (Ceramide-PEG_{2000}) were purchased from Avanti Polar Lipids (Alabaster, AL, USA). The appropriate amount of the lipids was

mixed at a 1:1 ratio in a round-bottom flask and dissolved in 1000 µl of chloroform (Sigma Aldrich, Bornem, BELGIUM). PEGylated liposomes were prepared by adding the desired amount of DSPE-PEG_{2000} or Ceramide-PEG_{2000}, corresponding to 3 mol% or 10 mol% of the total lipids.

The flask was then placed into the rotavapor (IKA, Staufen, Germany) and put in contact with a water bath pre-heated at 40°C. The pressure was reduced to 0.1 bar and the flask was rotated at 180 rpm for 15-20 min. The dried lipid film was then rehydrated in 0.2 ml distilled water and detached from the glass walls using glass pearls. The liposome suspension was then placed into a 0.5 ml vial and pulse-sonicated (10 s on, 15 s off) for 6 cycles using a probe sonicator (Branson Ultrasonics Digital Sonifier, Danbury, USA). The size and zeta-potential of the liposomes were checked using the Zetasizer Nano-ZS (Malvern, Worcestershire, UK) to ensure the liposomes had an acceptable size. Depending on the batch, liposomes had a size between 65 nm and 75 nm in diameter with a PDI that was always smaller than 0.25 and the zeta-potential was around +45 mV for the cationic liposomes and around +7 mV for the PEGylated liposomes. The obtained liposome solution had a concentration of 5 mM DOTAP and 5 mM DOPE.

PREPARATION OF pDNA

Two types of plasmid DNA were used, gWiz™ pDNA (≈ 5800 bp) and pBlueScript KS+ pDNA (≈ 3000 bp). The plasmids are multiplied in *E.coli* bacteria (Genlantis, San Diego, CA, USA) in a sterile LB-medium (NaCl; Sigma-Aldrich, St Louis, Missouri, USA / Yeast extract; Lab M, Heywood, UK / Tryptone; Lab M, Heywood, UK) to which the antibiotic Kanamycin (Sigma-Aldrich, St Louis, Missouri, USA) is added and the bacteria were

incubated overnight at 37°C, shaken at 300 rpm. We used the QIAGEN plasmid purification protocols (QIAGEN, Hilden, Germany) to obtain a purified pDNA solution. The purity and concentration of the solution was assessed using Nanodrop 2000C (ThermoFisher Scientific, Waltham, USA). The pDNA was labelled with Cy™5 (*Label* IT® Nucleic Acid Labeling Kits, Mirus Bio LLC, Madison, USA) by using 1 µl of Label IT Reagent for every 2 µg of pDNA. pDNA was purified from non-conjugated Cy™5 using the provided G50 Microspin Purification columns (Mirus, Madison, USA), as described by the manufacturer.

LIPOPLEX FORMATION AND PLASMID/NP EXPERIMENT

Lipoplexes were formed by mixing, in equal volumes, a fixed amount of 1 µg of labeled pDNA with DNase and RNase free water and a solution with the appropriate amount of liposomes to reach the desired charge ratio of N/P 6, 8, 10 and 12. The lipoplex solution, which had a total volume of 20 µl, was then vortexed and placed in the dark at room temperature for 30 minutes, to allow complex formation. The pDNA concentration of the solution was 50 ng/µl. Afterwards, the solution was diluted to a pDNA concentration of 0.3 ng/µl and the lipoplex concentration was measured with SPT. Variations in this protocol were introduced to monitor the influence on the resulting plasmid/NP ratio. In one set of experiments, the charge ratio was adapted by changing the amount of pDNA in the solution, while keeping the amount of liposomes fixed at 1.2 mM positive charges. In another set of experiments, both the pDNA and the liposome solutions were diluted ten and fifty times respectively, before complex formation, to study the role of the concentration in lipoplex formation. In other words, the volumes of the pDNA and liposome solutions that were mixed together were increased 10

and 50 times, while keeping the charge ratio constant (at N/P 8). The undiluted, 10 and 50 times diluted stock solutions used for complex formation are referred to as 50 ng/µl, 5 ng/µl and 1 ng/µl respectively, based on the pDNA concentration.
Also PEGylated lipoplexes were included in this study, formed by adding the desired amount of PEG (linker chain: DSPE or Ceramide) to the DOTAP and DOPE in the round-bottom flask (pre-insertion technique) or to the lipoplex solution after complexation (post-insertion technique). In the latter case, the solution was vortexed and maintained 1 h at 37°C under continuous stirring at 200 rpm.

GEL ELECTROPHORESIS

Complexation of pDNA with liposomes was verified using gel electrophoresis. 400 ng labeled pDNA/eppendorf was complexed with the appropriate amount of liposomes to reach the desired charge ratio (4, 6, 8, 10 or 12) and water was added to a total volume of 15 µl. Then 5 µl TBE buffer (Tris; Merck Millipore, Billerica, Massachusetts, USA / Borate; VWR, Haasrode, Belgium / EDTA; Merck KGaA, Darmstadt, Germany) and 5 µl Loading buffer (ThermoFisher Scientific, Waltham, USA) were added to each solution. The samples were loaded on a 0.7% agarose gel (ThermoFisher Scientific, Waltham, USA) and left to run at 100 V for 50 min. Results are shown in the appendix at the end of the chapter, Fig. 1 SI and 2 SI.

SINGLE PARTICLE TRACKING NUMBER CONCENTRATION

Single Particle Tracking is a well-known advanced microscopy technique that allows to analyze the mobility of nanoparticles. Briefly, SPT captures the motion of individual particles in time-lapse videos, which are then analyzed to reconstruct the

trajectories of each of these nanoparticles. From the analysis of the trajectories it is possible to calculate for instance the diffusion coefficient of each nanoparticle. Recently we developed a dedicated algorithm that allows to extract the absolute number concentration from SPT videos of nanoparticles diffusing freely in a liquid[9]. The number concentration is the average number of particles identified per frame divided by the detection volume V. As SPT is a microscopy based method, the lateral dimensions of V are simply the field of view of the microscope, which is easily calibrated with a graded ruler. The difficulty, however, is to precisely determine the effective axial dimension, which is unknown and impossible to calibrate *a priori* since it depends on several parameters, including the image processing settings used to detect the particles. It can, however, be derived from the time particles spend inside V, which can be measured directly from the SPT movies. Small and fast moving particles will spend less time within V as compared to larger and slower ones. Thus, thanks to the fact that the diffusion coefficient can be directly measured from SPT data and by making use of the statistical model reported by Roding et al.[9], the axial dimension of V can be readily determined for each SPT movie and used to calculate the absolute number concentration of the particles in the dispersion.

The plasmid/NP ratio, which is of interest in this study, is then simply calculated by dividing the concentration of pDNA in the solution before complexation by the concentration of LPX after complexation, with the assumption that all the plasmid DNA is complexed.

RESULTS

VALIDATION

First we evaluated if SPT is able to correctly measure pDNA and LPX concentration. A solution of gWiz™ pDNA was prepared at a concentration of 166 ± 3 ng/µl, corresponding to $2.84 \pm 0.05*10^{13}$ pDNA strands per ml. While SPT can be operated in light scattering mode, the best sensitivity is obtained in combination with fluorescence. Therefore, the experiments reported here were all done in fluorescence mode, with pDNA labelled covalently with a far-red fluorophore, Cy5, for optimal visualization with SPT. A dilution series was prepared from the stock solution at sufficiently low concentrations (0.006%, 0.013%, 0.019%, 0.025%, 0.032%) so that the diffusion of individual pDNA copies can be imaged with SPT. The pDNA number concentrations as measured with SPT are presented in Fig. 1 A. A linear trend line through the data extrapolated to 100% predicts a pDNA stock concentration of $2.66 \pm 0.23*10^{13}$ plasmid/ml, with an R^2 of 0.989, in excellent agreement with the actual concentration reported above. This shows that SPT is well suited to measure the number concentration of Cy5-labelled pDNA.

Next, we evaluated whether SPT allows to determine the number concentration of DOTAP:DOPE LPX containing Cy5-labelled pDNA. A dilution series was prepared from a LPX formulation and measured with SPT, as shown in Fig. 1 B. Charge ratio 8 was chosen to ensure complete complexation of the cargo while keeping the amount of carrier to a minimum to reduce cytotoxicity as much as possible. As expected, the LPX number concentration follows a linear trend, with an R^2 of 0.985. From the linear fit the LPX stock concentration is extrapolated to be $1.9 \pm 0.1*10^{11}$ particle/ml.

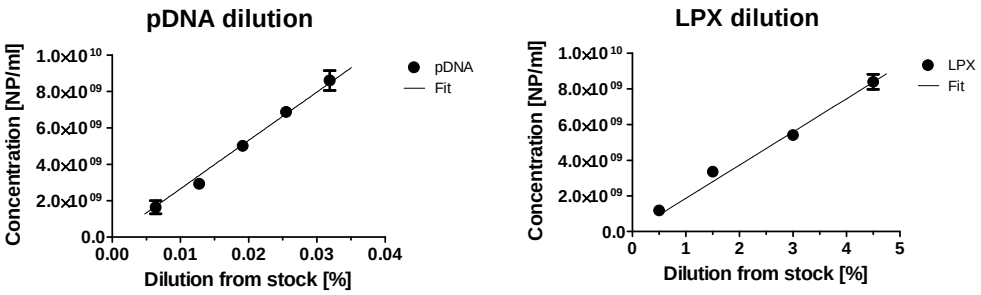

Fig. 1. SPT number concentration measurements of a dilution series of (A) Cy5-labelled gWiz pDNA and (B) DOTAP:DOPE LPX containing Cy5-pDNA at a charge ratio of 8.

Knowing the number concentration of plasmids and LPX, the average number of plasmids per LPX now readily follows from the ratio C_{pDNA}/C_{LPX}. The pDNA solution, when complexed with DOTAP:DOPE liposomes, was diluted 20 times. Thus, for the above mentioned LPX of charge ratio 8 it yields a plausible number of 7.0 +/- 0.7 plasmids per LPX. This result is based on the assumption that all pDNA is complexed (i.e. no remaining free pDNA). Based on gel electrophoresis this is the case here, as no uncomplexed pDNA could be detected (see the appendix at the end of the chapter). Further on we will discuss how the method can be extended in the future to also deal with partially uncomplexed pDNA.

INFLUENCE OF PLASMID SIZE

As a first application of the method we investigated if the number of plasmid/NP is influenced by the size of the plasmid, keeping the charge ratio constant. We prepared LPX at charge ratio 8 with gWiz™ pDNA (≈ 5800 bp) and pBlueScript KS+ pDNA of about half the size (≈ 3000 bp). 50 ng/µl pDNA was added to DOTAP:DOPE liposomes corresponding to 1.2 mM positive

charges. As can be seen in Fig. 2A we find that 2.2 ± 0.2 times as many plasmids per LPX are found for the smaller pDNA, which corresponds well with the difference in size of both plasmids. In any case it shows that the plasmid size can influence the number of plasmid/NP.

INFLUENCE OF THE CONCENTRATION OF PDNA AND LIPOSOMES

To explicitly investigate the influence of both pDNA and liposomes concentration on the number of plasmid copies per LPX, LPXs were prepared at a constant charge ratio 8 for different concentrations of pDNA and liposomes. Fig. 2B confirms that the plasmid/NP ratio is highly dependent on the concentration of the initial stock solutions that are mixed when the lipoplexes are prepared. At a pDNA concentration of 1 ng/µl the lipoplexes contain only 3 copies of pDNA, while it is about 6.5 at a concentration of 50 ng/µl. This again shows that the plasmid/NP ratio has the tendency to increase at higher concentrations of the interaction partners. Surprisingly, the lipoplex size showed the opposite trend, indicating that size alone is not sufficient to infer if lipoplexes have more or less copies of pDNA per particle.

INFLUENCE OF CHARGE RATIO

Next, we investigate how the number of plasmid/NP changes for various LPX charge ratios. We first start by keeping the concentration of lipids constant at 1.2 mM and adjust the amount of gWiz™ pDNA to obtain charge ratios of 6, 8, 10 and 12 (see "Fixed Lipid Content" in Table 1). All solutions are prepared in a constant total volume of 20 µl. The results in Fig. 2C (light green bars) show a clearly decreasing trend for the plasmid/NP ratio at increasing charge ratio. This can be explained by the fact that

more liposomes are available at higher charge ratios to complex the pDNA, so that it seems reasonable that complexes will be formed with less pDNA per particle. Although not very pronounced, this is to some extent also reflected in the LPX size as measured by SPT shown in Fig. 2C (light green line), with about 20% decrease in size between charge ratio 6 and 12.

The same charge ratio series can also be obtained by keeping the pDNA concentration constant at 50 ng/µl and adjusting the amount of lipids instead. In this case we find a slightly increasing trend for the plasmid/NP ratio as the charge ratio increases (Fig. 2C, dark green bars). At the same time a moderate size increase is observed (Fig. 2C, dark green line). An important difference with the previous charge ratio series is that the number concentration of pDNA and liposomes is different, as seen in Table 1.

For instance for the charge ratio of 12 we now have 50% more liposomes and pDNA as compared to the previous series. This means that the complexes are now formed at a higher concentration, which apparently leads to larger complexes containing more pDNA per particle. On the contrary, for a charge ratio of 6 we now have 25% less liposomes and pDNA as in the previous series, which leads to smaller complexes with less pDNA per particle. Therefore, it is clear that the plasmid/NP ratio is not only determined by the charge ratio, but also by the concentration at which the complexes are prepared, which will be further explored in the next section.

pDNA and liposomes Concentration				
Charge Ratio	Fixed Lipid Content		Fixed pDNA Content	
	C pDNA [ng/µl]	C liposomes [mM]	C pDNA [ng/µl]	C liposomes [mM]
6	67	1.2	50	0.9
8	50	1.2	50	1.2
10	40	1.2	50	1.5
12	33	1.2	50	1.8

Table 1. Concentration of plasmid DNA and lipids, expressed in ng/µl and nM of positive charges respectively, in the LPX dispersions. The volume was always kept constant at 20 µl. Fixed Lipid Content corresponds to 1.2 mM of lipids, and Fixed pDNA Content corresponds to 50 ng/µl pDNA.

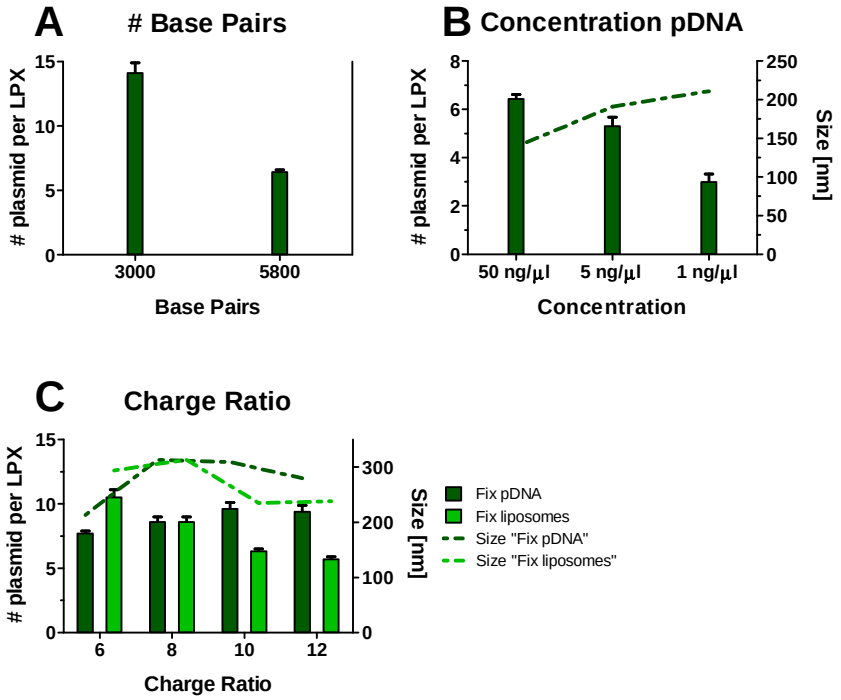

Fig. 2. The effect of pDNA size, LPX charge ratio and pDNA concentration on the number of plasmids per LPX. (A) Effect of plasmid size on plasmid/NP ratio. Halving the number of base pairs in the plasmid doubles the plasmid/NP ratio. (B) Effect of concentration on the plasmid/NP ratio. Both the pDNA and the liposome solutions were diluted ten and fifty times (pDNA concentrations from 50 ng/µl to 5 ng/µl and 1 ng/µl) to form LPXs at a fixed charge ratio of 8. The decrease in plasmid/NP ratio confirms that the complexation is concentration-dependent. (C) Plasmid/NP ratio in function of charge ratio. LPXs were complexed in a fixed volume (20 µl) by keeping the amount of plasmids constant at 50 ng/µl (dark green) or by keeping the amount of lipids constant at 1.2 mM (light green).

PEGylated lipoplexes

PEGylation of nanocarriers is a common strategy to improve their transport and stability in biological tissues. For instance, it can prevent mucoadhesion[19] and increases the nanoparticle half-life and colloidal stability in biofluids[20, 21]. However, PEG chains may also reduce the interaction strength between pDNA and liposomes, which in turn could affect the plasmid/NP ratio. Here, we investigate this for two common PEGylation strategies. In the first PEGylation approach, referred to as PRE-PEGylation, PEGylated lipids are added to the lipid mixture of the liposomes before complexation with pDNA[19, 22, 23]. In the second strategy the PEG chains are added to the LPX dispersion after formation of the complexes, referred to as POST-PEGylation[19, 23, 24]. We used DSPE-PEG_{2000} and tested the effect of PRE- and POST-PEGylation, as well as the influence of the amount of PEG on the plasmid/NP ratio of lipoplexes (at fixed charge ratio 8). The graph shown in Fig. 3 indicates a substantial drop in the plasmid/NP ratio of PRE-PEGylated lipoplexes as the amount of PEG increases. This can be explained by the steric hindrance of the PEG chains and the shielding of cationic charges due to which the interaction with pDNA is reduced. At the same time the LPX size increased, again showing that LPX size alone cannot be used to infer the plasmid/NP ratio. POST-PEGylation, on the other hand, did not have such a strong impact on the plasmid/NP ratio with only a very small reduction in the number of plasmid/NP. This is likely due to the fact that the LPX are already formed at the time that the DSPE-PEG is added so that (most of) the pDNA remains stably incorporated.

Finally, we tested if the anchor lipid that is used to post-functionalize LPX with PEG may have an influence. Therefore, we

evaluated POST-PEGylation with 10 mol% of Ceramide-PEG$_{2000}$ instead of DSPE-PEG. Ceramide-PEG is sometimes preferred to enhance the interaction with the anionic cellular membrane as it is less stably incorporated into LPX as compared to DSPE-PEG[21, 25]. Post-PEGylation with Ceramide-PEG again had no influence on the plasmid/NP ratio compared to the non-pegylated LPX, showing that it influences LPX composition even less than DSPE-PEG.

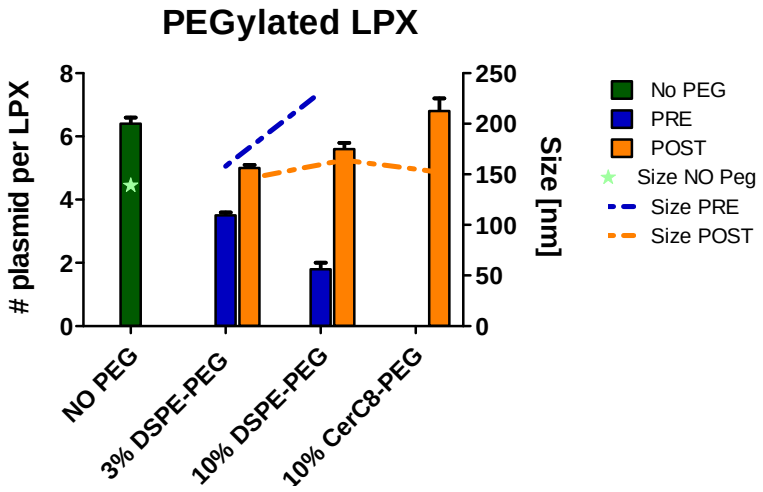

Fig. 3. Influence of PRE- and POST-PEGylation on the number of plasmid copies per LPX. Liposomes were PRE-PEGylated by incorporation of the indicated percentage of PEGylated DSPE lipids. POST-PEGylation of LPX was performed with both DSPE-PEG and Ceramide C8-PEG. All LPX were prepared at a charge ratio of 8.

DISCUSSION

To obtain a safe and efficient delivery of nucleic acid-based therapeutics, a complete and thorough characterization of the carrier-cargo complex is required. The efficiency of the carrier in encapsulating or complexing the therapeutic cargo molecules is an important parameter that may influence the effectiveness of the carrier. To our knowledge, we present here the first reported method for directly measuring the plasmid/NP ratio in a flexible manner. Another reported method makes use of photobleaching to count the number of therapeutic molecules each labelled with a single fluorophore. When continuously excited, the fluorophores will photobleach one after the other, resulting in a step-wise decrease in intensity. By counting the number of steps it is possible to calculate the amount of cargo molecules in the complex. Importantly, this method requires each NAms to be labelled with exactly one fluorophore. While there are methods to do that, such as the *in vitro* incorporation of modified nucleotides in the polynucleotide backbone, or the introduction of specific sequences in the plasmid DNA to allow sequence-specific fluorophore attachment[26], these are rather complex procedures and need to be considered carefully. Another limitation of the method is that it is inherently limited to a low number of molecules, because else the step-wise decrease in fluorescence is buried in the overall shot-noise. Instead, our approach based on SPT nanoparticle concentration measurements, does not pose any particular limit on the number of plasmids per nanoparticle. While in principle it does not require the nucleic acids to be labelled when operated in light scattering mode, we did label the plasmids in our study as in our hands it improves the detection sensitivity. In any case, the labelling requirements are not as stringent as in the

photobleaching method since the number of fluorophores per plasmid does not need to be controlled. Indeed, the only requirement is that the plasmids and complexes are visible in the SPT microscope. The downside, however, is that only the average number of plasmid/NP is obtained, while the photobleaching methods yield information on a single particle basis.

As a case study, we focused on DOTAP:DOPE liposomes as a model carrier and studied its plasmid/NP ratio for a variety of conditions. The influence of pDNA size, charge ratio of the lipoplexes and concentration of pDNA vs. liposomes were thoroughly investigated. Remarkably, each of those factors had an influence on the number of plasmids per carrier. First it was noted that lipoplexes formed with pDNA of half the size had double the amount of plasmids per LPX when prepared at the same charge ratio. It must be noted that by halving the size of the pDNA while keeping the weight concentration (in ng/μl) constant, the actual number of pDNA molecules doubled. Therefore, the doubling of the plasmid/NP ratio can be expected and provides a validation of the proposed method. Then a slight decrease in plasmid/NP ratio was noticed when the charge ratio was increased by keeping constant the amount of lipids and varying the pDNA concentration, while the opposite trend was observed when the charge ratio was modified by keeping the concentration of pDNA constant and adjusting the amount of liposomes. Thus the charge ratio itself is not the main factor that influences the number of plasmids per carrier. Finally, we observed that preparing lipoplexes of fixed charge ratio at lower concentrations of pDNA and liposomes reduces the number of plasmids per lipoplex.

In general, these observations indicate that the charge ratio itself is not the main factor that influences the number of plasmid per carrier, but it seems that the number of plasmids per nanoparticle

also depends on the potential collisions between the plasmids and the liposomes. Indeed, the number of plasmid per nanoparticle substantially increases when the concentration of the nanocarriers constituents increases and/or when the pDNA size is decreased, leading to a higher amount of pDNA molecules for the same weight concentration.

Another factor that we investigated was the influence of PEGylation on the number of plasmids per lipoplex. Functionalization of nanocarriers with PEG chains to improve their colloidal stability in buffers and biofluids, and to prolong their circulation time *in vivo* has been widely studied[19, 20, 22, 27]. Here we evaluated the effect of PEGylation on the number of plasmids per LPX, finding that the PEGylation method does have a significant impact. With PRE-PEGylated liposomes a decrease in the plasmid/NP ratio was observed with increasing PEG content. Instead, POST-PEGylation of LPX had virtually no effect on the incorporated number of plasmids per nanoparticle. This is most likely due to the fact that PRE-PEGylated liposomes have better colloidal stability, so that they have less tendency to agglomerate when the pDNA-LPX complexes are formed. As a result those LPX will contain less liposomes per NP, also leading to the complexation of less pDNA per LPX.

Optimization of nanoparticles for nucleic-based therapy should not focus only on the optimization of the carrier, but also of the carried nucleic acid molecules. As shown in Fig. 2A, the lower the number of base pairs, the higher the number of plasmids per particle. A smaller size is not only beneficial in the complexation process, but also during transfection. It has been reported that plasmid DNA bigger than 6000 bp have a substantially decreased expression compared to smaller constructs[28]. It is believed that this size-dependent reduced efficiency is due to the lower

mobility big plasmid DNA experience in the cytoplasm. Minicircle DNAs are the perfect solution for an optimized transfection efficiency. Minicircle DNAs are non-viral closed circular gene expressing vectors to which all the sequences not directly linked to gene transfection are removed. They are smaller and safer than the commonly used plasmids, since the sequence coding for antibiotic resistance is removed, and present longer gene expression due to the removal of their bacterial origin of replication[28, 29].

On the technological side, while we used a custom-built microscope in this study, it is of note that SPT instruments are also commercially available, like those from Malvern (NanoSight) and ParticleMetrix. They are gaining in popularity for nanoparticle characterization to complement DLS measurements. As such the reported method should find easy entrance in the nanomedicine community. For optimal accuracy we do advise though to make use of our reported concentration algorithms which were extensively validated to give correct absolute concentration values in a calibration-free manner[9-11, 13].

A current limitation of the method as reported here is that it requires complete complexation of the cargo and its carrier. Indeed, in case there is still free pDNA in the LPX dispersion, the visible particles in the SPT images cannot be unambiguously assigned to LPX so that its concentration cannot be reliably determined. A workaround could be to label the carrier with a different fluorophore so that LPX can be identified as particles having both colors while uncomplexed pDNA would only have one color. An alternative approach is to quantify and remove uncomplexed DNA by adding nucleases to the LPX sample after measuring its apparent concentration. The protocol would then require to measure the particle concentration two times, before

and after the addition of DNase I. The unbound DNA can thus be quantified as the difference between the particle concentration in the LPX solution (C_{NC}), measured before the addition of DNase I, and the lipoplex concentration C_{LPX}, measured after degradation of pDNA by the DNase. Thus the number of plasmids per particle in this case can be calculated from

$$\frac{pDNA}{NC} ratio = \frac{C_{complexed\ pDNA}}{C_{LPX}} = \frac{C_{pDNA} - (C_{NC} - C_{LPX})}{C_{LPX}}$$

where C_{pDNA} is the concentration of pDNA in the solution, complexed and unbound, and must be measured or calculated before complexation with the carriers.

Finally, it is important to note that the presented SPT method is not limited to plasmids, but could be used for other and smaller nucleic acids as well. The only requirements are that (1) the concentration of nucleic acids is known or can be measured precisely beforehand, (2) that 100% complexation is obtained, and (3) that the final complexes can be visualized by SPT (scattering or fluorescence). Furthermore, in case the (liposomal) carrier would be labeled, the same SPT method could be used to determine the carrier number concentration, which would allow to get even more detailed insight into the formation and composition of pDNA-carrier complexes.

CONCLUSIONS

Prior to fulfilling their therapeutic effect, nucleic acid/carrier complexes must overcome numerous barriers that vary according to the administration route. To exploit their full potential, such nanomedicines must be extensively characterized. However, differences in the complexation conditions, such as pDNA size, concentration of the components and type of protocol used to PEGylate the nanocarriers, introduce differences on the loading degree per nanoparticle. In future research it is of interest to investigate for lipoplexes but also for other carriers how that may influence the biological effectivity of the formulation. We have proposed to take advantage of SPT nanoparticle concentration measurements and apply it to determine the number of plasmids per nanoparticle, a type of characterization that was not possible before. Given the fact that SPT instruments are commercially available and are increasingly being used for nanoparticle characterization, we believe that the demonstrated method can find rapid acceptance in the field and contribute to the development of safer and more efficient nanoformulations for nucleic acids based-therapies.

APPENDIX

Gel electrophoresis

The method we developed to calculate the plasmid/NP ratio is based on the assumption that all pDNA is complexed with the liposomes. If this is the case, by measuring the concentration of pDNA before complexation, it is possible to calculate the concentration of pDNA that is effectively complexed with the liposomes. Gel electrophoresis is a practical and easy tool to check if there is complete complexation of plasmid DNA. The complexation of every sample considered in this paper is checked with gel electrophoresis. As it can be seen from Fig. 1 SI and 2 SI, the samples show complete complexation under the indicated conditions. The only exception is gWiz pDNA complexed with PRE-PEGylated DOTAP:DOPE and ceramide PEG. Since there isn't complete complexation, our method cannot yet be applied to this sample.

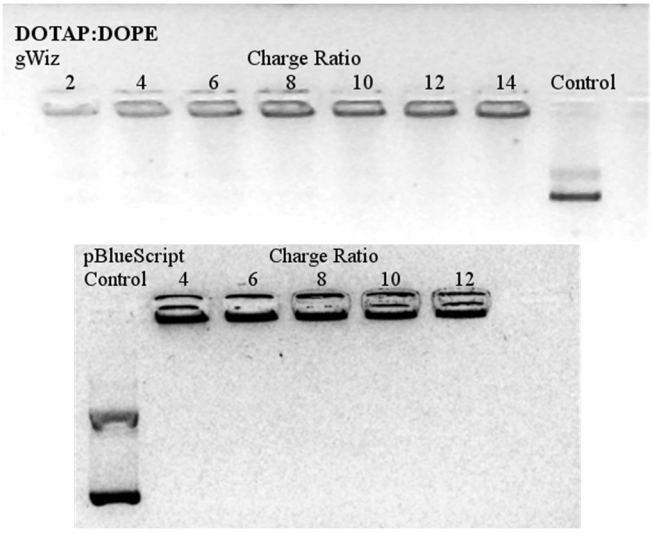

Fig. 1 SI. Complexation of gWiz pDNA and pBlueScript pDNA with DOTAP:DOPE 1:1 at different charge ratio. The plasmid DNA is totally complexed with the liposomes at the charge ratios chosen for the experiments (6, 8, 10 and 12).

PEGylated LPXs

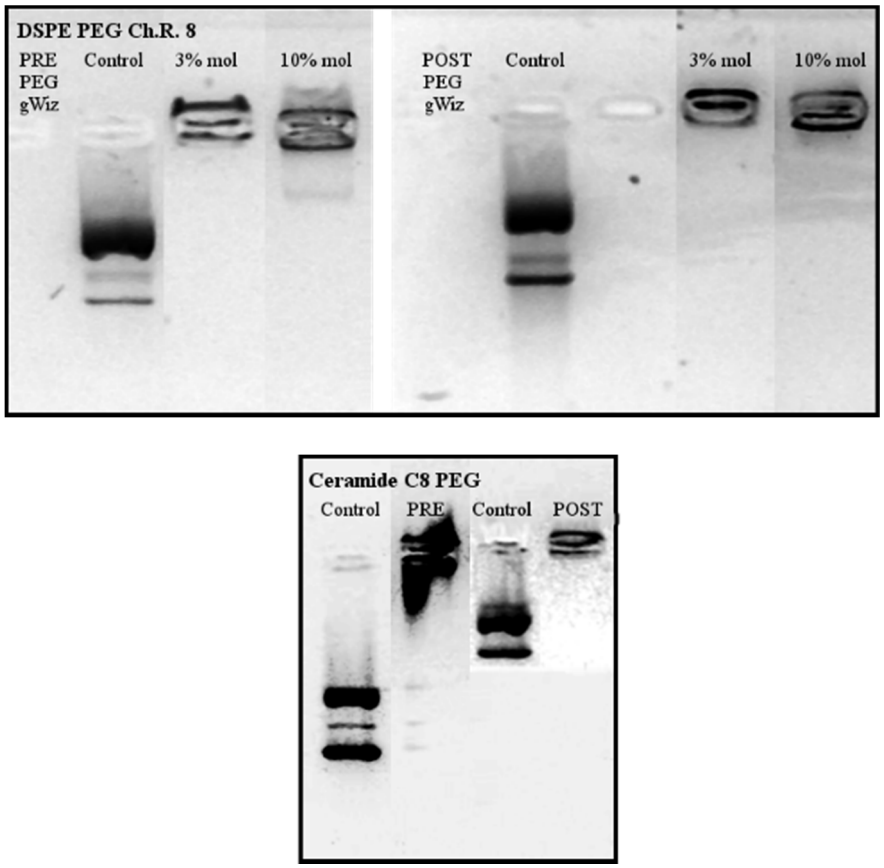

Fig. 2 SI. Complexation of gWiz™ pDNA and pBlueScript KS+ pDNA with PEGylated DOTAP:DOPE liposomes at charge ratio 8. Most of the samples show complete complexation, except for pBlueScript DSPE PRE-PEGylated LPX and gWiz Ceramide C8 PRE-PEGylated LPX.

Of note is the presence of a faint smear for the gWiz DSPE PRE-PEGylated complexes (see Fig. 2 SI). This is likely due to the fact that the high amount of PEG chains into PRE-PEGylated liposomes allows some strands to be only loosely attached to the complexes. When in the presence of a strong electric field, this weak bond breaks and some plasmid DNA strand detaches and travel through the gel. Since our samples, when measured with

SPT, are not subject to strong electric fields, we assume the fraction of loose/uncomplexed DNA to be negligible if not absent.

Zeta Potential

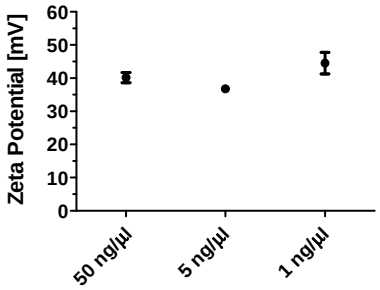

Fig. 3 SI. Zeta Potential of charge 8 DOTAP:DOPE lipoplexes complexed at different concentration of pDNA and liposomes, ranging from 50 ng/µl to 1 ng/µl. No substanzial difference in zeta-potential is found.

REFERENCES

1. Remaut, K.; Lucas, B.; Raemdonck, K.; Braeckmans, K.; Demeester, J.; De Smedt, S. C. Can we better understand the intracellular behavior of DNA nanoparticles by fluorescence correlation spectroscopy? *J Control Release* **2007,** *121*, (1-2), 49-63.
2. Soni, G.; Yadav, K. S. Nanogels as potential nanomedicine carrier for treatment of cancer: A mini review of the state of the art. *Saudi Pharm J* **2016,** *24*, (2), 133-9.
3. Dizaj, S. M.; Jafari, S.; Khosroushahi, A. Y. A sight on the current nanoparticle-based gene delivery vectors. *Nanoscale Res Lett* **2014,** *9*, (1), 252.
4. Ramamoorth, M.; Narvekar, A. Non viral vectors in gene therapy-an overview. *J Clin Diagn Res* **2015,** *9*, (1), GE01-6.
5. Jain, A.; Hosseinkhani, H.; Domb, A. J.; Khan, W., Cationic Polymers for the Delivery of Therapeutic Nucleotides. In *Polysaccharides: Bioactivity and Biotechnology*, Ramawat, K. G.; Mérillon, J.-M., Eds. Springer International Publishing: Cham, 2015; pp 1969-1990.
6. Zhang, H.; Guo, P. Single molecule photobleaching (SMPB) technology for counting of RNA, DNA, protein and other molecules in nanoparticles and biological complexes by TIRF instrumentation. *Methods* **2014,** *67*, (2), 169-76.
7. Delport, F.; Deres, A.; Hotta, J.; Pollet, J.; Verbruggen, B.; Sels, B.; Hofkens, J.; Lammertyn, J. Improved method for counting DNA molecules on biofunctionalized nanoparticles. *Langmuir* **2010,** *26*, (3), 1594-7.
8. Zagato, E.; Forier, K.; Martens, T.; Neyts, K.; Demeester, J.; De Smedt, S.; Remaut, K.; Braeckmans, K. Single-particle tracking for studying nanomaterial dynamics: applications and fundamentals in drug delivery. *Nanomedicine (Lond)* **2014,** *9*, (6), 913-27.
9. Roding, M.; Deschout, H.; Braeckmans, K.; Rudemo, M. Measuring absolute number concentrations of nanoparticles using single-particle tracking. *Phys Rev E Stat Nonlin Soft Matter Phys* **2011,** *84*, (3 Pt 1), 031920.
10. Roding, M.; Deschout, H.; Braeckmans, K.; Rudemo, M. Measuring absolute nanoparticle number concentrations from particle count time series. *J Microsc* **2013,** *251*, (1), 19-26.
11. Roding, M.; Deschout, H.; Braeckmans, K.; Sarkka, A.; Rudemo, M. Self-calibrated concentration measurements of polydisperse nanoparticles. *J Microsc* **2013,** *252*, (1), 79-88.

12. Roding, M.; Guo, M.; Weitz, D. A.; Rudemo, M.; Sarkka, A. Identifying directional persistence in intracellular particle motion using Hidden Markov Models. *Math Biosci* **2014,** *248*, 140-5.
13. Roding, M.; Zagato, E.; Remaut, K.; Braeckmans, K. Approximate Bayesian computation for estimating number concentrations of monodisperse nanoparticles in suspension by optical microscopy. *Phys Rev E* **2016,** *93*, (6), 063311.
14. Kim, B. K.; Hwang, G. B.; Seu, Y. B.; Choi, J. S.; Jin, K. S.; Doh, K. O. DOTAP/DOPE ratio and cell type determine transfection efficiency with DOTAP-liposomes. *Biochim Biophys Acta* **2015,** *1848*, (10 Pt A), 1996-2001.
15. Ciani, L.; Ristori, S.; Salvati, A.; Calamai, L.; Martini, G. DOTAP/DOPE and DC-Chol/DOPE lipoplexes for gene delivery: zeta potential measurements and electron spin resonance spectra. *Biochim Biophys Acta* **2004,** *1664*, (1), 70-9.
16. Falsini, S.; Ristori, S., Lipoplexes from Non-viral Cationic Vectors: DOTAP-DOPE Liposomes and Gemini Micelles. In *Non-Viral Gene Delivery Vectors: Methods and Protocols*, Candiani, G., Ed. Springer New York: New York, NY, 2016; pp 33-43.
17. Wasungu, L.; Hoekstra, D. Cationic lipids, lipoplexes and intracellular delivery of genes. *Journal of Controlled Release* **2006,** *116*, (2), 255-264.
18. Remaut, K.; Sanders, N. N.; De Geest, B. G.; Braeckmans, K.; Demeester, J.; De Smedt, S. C. Nucleic acid delivery: Where material sciences and bio-sciences meet. *Materials Science & Engineering R-Reports* **2007,** *58*, (3-5), 117-161.
19. Suk, J. S.; Xu, Q.; Kim, N.; Hanes, J.; Ensign, L. M. PEGylation as a strategy for improving nanoparticle-based drug and gene delivery. *Adv Drug Deliv Rev* **2016,** *99*, (Pt A), 28-51.
20. Braeckmans, K.; Buyens, K.; Bouquet, W.; Vervaet, C.; Joye, P.; De Vos, F.; Plawinski, L.; Doeuvre, L.; Angles-Cano, E.; Sanders, N. N.; Demeester, J.; De Smedt, S. C. Sizing nanomatter in biological fluids by fluorescence single particle tracking. *Nano Lett* **2010,** *10*, (11), 4435-42.
21. Mishra, P.; Nayak, B.; Dey, R. K. PEGylation in anti-cancer therapy: An overview. *Asian Journal of Pharmaceutical Sciences* **2016,** *11*, (3), 337-348.
22. Dakwar, G. R.; Zagato, E.; Delanghe, J.; Hobel, S.; Aigner, A.; Denys, H.; Braeckmans, K.; Ceelen, W.; De Smedt, S. C.; Remaut, K. Colloidal stability of nano-sized particles in the peritoneal fluid: towards optimizing drug

delivery systems for intraperitoneal therapy. *Acta Biomater* **2014,** *10*, (7), 2965-75.
23. Xu, H.; Paxton, J. W.; Wu, Z. Enhanced pH-Responsiveness, Cellular Trafficking, Cytotoxicity and Long-circulation of PEGylated Liposomes with Post-insertion Technique Using Gemcitabine as a Model Drug. *Pharm Res* **2015,** *32*, (7), 2428-38.
24. Santos, R. S.; Dakwar, G. R.; Zagato, E.; Brans, T.; Figueiredo, C.; Raemdonck, K.; Azevedo, N. F.; De Smedt, S. C.; Braeckmans, K. Intracellular delivery of oligonucleotides in Helicobacter pylori by fusogenic liposomes in the presence of gastric mucus. *Biomaterials* **2017,** *138*, 1-12.
25. Webb, M. S.; Saxon, D.; Wong, F. M.; Lim, H. J.; Wang, Z.; Bally, M. B.; Choi, L. S.; Cullis, P. R.; Mayer, L. D. Comparison of different hydrophobic anchors conjugated to poly(ethylene glycol): effects on the pharmacokinetics of liposomal vincristine. *Biochim Biophys Acta* **1998,** *1372*, (2), 272-82.
26. Rombouts, K.; Braeckmans, K.; Remaut, K. Fluorescent Labeling of Plasmid DNA and mRNA: Gains and Losses of Current Labeling Strategies. *Bioconjug Chem* **2016,** *27*, (2), 280-97.
27. Dakwar, G. R.; Braeckmans, K.; Demeester, J.; Ceelen, W.; De Smedt, S. C.; Remaut, K. Disregarded Effect of Biological Fluids in siRNA Delivery: Human Ascites Fluid Severely Restricts Cellular Uptake of Nanoparticles. *ACS Appl Mater Interfaces* **2015,** *7*, (43), 24322-9.
28. Gaspar, V.; de Melo-Diogo, D.; Costa, E.; Moreira, A.; Queiroz, J.; Pichon, C.; Correia, I.; Sousa, F. Minicircle DNA vectors for gene therapy: advances and applications. *Expert Opin Biol Ther* **2015,** *15*, (3), 353-79.
29. Chen, Z. Y.; He, C. Y.; Ehrhardt, A.; Kay, M. A. Minicircle DNA vectors devoid of bacterial DNA result in persistent and high-level transgene expression in vivo. *Mol Ther* **2003,** *8*, (3), 495-500.

CHAPTER 5

BROADER INTERNATIONAL CONTEXT, RELEVANCE AND FUTURE PERSPECTIVE

CURRENT TRENDS IN FLUORESCENCE MICROSCOPY

It is common knowledge that progress in science is a slow process, made of small steps that eventually lead to advancement in the field. However, sometimes science proceeds through a series of breakthroughs that lead to important developments in a particular field. It is certainly the case, in recent times, within the life sciences, which benefitted enormously from the recent blooming of new microscopy techniques. In a short time span, fluorescence microscopy has become a precious tool within the life sciences and a cornerstone of modern biological laboratories, with applications that range from basic research, to the pre-clinical and clinical applications. Certainly, the greatest advances in fluorescence microscopy are due to the discovery and subsequent development of fluorophores for live cell imaging, opening the path to studying molecular pathways and subcellular dynamics. However, whilst new methodologies for live cell labeling appeared, major advances have been achieved on the technology side as well. New illumination modalities have emerged. After the initial fast but low-contrast epi-fluorescence microscopes, confocal microscopes appeared, and in particular the laser-scanning confocal microscope. While slower than an epi-fluorescence microscope with CCD camera, it provides high axial resolution and high contrast thanks to its inherent ability to optically section the sample. However, optical sectioning is achieved by rejecting the out-of-focus light, thus high laser intensities and fluorophores emitting bright signals are required to collect high-quality images. Developed as an alternative confocal technique, spinning disk confocal microscopes combined with sensitive CCD cameras are designed to be faster and more light-sensitive, thus less toxic for the sample, but at the

cost of a somewhat diminished confocality. Although confocal microscopes are great tools to study cells with high density of intracellular components, their axial and lateral resolution is still limited by diffraction. Probing the molecular architecture of single proteins, protein complexes and subcellular structures at the nanometer scale in their natural environment required the development of a new class of microscopes able to circumvent Abbe's diffraction limit. Super-resolution microscopes are the answer to the crescent need to examine biological structures at the nanoscale [1, 2]. There are three main super-resolution techniques: structured illumination microscopy (SIM), stimulated emission depletion microscopy (STED), Photo-activated localization microscopy (PALM). SIM uses interference-generated light patterns to extract high-resolution information of the intracellular structure. Although it can be used with many common fluorophores and dyes and it is the least photodamaging technique, its lateral and axial resolution is still in the hundreds of nanometer range. In comparison PALM, which is based on the stochastic activation of fluorophores and the subsequent identification of their centroid, has very high lateral and axial resolution (for 3D localization), both in the tens of nanometer range. On the other hand recording an image is typically slow, taking several seconds to even minutes and it requires special, photoswitchable fluorophores. STED has the best temporal resolution at the highest spatial resolution, however it too requires particular photostable dyes and can cause moderate photodamage to the sample due to the high laser powers needed[1]. One of the toughest challenges when performing cell imaging on live organisms is the acquisition of high contrast images at the cellular and sub-cellular level deep within thick scattering samples. To this end, multiphoton microscopy has proven to be a

valuable tool. Since near infrared light interacts less with biological tissues than visible light, it penetrates deeper into the sample and suffers less from scattering effects. Also multiphoton microscopy is less harmful to the sample than confocal microscopy, thanks to the reduced photobleaching outside the focal plane[3]. Instead, for situations where the viability of the sample is of major concern, a gentler technique has been recently developed: Light sheet fluorescence microscopy (LSFM). LSFM, extensively discussed in the first chapter, allows fast imaging of samples for days at high resolution and with limited phototoxic effects.

Thanks to the development of new illumination strategies and super-resolution microscopy techniques, phenomena in tissues and living cells can be recorded, producing much richer and more detailed datasets. Yet, the collection of high resolution images and their analysis generate an ever increasing amount of data which sometimes research facilities struggle to manage[4]. For example, super-resolution approaches may require 30,000 images to generate a single final picture[4], while the rate and amount of data generated in a LSFM experiment is approximately three orders of magnitude higher than that of confocal microscopes[5]. As a result, the functionality of a laboratory may be hindered by sub-optimal data management. Such a problem is mostly felt when the microscope has been adapted to be able to perform high-throughput assays. High-throughput cell assays are traditionally used to perform systematic measurements of enzymatic activity and gene expression. The ability to test and screen on a large scale cellular responses to selected stimuli (e.g. proteins, nucleic acids molecules) provides a great way to quantify the variability of the sample and uncover stereotypic patterns that may lead to important findings.

Certainly, this fairly recent expansion of the biologist's toolkit required a close collaboration between traditionally separated fields, involving life sciences (biology, chemistry), natural sciences (physics, mathematics) and engineering (optics, mechanics and software development). Never before like in the last decades the power of collaborative efforts has been so fundamental for the development of new devices and the advance of knowledge into the life sciences. Such complex instrumentation and techniques demand a sufficient level of expertise in various fields of the end users as well. This means that the implementation of a new technique in a lab or a department is not only expensive, but also requires a substantial amount of time and effort to increase the expertise of the main users. Moreover, as every sample and every scientific question is different from project to project, the necessity of modifying the set-up to address a specific issue requires to re-design the set-up and thus necessitates the same level of collaboration used to develop the technique. This type of interdisciplinarity is not always readily available to the average biology lab. In addition, particular prototypes developed in certain labs are not easily transferrable and not as robust as commercialized products.

As a matter of fact, one of the important challenges nowadays is to make these advanced microscopy techniques accessible to the general biologist. Without any doubt, commercial providers play a key role in the development and expansion of new technologies to the market. However, for a particular technique to become commercially available the demand must be high enough to cover the cost of its optimization and marketing. Only time will tell if this is the case for the advanced techniques mentioned above, which are highly complex and not as broadly applicable as the more traditional fluorescence and confocal microscopes.

SINGLE LENS LIGHT SHEET FLUORESCENCE MICROSCOPY

In this research project, we focused on increasing access to LSFM, which is a fast but gentle microscopy technique and, on paper, it is the dream of many biologists. It can quickly record 3-D images of mm-sized samples and collect high resolution images with low rates of photobleaching and minimal light-induced adverse effects on the sample. It has already proven beneficial in many studies and the range of applications increases by the year. However, LSFM is also the perfect example of a technique that requires a high level of collaboration between different scientific disciplines to be implemented, optimized and/or adapted to the particular sample of interest. Indeed, commercial systems have only very recently appeared on the market, which should be helpful as well to make it more widely available to technologically less experienced laboratories and research groups.

Our work has thus been focused on developing a system that would allow an easy implementation of high-resolution light sheet microscopy on standard microscopes bodies, like the ones of normal fluorescence microscopes that are ubiquitously available in many life sciences labs. The whole concept was based on creating a high-quality light sheet without the need of a second objective lens typically used for illumination in LSFM. Indeed, as already explained in chapter 1 and 2, most LSFM set-ups require two perpendicular objective lenses, one for illumination, one for detection. Such a configuration prevents the use of high-resolution objective lenses due to their bulky figure and their short working distances. Moreover, an easy implementation of LSFM on standard microscope bodies is hindered by their own architecture, since the large majority of them have been designed for single-lens use. In response to these issues, we designed,

tested and optimized special sample holders with integrated tilted micromirrors to enable light sheet illumination on-chip. The sample holders were prepared with a set of open channel, so as to allow imaging of many samples at the same time. Special attention has been given to choose a simple and cost effective design that would permit easy replication of the sample holders, to decrease costs of fabrication and allow the sample holders to be treated as disposables.

During the course of this project, the idea of using a mirror to reflect a light sheet on the sample was also developed by some other groups as well. Notable examples are the microfluidic sample holders developed by Galland and coworkers[6] and by Meddens and coworkers[7]. While conceptually similar, each work differs from the others. For example, the sample holders developed by Meddens and coworkers are meant to be used to perform 3D single molecule super-resolution imaging on single cells, thus their set-up is designed to produce very thin light sheets (1.1-1.6 μm at λ: 642 nm) with a DoF of 12 μm. To properly perform dSTORM, they developed a plastic laminated package to house the sample holder, with an inlet and an outlet to rapidly change buffers in the channels. In comparison, Galland and coworkers built a more flexible system, with capabilities that range from single molecule detection in single cells and cell clusters to whole embryo imaging. As a consequence, their light sheet can be tuned in thickness and size, ranging from a light sheet of 265x500x5.2 μm^3 to a light sheet of 13x30x1.2 μm^3. However, in both cases the fabrication process is quite labor-intensive. Our work differs from those in the sense that we evaluated a less complicated approach to fabricate the micromirrors. We chose to start from inexpensive polyimide wafers, polished and cut into smaller part, then coated with metal

to create a micromirror. The sample holder was then used as a master mold to create replicates that would be then coated in gold or aluminum. Results show that the replicated sample holders perform well in terms of beam waist and depth of field (1.9 µm and 17 µm respectively). Also important, we demonstrated that our approach based on inexpensive polished polymer plugs is very well suited for upscaling of sample holders with integrated micromirrors for single-lens LSFM.

However, compared to the systems cited above, in its actual configuration our sample holder does not yet comprise channels for easily seeding cells, exchanging cell media etc. Medden's and Galland's sample holders are thus better adapted at this stage to image live cells for long periods of time.

All these sample holders allow simultaneous imaging of several samples within the same experiment and enable broad modularity, considering that wide-field, high resolution and super-resolution imaging can be readily performed on the same microscope. Compared to other Reflected LSFM set-ups, these single-lens sample holders are a cheap and simple alternative to more complicated and expensive dedicated optical systems. Indeed, although Reflected LSFM set-ups enable the use of high NA lenses[8], the most known Reflected LSFM set-ups are quite complex and still require two objective lenses that need to be critically aligned. Gebhardt's set-up for instance used a specially manufactured AFM cantilever holder and special optics to provide light sheet illumination onto the AFM cantilever, all mounted to a fluorescent microscope. Leica also developed a reflected LSF microscope in which light is coupled through the diascopic arm and is reflected horizontally by two opposing mirrors mounted on the condenser lens. Their microscope is well suited to image large samples, but less so to image adherent cell

cultures. A similar but simpler solution has been put forward by Greiss and coworkers, which mounted the optic component on a custom-made breadboard attached on an inverted microscope. The laser light, coming from the opposing direction of the detection lens, is reflected on a micro-prism custom-attached to a microscopy coverslip[9]. Thanks to their thin light sheet (>1 μm), their set-up can image embryos but it can also be used for single-cell studies, however only if the cells are placed a few micrometers above the coverslip.

All considered, Reflected LSFM and particularly single-lens LSFM seems a budget-friendly and valid alternative to other LSFM set-ups for standard experiments. The sample holders are able to image samples ranging from whole embryos to single cells, it is possible to grow cells on the sample holders if necessary and they are well suited for single molecule super-resolution imaging. In the future, it would be interesting to extend their field of view by using self-reconstructing beams, like Bessel or Airy beams, instead of Gaussian beams or by using a TAG device, like done by Zong et al.[10], to quickly scan the focal spot along the illumination axis.

About the future of microscopy for biomedicine, it is clear that further innovations will continue to depend on close collaborations between different branches of science. A great effort remains needed to scientist to share their expertise, knowledge and experience. The great popularity of imaging courses around the world [11] reflects the interest and demand for transfer for expertise. Efforts to increase access to imaging technologies, like the OpenSpim project [12], are critical to pursue top-notch research worldwide.

Our newly developed sample holders are a step in that direction, yet they can still be improved further. A first important

improvement would be to automate the optic set-up so as to allow rapid double-sided light sheet illumination on the sample holders. Sample holders with two tilted mirrors facing each other have already been reported, but an efficient double-side illumination was prevented by the difficulties of manually moving the beam from one tilted wall to the other. An accurate automatization of the process would certainly improve the system's usability as well as image quality.

Also, automation would allow to perform multiple experiments at the same time. Multiple tilted mirrors could be built onto the same chip, each with their own space to place the sample, so that samples subject to different conditions can be investigated simultaneously. This would increase throughput, similar to the use of multi-well titer plates.

While our optical set-up is quite simple compared to other set-ups, it still requires a considerable amount of time and expertise to be assembled in less-specialized laboratories. To make the transition to less specialized labs, the beam shaping /steering optics should be packaged into an add-on module that can be easily connected to the microscope bodies of the main manufacturers, similar to confocal scanners. Another drawback is that, right now, the process to fabricate the sample holders is quite labor-intensive and it produces a relatively low number of replicated sample holders. However our fabrication process was especially chosen for rapid up-scaling of the sample holders so to decrease their fabrication cost per unit and to allow them to be used as disposables, to avoid contamination between samples.

In general terms, the up-scaling process should take advantage of modern replication technologies such as micro-injection molding, hot embossing or (nano)imprint lithography. The last is a low cost, high resolution and high throughput process that

creates patterns into a polymer material that is cured by heat or by UV-light during imprinting. Once a final design is available, a so-called master mold can be made consisting of a large number of sample holders in a matrix. This can for example be fabricated on a 4 inch (or larger) Si wafer. From this master, a flexible stamp can then be made by covering the sample holders with a UV-curable resin (such as PDMS or PFPE). Upon UV exposure, the resin turns into a transparent flexible polymer material which can be easily peeled off from the master. This sheet of polymer material with the inverse of the master patterns can now be used multiple times as a stamp to imprint another UV-curable photoresist. Thereto, a suitable UV-curable photoresists (e.g. an epoxy) is coated on a substrate (typically having the same size as the master) and the stamp is pressed or laminated on top of it. The resist is then cured by exposing it to UV through the stamp, after which the stamp can be detached and a full-wafer replica of the master is achieved in the photoresist. Those structures can subsequently be coated with aluminum and can afterwards be cut into individual sample holders by a wafer dicer. Finally, a microscopy coverslip provided with inlet and outlet holes can be attached to the sample holders using for example an UV-sensitive glue or adhesive tape. Alternatively, micro-injection molding could be used to realize a large number of sample holders. Therefore, a 3D metal mold with an inset being the inverse of the sample holder can be created, in which a thermoplastic material is then injected under pressure and elevated temperature. However, this yields individual, freestanding components, which might be more difficult to coat with metal.

Application of the device shouldn't be limited to LSFM imaging. The simple fabrication process and the limited requirements to create light sheet illumination should make it possible to

completely integrate the tilted micromirror in a lab-on-chip device. A lab-on-chip device has the advantage to manipulate and label the sample prior to investigation, and also allows sorting of cells with interesting features that can be later studied in details[13]. They save time and ensure standardized treatment of the sample, which prevent variability in the results due to human errors. We think our device would be a nice addition to many multitasking devices.

SPT FOR PARTICLE CHARACTERIZATION

In parallel with this project, we focused on expanding the biochemist's toolkit by means of SPT. As discussed in chapter 3, SPT is a well-known technique currently employed to characterize the behavior of nanoparticles in a given (biological) environment. Modern SPT-based commercial instruments for nanoparticle characterization, like NanoSight NS300 (Malvern) and Zetaview (ParticleMetrix), record and analyze the motion of individual nanoparticles to simultaneously determine their size distribution, their absolute number concentration and sometimes even their zeta potential. As an optical technique it is non-invasive, and over the years has proven to be fundamental for a rational optimization of gene-based macromolecular therapeutics. Reported uses of the instruments cited above indeed vary from extracellular vesicles characterization to research on protein aggregation, focusing also on research on viral vaccines and on research and development of drug- and gene-delivery systems. It is common belief among nucleic acid- and gene-delivery researchers that a successful gene-based treatment rely on the capacity of biocompatible carriers to protect nucleic acid molecules (NAms) and deliver them to their target cells. Engineering well-performing NAms delivery systems is thus a

common goal, and a thorough characterization of NAms delivery systems is of the utmost importance. However, while parameters like size, degree of aggregation, surface chemistry, zeta potential and even concentration can be easily measured or calculated, the average number of NAms per carrier is mostly unknown. We thus developed the first method (to our knowledge) that directly measures the number of NAms per carrier. Thanks to our method, the differences in the loading degree of the nanocarrier, mostly due to small differences in the complexation conditions, can be monitored and exploited to ensure maximal effectivity of the NA molecule/carrier formulation. The results indicated that pDNA size and concentration have a clear influence on the number of pDNA copies per DOTAP:DOPE lipoplex (LPX). Also, we proved that the approach used to PEGylate the surface of the carrier has direct consequences on the lipoplexes complexation. Thus, our method gives important information on which conditions exactly affects complexation and it is certainly useful for a rational optimization of the NA molecule/carrier complex. For instance, with our methods different protocols to complex nanoparticles may be tested to increase (or decrease, if preferred) the number of molecules per carrier. Techniques to decrease the size of the NAms without affecting their functionality may be adopted, like using Minicircle DNAs. Cell uptake and transfection efficiency may be considered in relation to the actual number of NAms per carrier, since tuning the pDNA/NP ratio is now possible.

While we could successfully demonstrate the method's principle, further improvement is certainly needed. First of all, as the method currently requires complete complexation of the NAms cargo with its carrier, it can now be applied to only a limited set of situations/conditions. Strategies that can quantify the percentage of uncomplexed NAms would be beneficial for the

technique and would expand its range of applications. For example, as suggested in chapter 4, uncomplexed NAms may be quantified by labeling both the NAms and the carrier with different fluorophores, so that uncomplexed DNA would have only one color. Also, by choosing the two fluorophores wisely, fluorescence resonance energy transfer may be used to directly discriminate between complexed and uncomplexed NAms. Another option may be to quantify and remove uncomplexed NA molecules by adding nucleases to the complexed sample after measuring their apparent concentration. Second, the method as it is now has been evaluated using fluorescently labeled NAms. However, in principle the method should be readily extended to unlabeled samples. For instance, some commercial instruments like Nanosight can perform SPT measurement based on light scattering and their presence into laboratories is increasing. As a last remark, the method has been tested only to check complexation of fluorescently labelled plasmid DNA. Nevertheless, there's no reason to believe that the method cannot be applied to monitor the complexation of any other molecule, as long as the concentration of this molecules can be precisely calculated beforehand.

As a last remark, it has been reported that SPT has benefitted from light sheet illumination[14, 15 16 17 18]. Thanks to the background noise reduction and the increased signal to noise ratio (SNR), the localization precision of nanoparticles with intrinsically weak signals is increased. Combining our method with light sheet illumination would thus increase its accuracy. In our laboratory we developed two LSFM systems, one based on a tilted mirror[19], the other based on a planar waveguide[18]. In the latter case, an optical fiber is butt-coupled to a waveguide on a silicon or glass substrate and a 9-µm-thick light sheet is formed in the channel.

Design-wise, the set-up developed by Deschout et al. is simpler than the one developed in this thesis with tilted mirrors. However, alignment of the fiber with the planar waveguide was not easy and its light sheet was 4.7 times thicker than the light sheet measured in the replicated polymer based sample holder, apart from the fact that the z-position of the light sheet could not be changed. As such I believe that the design proposed in this thesis is a substantial improvement and is expected to be of benefit for SPT based nanoparticle characterization. At present it remains to be seen if the contrast and SNR obtained with our LSFM systems can rival the contrast and SNR obtained with spinning disk confocal microscopy. From my personal experience, while using a spinning disk microscope I had sometimes to deal with annoying artifacts, especially "ghost particles" that appeared when very bright particles entered the field of view. Owing to this, I would personally rather use a LSFM microscope than a spinning disk microscope for SPT applications.

In summary, these are exciting times for life-science researchers. The rapid expansion of advanced microscopy techniques produced a symbiosis between life sciences and microscopy never seen before. To fully profit from these new technological tools, a high degree of collaboration between different fields and a willingness to explore other branches of science are necessary. Projects aimed to share knowledge, expertise and open source programs are gaining in popularity. Online tutorials and imaging courses are spreading and generally well attended. After all, new exciting discoveries are beyond the corner, as long as the right tool for the job is available. In this work, we aimed to expand the researchers toolbox by proposing a new method for characterization of NAms-loaded nanocarrier and by developing sample holders for a widespread adoption of LSFM.

REFERENCES

1. Sydor, A. M.; Czymmek, K. J.; Puchner, E. M.; Mennella, V. Super-Resolution Microscopy: From Single Molecules to Supramolecular Assemblies. *Trends in Cell Biology 25*, (12), 730-748.
2. Schermelleh, L.; Heintzmann, R.; Leonhardt, H. A guide to super-resolution fluorescence microscopy. *The Journal of Cell Biology* **2010,** *190*, (2), 165-175.
3. Hoover, E. E.; Squier, J. A. Advances in multiphoton microscopy technology. *Nat Photon* **2013,** *7*, (2), 93-101.
4. Wallace, C. T.; St. Croix, C. M.; Watkins, S. C. Data management and archiving in a large microscopy-and-imaging, multi-user facility: Problems and solutions. *Molecular Reproduction and Development* **2015,** *82*, (9), 630-634.
5. Schmid, B.; Shah, G.; Scherf, N.; Weber, M.; Thierbach, K.; Campos, C. P.; Roeder, I.; Aanstad, P.; Huisken, J. High-speed panoramic light-sheet microscopy reveals global endodermal cell dynamics. **2013,** *4*, 2207.
6. Galland, R.; Grenci, G.; Aravind, A.; Viasnoff, V.; Studer, V.; Sibarita, J. B. 3D high- and super-resolution imaging using single-objective SPIM. *Nat Methods* **2015,** *12*, (7), 641-4.
7. Meddens, M. B.; Liu, S.; Finnegan, P. S.; Edwards, T. L.; James, C. D.; Lidke, K. A. Single objective light-sheet microscopy for high-speed whole-cell 3D super-resolution. *Biomed Opt Express* **2016,** *7*, (6), 2219-36.
8. Gebhardt, J. C.; Suter, D. M.; Roy, R.; Zhao, Z. W.; Chapman, A. R.; Basu, S.; Maniatis, T.; Xie, X. S. Single-molecule imaging of transcription factor binding to DNA in live mammalian cells. *Nature Methods* **2013,** *10*, (5), 421-6.
9. Greiss, F.; Deligiannaki, M.; Jung, C.; Gaul, U.; Braun, D. Single-Molecule Imaging in Living Drosophila Embryos with Reflected Light-Sheet Microscopy. *Biophys J* **2016,** *110*, (4), 939-46.
10. Zong, W.; Chen, X.; Zhao, J.; Zhang, Y.; Fan, M.; Zhou, Z.; Cheng, H.; Sun, Y.; Chen, L. In *Two-photon three-axis digital scanned light-sheet microscopy (2P3A-DSLM)*, CLEO: 2014, San Jose, California, 2014/06/08, 2014; Optical Society of America: San Jose, California, p AW3L.7.
11. Swedlow, J. R. Innovation in biological microscopy: current status and future directions. *Bioessays* **2012,** *34*, (5), 333-40.
12. Marx, V. Microscopy: OpenSPIM 2.0. *Nat Meth* **2016,** *13*, (12), 979-982.

13. Wyatt Shields Iv, C.; Reyes, C. D.; Lopez, G. P. Microfluidic cell sorting: a review of the advances in the separation of cells from debulking to rare cell isolation. *Lab on a Chip* **2015,** *15*, (5), 1230-1249.
14. Ritter, J. G.; Veith, R.; Siebrasse, J. P.; Kubitscheck, U. High-contrast single-particle tracking by selective focal plane illumination microscopy. *Opt Express* **2008,** *16*, (10), 7142-52.
15. Ritter, J. G.; Veith, R.; Veenendaal, A.; Siebrasse, J. P.; Kubitscheck, U. Light sheet microscopy for single molecule tracking in living tissue. *PLoS One* **2010,** *5*, (7), e11639.
16. Spille, J. H.; Kaminski, T.; Konigshoven, H. P.; Kubitscheck, U. Dynamic three-dimensional tracking of single fluorescent nanoparticles deep inside living tissue. *Opt Express* **2012,** *20*, (18), 19697-707.
17. Yu, B.; Yu, J.; Li, W.; Cao, B.; Li, H.; Chen, D.; Niu, H. Nanoscale three-dimensional single particle tracking by light-sheet-based double-helix point spread function microscopy. *Appl Opt* **2016,** *55*, (3), 449-53.
18. Deschout, H.; Raemdonck, K.; Stremersch, S.; Maoddi, P.; Mernier, G.; Renaud, P.; Jiguet, S.; Hendrix, A.; Bracke, M.; Van den Broecke, R.; Roding, M.; Rudemo, M.; Demeester, J.; De Smedt, S. C.; Strubbe, F.; Neyts, K.; Braeckmans, K. On-chip light sheet illumination enables diagnostic size and concentration measurements of membrane vesicles in biofluids. *Nanoscale* **2013**.
19. Zagato, E.; Brans, T.; Verstuyft, S.; van Thourhout, D.; Missinne, J.; van Steenberge, G.; Demeester, J.; De Smedt, S.; Remaut, K.; Neyts, K.; Braeckmans, K. Microfabricated devices for single objective single plane illumination microscopy (SoSPIM). *Opt. Express* **2017,** *25*, (3), 1732-1745.

SUMMARY AND GENERAL CONCLUSIONS

The human body is a true wonder. It is composed by an average of 3.7 trillion cells, subdivided in more than 200 different cell types, each with its function and its own specialization. Yet, life is possible only if those cells manage to communicate and closely collaborate with each other, to reach their common goal. Clearly, collaboration is the key to evolution and progress. This is no different in science. The technological progresses of this era, such as in the field of optical microscopy, have given an inestimable contribution to the progresses recently achieved in the life sciences. In turn, the challenges encountered while studying those microscopic, remarkably complex biological systems have been a fertile ground for the development of new, specialized technological systems. Such a close collaboration across scientific fields clearly is a driver for innovation and scientific progress. However, increased technological capabilities comes with increased complexity as well. Hence, to implement a novel state-of-the-art technique, such as LSFM and SPT in this work, research groups must commit an increasing amount of resources, in terms of time, funding and efforts to properly use those techniques to their full capabilities and in training its main users.

In this thesis we aim to increase the accessibility of a recently developed technique to the general biology laboratory. In first instance, in **chapter 1** the implementation of the various existing light sheet fluorescence microscopes (LSFM) is described in detail. The review at first focuses on the advantages and disadvantages of multiview imaging, the benefits of using self-healing beams compared to traditional beams, and suggests how to improve the performance of the microscope by modifying the detection path.

The second part of the review discusses the various possibilities to get started with LSFM as a non-expert. Commercially available instruments are hence presented, together with the tutorials, available on-line, that describe step-by-step how to build a LSFM with basic optical components. Special attention is given to those solutions that allow a rapid implementation of a LSFM system on epi-fluorescent microscopes, since those kind of microscopes are commonly present in biological research labs.

One of those solution is presented in **chapter two**. To increase access to the technique, we designed, developed and replicated special microfluidic sample holders with integrated optical components to allow single lens light sheet microscopy directly on-chip. The sample holders make use of a micromirror to reflect in the channel the light that comes from the objective lens, while the same objective lens is used for imaging of the sample in the sample holder. This clever design eliminates *de facto* the need for (at least) two objective lenses as is needed for traditional LSFM.

Two designs have been proposed, tested and replicated in an inexpensive UV-curable epoxy. The quality of the beam generated in the microchannels has been dutifully assessed. The light sheet in the channel presents a beam thickness of approximately 2 μm, comparable to the light sheet thickness of most LSFM. Also, the sample holders perform well in terms of contrast achieved in the presence of a high background noise and proved to be adapt to acquire high-quality images of spheroids.

The second part of the thesis focused on a different sort of advanced microscopy technique, Single Particle Tracking. SPT is described in **chapter three**, explaining its fundamentals and its application to study drug- and gene-delivery oriented biocomplexes in extra- and intra-cellular environments. SPT is a highly sensitive, non-invasive optical technique that is able to

study the behavior of the nanoparticles at a single particle level. It has proven to be particularly beneficial in studies where monitoring the size distribution, degree of aggregation and concentration of the nanoparticle is crucial. Therefore, in **chapter four** we exploited the unique characteristic of the technique to devise a novel method for the characterization of nucleic acid-loaded nanocomplexes. Nucleic acid molecules (NAms) based therapeutics show great potential for the treatment of genetic disorders and cancer. However, the many environments the therapeutics need to cross to reach its desired target alter the physicochemical properties of the nanocomplex and more often than not result into degradation of the complex and of its precious cargo. Moreover, the nanocomplex itself, if poorly designed, may trigger acute inflammatory responses *in vivo* and be toxic for its target cells. Consequently, a thorough characterization of NAms based complexes is of the utmost importance to properly engineer safe and effective NAms based therapeutics. One property of the nanocomplexes that has been mostly overlooked is the actual number of NAms complexed per nanocarrier. We focused on DOTAP:DOPE liposomes as a model carrier and studied which conditions affect the number of pDNA molecules that are incorporated per lipoplex. We discovered that the pDNA/carrier complexation is highly influenced by their chance on collision when the carrier and cargo are mixed. Thus the average number of plasmid per nanocomplex depends on the concentration of carrier and cargo, on the size of the pDNA and whether or not the carrier is PEGylated.

In future research it will be of interest to apply the SPT method to different types of cargo and carriers and to see how the number of cargo molecules per complex influences the final biological effect.

SAMENVATTING EN ALGEMENE BESLUITEN

Het menselijke lichaam is echt wonderbaarlijk. Het is opgebouwd uit gemiddeld 3.7 biljoen cellen, onderverdeeld in meer dan 200 verschillende celtypes die elk hun eigen functie en specialisatie hebben. Al deze cellen moeten met elkaar kunnen communiceren en samenwerken om gezond te kunnen leven. Het is dus duidelijk dat samenwerking de sleutel is tot evolutie en vooruitgang. Binnen de wetenschap is dit ook zo, de technologische vooruitgang in één veld, zoals bijvoorbeeld de optische microscopie, zijn vaak van groot belang voor de vooruitgang in andere velden, de levenswetenschappen. Op hetzelfde moment zijn de moeilijkheden die gepaard gaan met het bestuderen van microscopische, uiterst complexe biologische systemen de drijfveer voor de ontwikkeling van nieuwe, zeer gespecialiseerde technologische systemen.

Deze nauwe relaties en samenwerkingen tussen verschillende wetenschappelijke domeinen dragen dan ook zeer duidelijk toe aan de hedendaagse innovatie en de wetenschappelijke vooruitgang. Echter brengen de verbeterde technologische mogelijkheden en verbeterde technieken ook een verhoogde complexiteit met zich mee. Bijgevolg dienen onderzoeksgroepen, bij de implementatie van een nieuwe state-of-the-art techniek zoals LSFM en SPT, over steeds grotere hoeveelheden aan middelen te beschikken zoals geld, tijd en opleiding om deze technieken efficiënt te kunnen gebruiken.

In dit werk trachten we de toegankelijkheid van een recent ontwikkelde techniek te verhogen voor biologische laboratoria. Als eerste wordt, in **hoofdstuk 1**, de implementatie van de verschillende bestaande “light sheet fluorescence microscopes” (LFSM) in detail beschreven. In het eerste deel van deze review worden de voor en nadelen van multiview beeldvorming, de voordelen van het gebruik van een “self-healing beam” in

vergelijking met de traditionele belichting besproken en worden een aantal voorstellen gemaakt om de prestaties van een microscoop te verbeteren door aanpassingen door te voeren aan het detectiepad.

Het tweede deel van de review bespreekt de verschillende mogelijkheden om als niet expert van start te gaan met LSFM. Hiervoor worden commercieel beschikbare instrumenten besproken alsook on-line beschikbare handleidingen die stap voor stap beschrijven hoe een LSFM kan gebouwd worden met standaard optische componenten. Hierbij wordt extra aandacht gegeven aan oplossingen die een snelle implementatie van LSFM systemen mogelijk maken op epi-fluorescentie microscopen aangezien dit soort microscopen algemeen aanwezig zijn in biologische onderzoekslaboratoria.

Een van deze oplossingen wordt voorgesteld in **hoofdstuk 2**. Om de toegang tot LFSM te verhogen werd een speciale microfluïdische staalhouder ontworpen, ontwikkeld en gerepliceerd die geïntegreerde optische componenten bevat die toelaten om "light sheet" microscopie uit te voeren op epi-fluorescentie microscopen met één enkele objectieflens. Deze staalhouder maakt gebruik van een micromirror om het licht afkomstig van de objectief lens te reflecteren in het kanaal waar het staal zich bevindt, waarna dezelfde objectieflens ook gebruikt wordt voor de beeldvorming van het staal in de staalhouder. Dit ontwerp elimineert *de facto* de noodzaak voor minstens twee objectief lenzen zoals bij traditionele LFSM instrumenten.

Twee ontwerpen werden voorgesteld, getest en gerepliceerd met een goedkope UV-uithardbare epoxy. De kwaliteit van de, in het kanaal gecreëerde, lichtstraal werd geëvalueerd en uit de evaluatie blijkt dat de lichtstraal (light sheet) in het kanaal een dikte heeft van ongeveer 2µm, hetgeen vergelijkbaar is met de light sheet dikte in de meeste LSFM systemen. Verder presteren

de staalhouders goed wat betreft het behaalde contrast in de aanwezigheid van een hoge background noise en zijn ze in staat om beelden van hoge kwaliteit te bekomen van sferoïden.

Het tweede deel van dit werk besteedt aandacht aan een ander soort geavanceerde microscopische techniek namelijk "Single Particle Tracking" (SPT). Deze techniek wordt besproken in **hoofdstuk 3**, waarin de basisprincipes van de techniek alsook de toepassing ervan voor het bestuderen van geneesmiddel en gene-delivery georiënteerde biocomplexen in extra- en intra-cellulaire omgevingen. SPT is een zeer gevoelige, niet invasieve optische techniek die toelaat om het gedrag van nanopartikels te bestuderen tot op het niveau van één enkel partikel en heeft reeds zijn nut aangetoond voor studies waarbij het belangrijk is om de grootteverdeling, mate van aggregatie en concentratie van nanopartikels te bestuderen. Daarom werden, in **hoofdstuk 4**, de unieke karakteristieken van SPT gebruikt om een nieuwe methode te ontwikkelen om nanocomplexen gevuld met nucleïnezuren te karakteriseren. Therapeutica gebaseerd op nucleïnezuur moleculen (NAms) zijn veelbelovend voor de behandeling van genetische aandoeningen en kanker. Echter dienen deze therapeutica verschillende omgevingen te doorkruisen om het gewenste doelgebied te bereiken en al deze omgevingen kunnen de fysicochemische eigenschappen van het nanocomplex beïnvloeden. Deze veranderde fysicochemische eigenschappen leiden zeer vaak tot de degradatie van het nanocomplex en zijn kostbare inhoud. Bovendien kan het nanocomplex zelf, indien deze slecht ontwerpen is, een acute inflammatoire reactie teweegbrengen en kan deze giftig zijn voor de doelcellen. Bijgevolg is een duidelijke karakterisatie van op NAms gebaseerde complexen van zeer groot belang om veilige en efficiënte op NAms gebaseerde therapeutica te kunnen ontwikkelen. Eén eigenschap van nanocomplexen die hierbij vaak

over het hoofd werd gezien is het effectieve aantal NAms die gecomplexeerd zijn per nanocarrier.

In deze studie werd gekozen om DOTAP:DOPE liposomen als model carrier te gebruiken en te bestuderen welke condities een invloed hebben op het aantal pDNA moleculen die geïncorporeerd worden per liposoom. We hebben hierbij ontdekt dat pDNA/carrier complexatie sterk beïnvloed wordt door de kans op botsingen wanneer de carrier en hun lading worden gemengd. Bijgevolg hangt het gemiddelde aantal plasmiden per nanocomplex af van de concentratie aan carriers en hun lading, de grootte van het pDNA en van het feit of de carrier gePEGyleerd is.

Voor toekomstig onderzoek is het interessant om deze nieuwe SPT methode toe te passen op verschillende soorten carriers en lading om te zien hoe het totale aantal lading moleculen per complex het uiteindelijke biologische effect beïnvloeden.

Curriculum Vitae

Education

1/2013 – now: **PhD Candidate** at the Lab of General Biochemistry and Physical Pharmacy, Faculty of Pharmaceutical Sciences, Ghent University, Belgium.

Promoters:
Prof. Dr. Kevin Braeckmans,
Prof. Dr. Kristiaan Neyts
Prof. Dr. Katrien Remaut

2009 – 2012: **Master in Biophysics** *(107/110)*
Università degli Studi di Milano-Bicocca - Italy

Master thesis: "Fluorescence Correlation Spectroscopy and Single Particle Tracking to study the complexation behaviour of plasmid DNA with non-viral delivery carriers."

Promoters:
Prof. Dr. Giuseppe Chirico
Prof. Dr. Kevin Braeckmans

2006 – 2009: **Bachelor in Physics** *(110/110 cum laude)*
Università Cattolica del Sacro Cuore - Italy

Master thesis: "Study of a molecular sensor based on surface acoustic waves formed on nanostructured materials."

Promoters: Prof. Dr. Francesco Banfi,
Prof. Dr. Gabriele Ferrini

ADDITIONAL COURSES

2013:	Particle Characterization (Belgian Particle, Colloid and Interface society, Belgium)
2014:	Effective Scientific Communication (Doctoral Schools, Ghent University)

Academic curriculum

PUBLICATIONS

Zagato E, Forier K, Martens T, Neyts K, Demeester J, De Smedt SC, Remaut K, Braeckmans K.
"Single-particle tracking for studying nanomaterial dynamics: applications and fundamentals in drug delivery." *Nanomedicine*, 2014

Zagato E, Brans T, Verstuyft S, Van Thourhout D, Remaut K, Missinne J, Van Steenberge G, Demeester J, De Smedt S, Neyts K, Braeckmans K
"Microfabricated devices for single objective single plane illumination microscopy (SoSPIM)", *Optics express*, 2017

Zagato E, Brans T, De Smedt S, Remaut K, Neyts K Braeckmans K
"Technical implementation of Light Sheet Microscopy", *Microscopy Research and Technique*, 2018

Zagato E, Vermeulen L, Dewitte H, Van Imschoot G, Vandenbroucke R E, Demeester J, De Smedt S, Neyts K, Remaut K, ,Braeckmans K
"Quantifying the average number of nucleic acid therapeutics per nanoparticle by Single Particle Tracking", *Molecular Pharmaceutics*, 2018 (under consideration)

Santos RS, Dakwar GR, **Zagato E**, Brans T, Figueiredo C, Raemdonck K, Azevedo NF, De Smedt SC, Braeckmans K.

"Intracellular delivery of oligonucleotides in Helicobacter pylori by fusogenic liposomes in the presence of gastric mucus", *Biomaterials* 2017

Röding M, **Zagato E,** Remaut K, Braeckmans K
"Approximate Bayesian computation for estimating number concentrations of monodisperse nanoparticles in suspension by optical microscopy" *Physical Review E*, 2016

Colzani B, Speranza G, Dorati R, Conti B, Modena T, Bruni G, Zagato E, Vermeulen L, Dakwar GR, Braeckmans K, Genta I.
"Design of smart GE11-PLGA/PEG-PLGA blend nanoparticulate platforms for parenteral administration of hydrophilic macromolecular drugs: synthesis, preparation and in vitro/ex vivo characterization." *International Journal of Pharmaceutics*, 2016

Furst T,.Dakwar GR, **Zagato E**, Lechanteur A, Remaut K, Evrard B, Braeckmans K, Piel G.
"Freeze-dried mucoadhesive polymeric system containing pegylated lipoplexes:Towards a vaginal sustained released system for siRNA", *Journal of controlled Release*, 2016

Pärnaste L, Arukuusk P, **Zagato E**, Braeckmans K, Langel Ü.
"Methods to follow intracellular trafficking of cell-penetrating peptides." *Journal of Drug Targeting*, 2015

De Cock I, **Zagato E**, Braeckmans K, Luan Y, de Jong N, De Smedt SC, Lentacker I.
"Ultrasound and microbubble mediated drug delivery: Acoustic pressure as determinant for uptake via membrane pores or endocytosis" *Journal of Controlled Release*, 2014

Dakwar GR, **Zagato E**, Delanghe J, Hobel S, Aigner A, Denys H, Braeckmans K, Ceelen W, De Smedt SC, Remaut K.

"Colloidal stability of nano-sized particles in the peritoneal fluid: Towards optimizing drug delivery systems for intraperitoneal therapy" *Acta biomaterialia*, 2014

CONFERENCES ATTENDED

2014: DIATECH2014, Leuven, Belgium -
POSTER presentation
On-chip light sheet microscopy for nanoparticle characterization and cell imaging

2014: MICROFLUIDICS2014, Heidelberg, Germany –
POSTER presentation
On-chip light sheet microscopy for nanoparticle characterization and cell imaging

2014: NANOBIOTECH, Montreaux, Switzerland –
POSTER presentation
On-chip light sheet microscopy for nanoparticle characterization and cell imaging

2015: Focus On Microscopy 2015, Gottingen, Germany –
POSTER presentation
On-chip light sheet microscopy for nanoparticle characterization and cell imaging

2015: 2nd LSFM International Conference, Genoa, Italy –
ORAL presentation
Single Lens Light Sheet Microscopy enabled by Optofluidics Device with integrated Micromirrors

2016: MicroTAS2016, Dublin, Ireland –
POSTER presentation
Single Lens Light Sheet Microscopy On-chip

TEACHING EXPERIENCE

2016: Supervision and evaluation of 1st year Master in Pharmaceutical Sciences student during her thesis

2014: Supervision and evaluation of 1st year Master in Pharmaceutical Sciences student during her thesis

MEMBERSHIP OF PROFESSIONAL BODIES

RBSM Royal Belgian Society for Microscopy

ACKNOWLEDGEMENT

“Success isn’t about how much money you make. It’s about the difference you make in people’s lives.” said Michelle Obama once. I don’t know if she’s right or wrong, but in these last four years I’ve been lucky enough to meet people she’ll definitely define “successful”. Here’s the time to thank them.

First, I would like to express my gratitude to my advisor, Prof. Kevin Braeckmans, for his continuous support, his patience and his guidance. I never felt alone, even in difficult times, and I owe it to him if I eventually managed to finish my research and writing my thesis. I feel lucky he choose me to be part of his team.

Besides my advisor, I would like to thank my co-promotors, Prof. Katrien Remaut and Professor Kristiaan Neyts. Katrien, thank you for sharing your knowledge with me and for your insightful comments end encouragement. Kristiaan, I am very grateful to you for providing me the opportunity to join your team and share your lab and resources. It was a pleasure to work with such a skilled and good hearted team.

My sincere thanks to the members of my thesis committee, for their enthusiasm, the stimulating discussion and the interesting questions and remarks. It was a pleasure to discuss my thesis with you.

Prof. De Smedt and Prof. Demeester, it was a pleasure working with you. Your enthusiasm and passion stimulated and motivated me when I needed it the most. My sincere gratitude for every time I felt you cared for me and my research.

I thank my fellow labmates with all my heart and soul. Sadly, I don’t have time to thank all of you one by one, also because we are a large group, so I will focus on the ones that most influenced my life in the last four years.

First of all, I need to thank Lotte Vermeulen, Koen Rombout and Freya Joris. Koen, you are a great person and I feel lucky I had the possibility

to spend these years with you. You were like a mentor to me, the first one I would ask for help, the one I relied on the most. I enjoyed your silences, I enjoyed your smiles, your jokes and your sudden outburst of loquacity. I still have the blackberry plant you bought for us in the office, it is alive and well, and I can't wait for it to produce some fruit and share them with you.

Freya, you are truly amazing. Your smile warms up the room and I envy your strength and determination. Thanks for sharing your dreams with me, as I shared mines with you. Thanks for your compassion and kindness, thanks for all the interesting discussions, thanks for listening when I needed to ventilate my frustration.

Lotte, I have high admiration for you. I love your no-nonsense attitude. I value your sincerity and integrity. Also, you went through tough times with a strength I don't think I possess. Thank you for sharing my tears, thank you for sharing my frustration, thank you for the laugh we had. You truly made my four years here special.

Next in line, Karen Peynshaert. I am mesmerized by you and your personality. Eventually, you became a model to me, the kind of researcher I would have wanted to be, eclectic, enthusiastic, compassionate, self-driven, able to make people smile and able to conquer other people's heart in a few minutes. Thank you for sharing your good and bad moments with us. I know you have a brilliant career in front of you, since you are a brilliant person yourself.

Katrien Forier, I miss you. You are a true friend to me and your is the presence I miss the most. You are one of the most fun and interesting people I know, I love your creativity and fantasy. Pity you couldn't come to the defense, I really wanted to share the moment with you.

Of course, there are other 30 people or so I should thank. Every colleague I had contributed to my personal success, sometimes by sharing their opinion, sometimes by encouraging me, sometimes by smiling and contributing to the great atmosphere in the lab.

Last but not least, I need to thank my husband and his mother, Stijn and Nella. I couldn't have made it without you. No words will ever describe my gratitude, but words between us are not necessary. You know I love you.
To my family, friends and supporters in Italy: I know you would have wanted to be here. I miss you so much! I feel and have felt your love and support throughout this PhD. Thanks.
And to Leon: my dear son-to-be, these last months were hard, and you know it most than anyone else. Well, thank you for being calm and quiet during the internal defense. I love you and can't wait to meet you, in person, for the first time ever.